AECL-9684

Atomic Energy of Canada Limited

L'Energie Atomique du Canada Limitée

PROPOSAL FOR A NATIONAL FACILITY
Proposition d'une installation nationale

MARS

A MULTIDETECTOR ARRAY FOR REACTION STUDIES

Un système multidétecteur pour l'étude de réactions

G.C. Ball, W.G. Davies, J.S. Forster, E. Hagberg, D. Horn, M.A. Lone, C. Pruneau, L. Potvin, C. Rioux, R. Roy, C. St-Pierre, T. Drake and A. Galindo-Uribarri

Chalk River Nuclear Laboratories - Laboratoires Nucléaires de Chalk River
Chalk River, Ontario K0J 1J0

March 1988 mars

ATOMIC ENERGY OF CANADA LIMITED

PROPOSAL FOR A NATIONAL FACILITY

MARS

A Multidetector Array for Reaction Studies

by

G.C. Ball, W.G. Davies, J.S. Forster, E. Hagberg,
D. Horn, M.A. Lone, and C. Pruneau
Atomic Energy of Canada Limited, Chalk River Nuclear Laboratories

L. Potvin, C. Rioux, R. Roy, and C. St-Pierre
Université Laval

T. Drake and A. Galindo-Uribarri
University of Toronto

Nuclear Physics Branch
Chalk River Nuclear Laboratories
Chalk River, Ontario K0J 1J0
1988 February

AECL-9684

L'ÉNERGIE ATOMIQUE DU CANADA, LIMITÉE

PROPOSITION D'UNE INSTALLATION NATIONALE

MARS

Système Multidétecteur pour l'étude de Réactions

par

G.C. Ball, W.G. Davies, J.S. Forster, E. Hagberg,
D. Horn, M.A. Lone, and C. Pruneau
L'Énergie Atomique du Canada, Limitée
Laboratoires Nucléaires de Chalk River

L. Potvin, C. Rioux, R. Roy, and C. St-Pierre
Université Laval

T. Drake and A. Galindo-Uribarri
Université de Toronto

Résumé

On présente dans le rapport la proposition d'installation MARS (Système Multidétecteur pour Études de Réaction). MARS comprend un grand réservoir sous vide poussé renfermant un ensemble de 128 détecteurs à scintillation devant servir à des études de collision d'ions lourds dans l'installation combinée TASCC (Accélérateur Tandem Cyclotron Supraconducteur). L'installation sera financée par l'EACL et le CRSNG (Conseil de Recherches en Sciences Naturelles et en Génie) et appartiendra à ces deux organismes.

Physique nucléaire
Laboratoires Nucléaires de Chalk River
Chalk River, Ontario K0J 1J0
1988 mars

AECL-9684

ATOMIC ENERGY OF CANADA LIMITED

PROPOSAL FOR A NATIONAL FACILITY

MARS

A Multidetector Array for Reaction Studies

by

G.C. Ball, W.G. Davies, J.S. Forster, E. Hagberg,
D. Horn, M.A. Lone, and C. Pruneau
Atomic Energy of Canada Limited, Chalk River Nuclear Laboratories

L. Potvin, C. Rioux, R. Roy, and C. St-Pierre
Université Laval

T. Drake and A. Galindo-Uribarri
University of Toronto

Abstract

The proposal for MARS, a Multidetector Array for Reaction Studies is presented. MARS consists of a large, high-vacuum vessel enclosing an array of 128 scintillation detectors for use in studies of heavy-ion collisions at TASCC. The instrument will be funded and owned jointly by AECL and NSERC.

Nuclear Physics Branch
Chalk River Nuclear Laboratories
Chalk River, Ontario K0J 1J0
1988 February

AECL-9684

ACKNOWLEDGEMENTS

We are indebted to J. Barrette, now at McGill University, for stimulating discussions about the physics and the experimental aspects of this proposal. Many features and refinements of this proposal have evolved from points raised at the Toronto workshop on large arrays (March 1987) and from suggestions made by the TASCC Technical Review Committee.

The design, construction, and testing of prototype modules and electronics have required the skill and patience of R. Bertrand, R. Deal, M. Montaigne, G. Sims, H. Spenceley, and M.G. Steer. Mark McKendry contributed heavily to the design of the stabilization system. Engineering studies of the vacuum chamber were done by M. Ali, and the overall design considerations for the entire assembly were worked out by J. Morralee and his staff. We wish to express our sincere thanks to each one for his particular contribution towards the project.

Special thanks are due to H. Heubner for typing the proposal manuscript.

TABLE OF CONTENTS

PART ONE: EXECUTIVE SUMMARY

1. INTRODUCTION

The Multidetector Array for Reaction Studies (MARS) will be a device, with performance unmatched elsewhere in the world, for the study of heavy-ion reaction mechanisms. It will exploit beams from the new superconducting cyclotron at Chalk River Nuclear Laboratories in studies of heavy-ion reaction dynamics and the properties of excited nuclear matter. Existing collaborations between University and AECL physicists have led to the initiation of this proposal. The construction, commissioning and initial operation of the device will be by research groups from the Université Laval, the University of Toronto, and Chalk River. A McGill University group will participate in detector development and testing as well as in experiments. MARS will be a world-class facility in nuclear physics, and will be available for use by all qualified investigators.

The costs of the facility would be shared equally by the Natural Sciences and Engineering Research Council (NSERC) and AECL, in an arrangement which furthers the mandates of both organizations and strengthens the relationship between the Universities and the National Laboratory functions of the federal crown corporation.

Part I of this proposal gives brief summaries of the scientific justification and the technical specifications, which are discussed in detail in Parts II and III, respectively. Part I also treats various administrative, logistical, and financial matters.

2. HIGHLIGHTS OF THE SCIENTIFIC JUSTIFICATION

Most of the observed mass of our universe, from the very dense material of neutron stars to the dilute gases of space, is comprised of nuclear matter. Despite the wide range of temperature and densities in which it can exist, nuclear matter has traditionally been studied in its terrestrially most abundant form, the atomic nucleus. The nucleus is a specific and limited manifestation of nuclear matter: a cold, equilibrated system of a few hundred nucleons or less, approximately constant in density and proton-to-neutron ratio. Even when prepared by a heavy-ion collision from the previous generation of accelerators (beam energies typically less than 10 MeV per nucleon), a nuclear system generally has "normal" density and only a few MeV of excitation energy per nucleon (low temperature). Thermal equilibration of the system is fast compared with the collision time, and its behavior can be well characterized by a mean field. High energy collisions, on the other hand, are dominated by the nucleon-nucleon interaction: a projectile ion behaves like a collection of protons and neutrons, each interacting independently with the protons and neutrons of the target.

The range of energies available from TASCC (10-50 MeV/u) allows us to bridge the gap between mean field and nucleon-nucleon phenomena. Recent results from a number of new accelerators in the United States and France indicate that this transitional energy range does indeed contain fundamental thresholds in nuclear behavior. For example, the velocity of "sound" in nuclear matter corresponds to 15-20 MeV/u, and the Fermi energy of nucleons in a nucleus lies at

30-40 MeV. Exceeding the former value permits the creation of density and temperature variations; exceeding the latter triggers a substantial change in the number of available states, with profound implications for the subsequent opacity of the nucleus to incident nucleons.

Topics currently of interest world-wide include nuclear transparency, projectile fragmentation, onset of multifragmentation, localized high temperature sources, jets, limits to momentum transfer, limits to excitation energy, entropy production, explosive events, "subthreshold" pion production, and many other phenomena which the array proposed herein will allow us to address. In our discussion we concentrate on two general reaction categories: (i) peripheral processes, in which nuclei collide at large impact parameters, and (ii) central processes, in which the nuclei collide head-on.

Peripheral collisions are of particular interest when the projectile's speed is in the region of the nuclear sound velocity. The interaction time of the collision is then on the order of the time a disturbance takes to propagate across a nucleus. This limits thermal equilibration and the reactions evolve, with increasing beam energy, to fit the participant/spectator picture with three independent velocity components: one target-like, one projectile-like, and one corresponding to the interaction region. What are the stages of this evolution from equilibrated systems to separated sources, and by what influences is it driven? When a projectile-like component is clearly defined it often appears to

come from a simple or multiple breakup of the beam ion into fragments. Instances of excitation followed by equilibrium decay of the projectile remote from the target have been identified; are there also dynamical processes during the projectile-target interaction time that lead to a "prompt" fragmentation?

Central collisions deposit the largest amount of energy into the nuclear system and produce the highest temperatures in this energy range. They are therefore the most interesting for studying the properties of nuclear matter. There are many approaches to the question of how a system holds this excitation. They include searches for the onset of multifragmentation, exploration of the thermodynamic picture (gas/liquid phases, T_c), and tests of the limits to momentum transfer and excitation energy. The region of temperatures and pressures at which a piece of nuclear matter begins to disintegrate has not yet been mapped experimentally, and experiments to determine the cause of the breakup have so far been inconclusive. The reason for this situation to date has essentially been the lack of instrumentation to determine simultaneously the multiplicity, mass distributions, excitation energy and source velocities on an event-by-event basis. The instrument proposed here addresses such issues explicitly. It has been designed expressly to answer questions concerning transitional energy reaction dynamics and properties of excited nuclear matter, but it will also be valuable in a variety of other studies, from investigations of equilibrium phenomena to measurements of production mechanisms for high-energy quanta. At present, TASCC has no major facility to perform such experiments.

In broader terms, the physics probed by intermediate-energy heavy-ion collisions is fundamental to our understanding of the cosmos. It is well within the resources of Canadian science to play a leading role in this area of research. The largest step, construction of a suitable heavy-ion accelerator, has already been taken; all that remains is to assure its prompt and effective exploitation with the appropriate experimental facility.

3. PROPOSED FACILITY

Because most of the energy and most of the kinematic information concerning the reaction are carried by the charged reaction products, light and heavy ions, a system of charged particle detectors was designed. In order to identify the reaction products as well as measure their energy, these detectors are operated as ΔE-E telescopes. A heavy projectile brings a great deal of linear momentum into the collision, causing most reaction products to travel forward. Therefore, the detection system is located at forward angles, and is centered on the direction of the beam. Furthermore, in order to miss as few components as possible in any collision, the detectors are closely packed, with a minimum of inactive space between them. This, together with a desire for high counting rate capability, low cost, reliability, ease of operation, and a resistance to radiation damage, leads to the choice of scintillation counters as the main detector elements.

A few principles outlined above already determine the essential form of MARS. Refinement of the design in the face of additional requirements and considerations involved a complex set of tradeoffs

based on physics priorities; this is discussed in Part III of the proposal. Here we will simply list the properties of the array and its vacuum vessel.

The vacuum chamber is a horizontal-axis steel cylinder, 3 m in diameter by 3.7 m in length. It has a steel table inside, for mounting detectors and targets, which is supported independently of the chamber walls, since these suffer some deformation under vacuum. The operating pressure is 1×10^{-6} torr. The array consists of 128 plastic scintillator detectors, mounted in a "bull's eye" geometry of eight rings having 16 detectors each. The two innermost rings are simple transmission detectors, while the remaining 96 detectors are ΔE-E telescopes, each viewed from behind by a single photomultiplier tube in a phoswich arrangement. The array is positioned 2 m from the target and covers a cone of 38° half-angle, with a central 2° opening to accommodate the exiting beam. It can also be operated at smaller distances, e.g. 1 m from the target, for an increase in efficiency at a corresponding loss in granularity. An artist's view of MARS is shown in Figure 1.

A comparison with detector arrays addressing similar physics at other laboratories with access to "Fermi-energy" beams is in order. Of these, the Plastic Wall at GANIL is the oldest. It has 96 plastic scintillators of the ΔE type, which means that element identification must be done by ΔE-time-of-flight techniques. That facility has recently been retrofitted with the "Barrel" (plastic scintillator strips for light ion detection) and "DELF" (gas-filled detectors for heavier ions) which cover much of the remaining sphere. AMPHORA, at the accelerator SARA, is a more integrated array. It covers 84% of 4π steradians with 140 plastic/CsI phoswich detectors. Finally, the

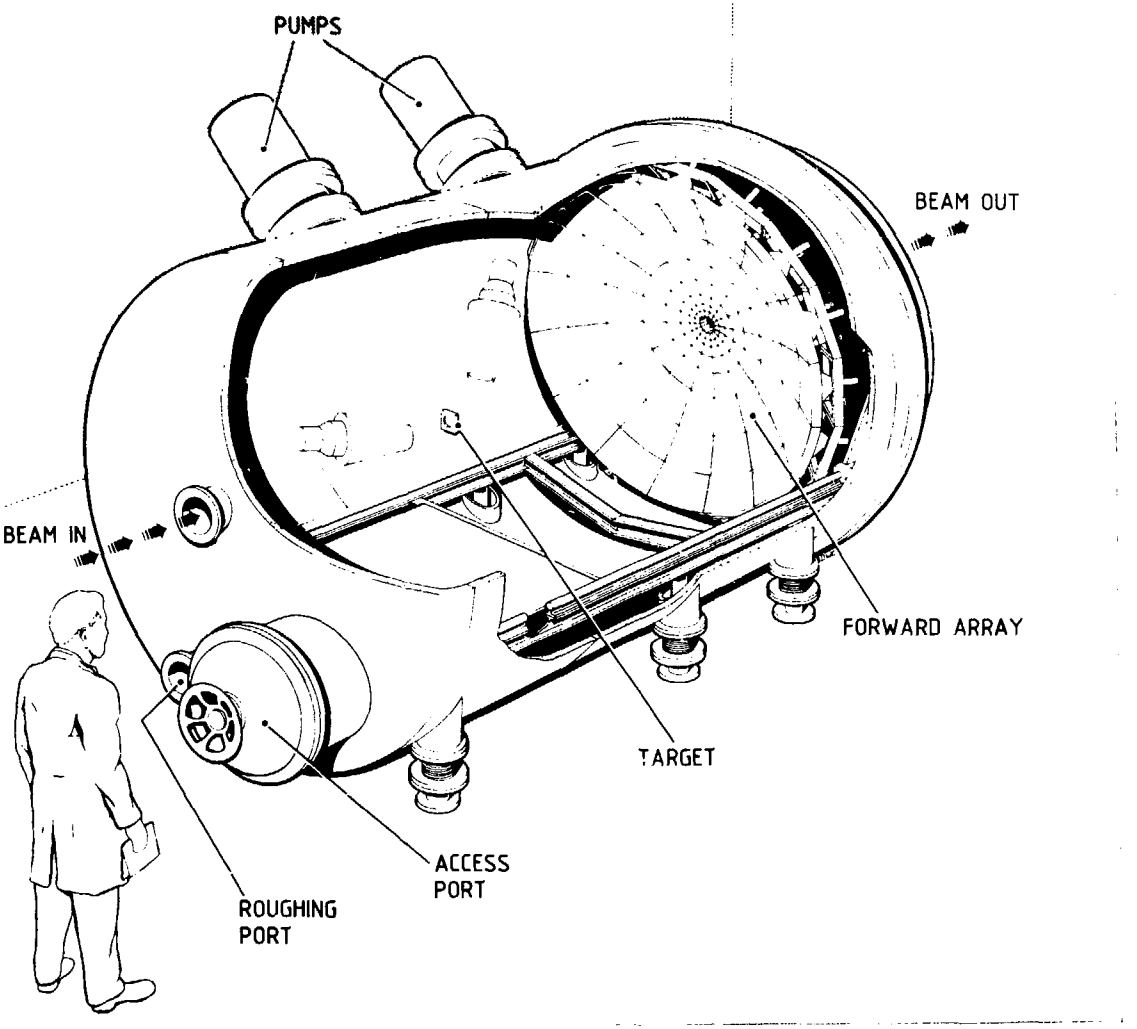

Figure 1. Artist's conception of the Multidetector Array for Reaction Studies (MARS), showing a cutaway of the vacuum chamber to expose the detector array and support hardware. Two auxiliary detectors are shown, though they do not form part of this proposal; neither their supports nor those for the target ladder are shown in this illustration.

Michigan State 4π Array covers a similar fraction of a sphere with 30 gas-filled detectors backed by 170 plastic phoswich telescopes, but has no forward wall. The MSU and SARA arrays are both in the commissioning stages.

None of these arrays is better suited to projectile fragmentation work than that proposed here. The GANIL array has similar granularity, but inferior identification; AMPHORA has good identification, but only 48 detectors in the forward wall; and MSU has no forward array. For central collisions, MARS offers about 75% efficiency for light ions when positioned at 1 m target distance, which is somewhat lower than the French and American facilities. However, our design provides isotope resolution for light ions, unlike the Barrel/Wall; it provides room in the area around the target for installation of auxiliary counters such as gas-filled detectors for heavy fragments, unlike the very compact geometry of AMPHORA, and it provides an efficient anticoincidence filter for projectile-like fragments, unlike the MSU array. Thus, the proposed array would be unmatched for studies of peripheral collisions and a major contender in the field of central collision physics.

The proponents of MARS view a large vacuum vessel with a forward array as a minimum basis for successful entry into this field at the international level. Therefore, the design provides both the space and the mechanical foundation to enhance the capability should future developments demand. One possible development could be in the direction of full 4π coverage for a broad dynamic range of charged particles. Other options include large-area avalanche counters or deep ion chambers. In any event, the immediate aim is to exploit fully the extremely competitive device described in these pages.

4. PROPOSED RESEARCH ACTIVITIES

The research programs planned by the users of MARS have largely determined the following array characteristics, listed as design goals in section 3.1:

- High efficiency for detecting products from both peripheral and central collisions.
- High granularity to avoid double hits in high-multiplicity events and to maximize event rate by reducing pileup.
- Good detector response (low thresholds, high element and energy resolution, identification of neutrons).
- Long (2 m) flight path for time-of-flight resolution.
- Fast decision capability to permit use of the array as an event tag.
- Compatibility with auxiliary detector systems.

A number of research activities are listed below in outline form. These represent the interests to date of the presently identified major users. They are, of course, subject to change as new developments arise or new collaborators appear. Items 1 and 2 are expected to form the scientific core of the collaboration's work over the next few years. These require the full capability of the array. Items 3-5 require MARS as an event selector and a coincidence detector in order to define the reaction channel and improve on earlier, inclusive measurements.

1. Activity: Study dynamics of projectile fragmentation

   [the impact of the array on this field is given in Section 3 of Part II].

Measurements: Fragment masses, energies, multiplicities, angular correlations, crystal blocking patterns.

Objectives: Source properties (sizes, velocities, excitation, decay modes, lifetimes).

Competition between nucleon-nucleon and mean field effects.

Reaction trajectories (dependence on beam energy and mass asymmetry).

2. Activity: Study fragments from central collisions

[the impact of the array on this field is given in Section 4 of Part II].

Measurements: Fragment masses, energies, multiplicities, and correlations in mass and energy; neutron yields and spectra.

Objectives: Source properties (velocities, excitation, decay modes).

Response of nuclear matter to high excitation, thermodynamic properties.

Limits to excitation before multifragmentation.

3. Activity: Use "nuclear interferometry" techniques.

[the impact of the array on this field is given in Section 4 of Part II].

Measurements: Small-angle, light-ion correlations in auxiliary detector lattice.

Event tag by multiplicity, ion types, hit pattern in large array.

Objectives: Size, temperature, lifetime of emitting region. Evolution of localization phenomena, duration.

4. Activity: Detect subthreshold pions in coincidence with remainder of nuclear system

[the impact of the array on this field is given in Section 5.1 of Part II].

Measurements: Detect pion production cross sections and energy spectra in specialized counter, detect coincident particles in array (energies, masses, angles).

Objectives: Identify mechanism for coherent pion production.

5. Activity: Study total cross sections and reaction cross sections for heavy-ion collisions

[the impact of the array on this field is given in Section 5.2 of Part II].

Measurements: Elastic and inelastic scattering angular distributions, beam attenuation measurements (long flight path in chamber for TOF discrimination and more complete anticoincidence in array).

Objectives: Reaction cross sections, transparency. Competition of quasifree scattering with mean field effects.

Clearly, the five research programs listed here represent only a fraction of the potential scientific impact of this device. A more detailed exposition of the array's potential for new and exciting research may be found in Part II of this proposal.

5. LOCATION

The detector array will be installed at TASCC, the Tandem Accelerator and Superconducting Cyclotron complex recently built at Chalk River. The designers of the beam transport and experimental areas have reserved a target room for a reaction facility, as indicated by the location of the large scattering chamber in Figure 2. This particular location was chosen because it has the best spatial and temporal beam qualities.

Many University groups, both Canadian and foreign, have had research programs at Chalk River. A very recent and very successful example is the 8π Spectrometer collaboration, which has demonstrated the accessiblity of AECL facilities to outside users. As a national facility, the array will be open to all qualified investigators.

6. USERS

An assocation of TASCC users, currently chaired by J.C. Waddington, has been instrumental in keeping the Canadian physics community informed of general progress at TASCC. It has also funded a workshop on reaction studies with large arrays at the University of Toronto (1987 March 26-27), attended by 32 physicists from 8 Canadian institutions, in addition to the invited speakers; proceedings of that workshop are attached to this proposal. Prospective users of the facility have also been informed by newsletters, seminars and talks at CAP conferences.

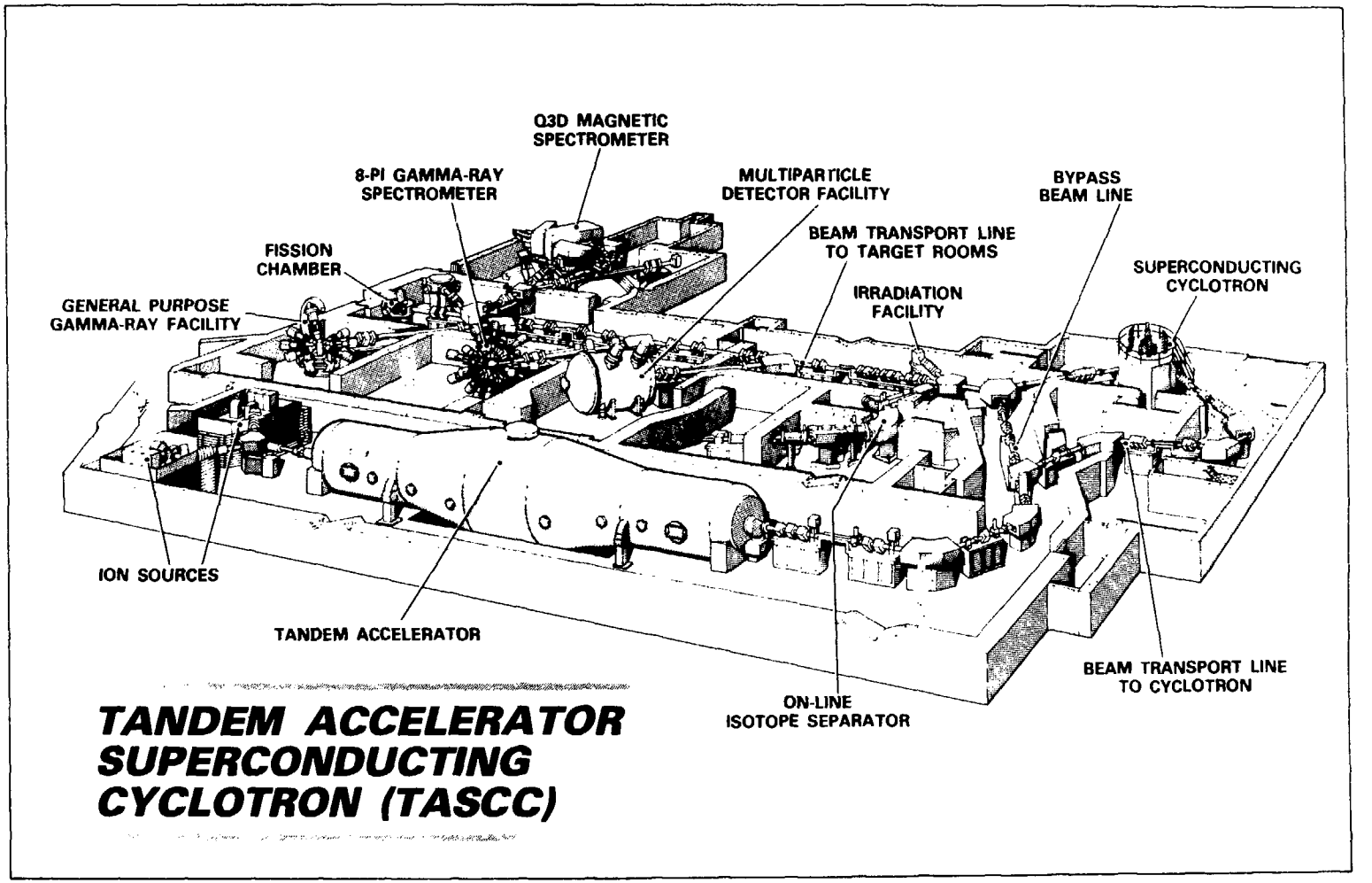

Figure 2. Location of the Multidetector Array for Reaction Studies indicated on this overview of the TASCC facility by the large vacuum chamber in the center of the illustration.

The physics program at MARS will be the major research effort of two University groups (Rioux et al. at Laval and Drake et al. at Toronto) and of a core of 3-4 physicists at CRNL (Horn et al.). J. Barrette et al. of McGill University have also expressed an intention to use the facility and have offered to help with detector development and testing. Within the MARS collaboration, a broad base of research accomplishments in heavy ion reaction studies can be found in areas such as scattering, projectile fragmentation, total reaction cross sections, compound nuclear lifetime measurements, heavy ion stopping powers, mass measurements, and intermediate mass fragment production. A list of users, defined as those spending more than 10% of their research effort on this device, is shown in Table 1. While AECL does not have the student resources that the Universities do, it does usually have a postdoctoral fellow (currently C. Pruneau) associated with the group.

7. BUDGET, CASH FLOW, AND SCHEDULE

The primary considerations in the design have been related to the array's performance in physics experiments. However, thought has also been given to practical matters such as reliability, ease of construction, and cost effectiveness.

Table 2 gives the cost estimates for construction. A more detailed discussion of the figures, including a breakdown of the contingency assignments, may be found in Part III, Section 8. Some approximate costs have been marked by asterisks. These represent infrastructure funding provided directly by the Universities, by NSERC through an infrastructure grant (see accompanying request) or

TABLE 1: LIST OF USERS

UNIVERSITE LAVAL

C. Rioux

R. Roy

C. St-Pierre

UNIVERSITY OF TORONTO

T. Drake

AECL

G.C. Ball

W.G. Davies

J.S. Forster

E. Hagberg

D. Horn

M.A. Lone

McGILL UNIVERSITY

J. Barrette

TABLE 2: COST ESTIMATES FOR THE FACILITY IN K$ (CDN) 1987

Items marked with an asterisk constitute infrastructure funding and are not included in the total for this request.

	NSERC	AECL
CHAMBER AND SUPPORTS		
Design Work, Engineering, Drafting		57.8
Chamber		233.3
Mech. Supports		64.0
Mounting & Alignment Structure		116.0
Site Preparation and Installation		37.0
High-Vacuum Pumps		166.5
Roughing System		37.0
Plumbing, Feedthrus Misc.		40.0
Commissioning		40.0*
DETECTORS		
Scintillator	106.4	
Photomultipliers	120.3	
Other Detector Components	16.4	
Machining of Scintillator	52.0*	
Assembly of Detector Modules	48.3*	
ELECTRONICS		
CAMAC	201.7	40.0*
NIM	167.2	
Custom Built Components	83.7	67.9
	48.3*	80.0*
HV	53.0	
Monitoring, Control	21.5	
Cabling & Racks	53.7	
Subtotals	824.0	819.5
Contingencies	122.5	130.7
Totals	946.5 +	950.2 = 1896.7

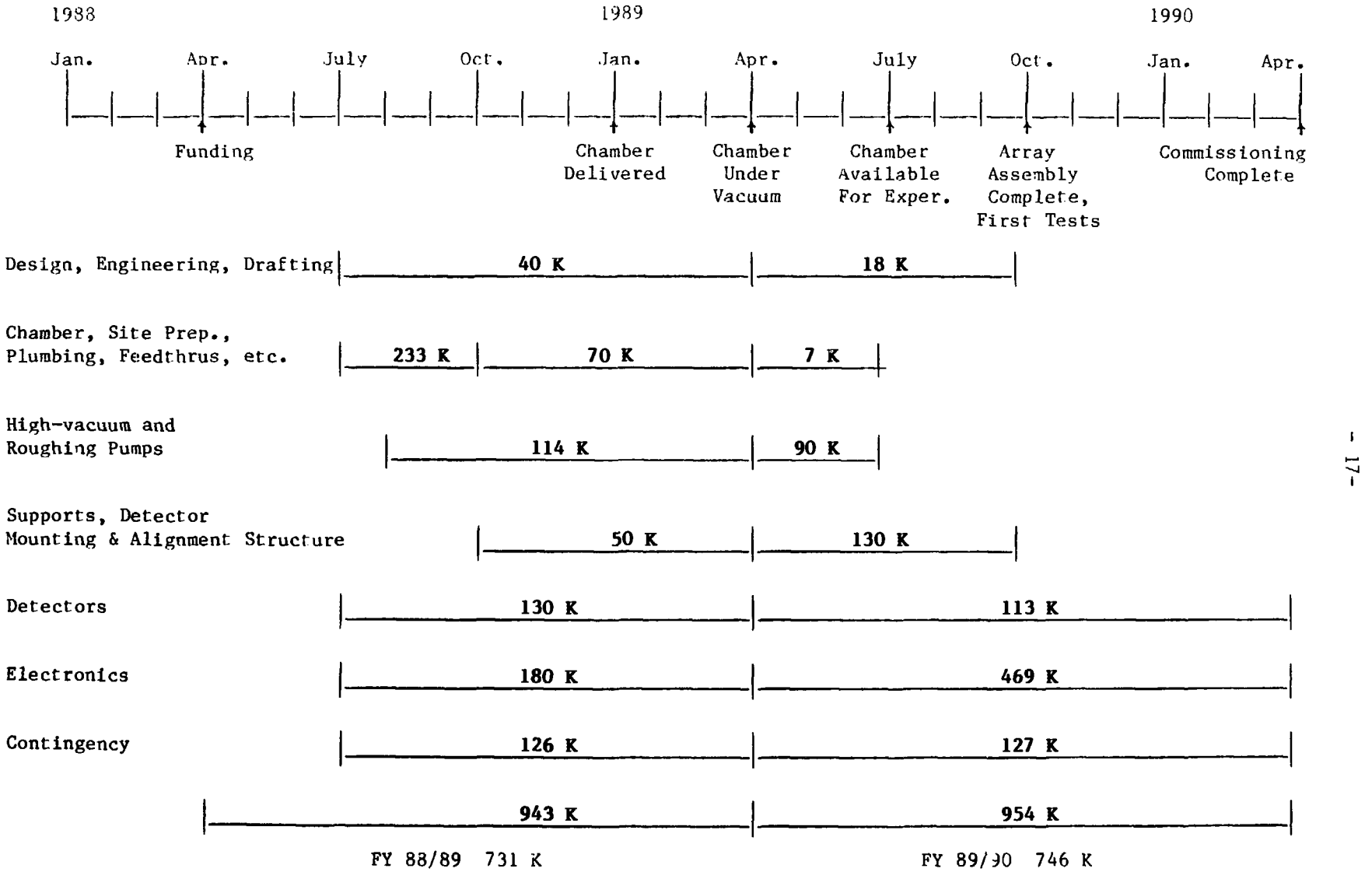

Figure 3. Schedule and Cash Flow

by AECL. They are not a part of this request and have not been added into the total. In general, detectors and electronics will be bought with NSERC funds and the chamber and support structures will be bought by AECL. This particular division is logical for several reasons. Since the facility is located at Chalk River, it makes sense for the non-portable items to be owned by AECL. Also detector materials and electronics are purchased items, some from abroad. It is therefore more economical for the Universities, which pay no import duty or federal tax, to buy those items while AECL, which must pay all duties and taxes, covers construction costs and the largely domestic content of the chamber and mechanical supports.

Two years will be required between the date of funding and the final commissioning. A major factor in the timing is that site preparation and installation of the scattering chamber take place during 1988 so that no temporary relocation of the existing small vacuum vessel would be necessary. This would insure the least disruption and the earliest possible availability of the large vacuum vessel for interim experiments. Such experiments are important in maintaining and developing the research interests of the contributing research groups. Construction of the support structure machining of the detectors and development of the electronics hardware/software are fairly time-consuming and could take over a year. It is therefore possible to spread the cash flow over two years, FY 88/89 and FY 89/90 as shown in Figure 3.

8. CANADIAN CONTENT

The benefits to Canadian business and industry from implementation of the MARS proposal are considerable. The chamber

would be bought from one of three Canadian manufacturers; the mechanical supports, roughing system with plumbing, and a substantial amount of electronics would be built locally, at the Universities and at CRNL. The cost of Canadian-built components is thus 884 K$ including the appropriate contingencies. A number of components, such as specialized electronic modules, are not made in Canada. For these unavoidable foreign purchases, the only direct Canadian component is in the duties and taxes (120 K$), applicable to the various transactions. The total direct Canadian content is then 1004 K$, or greater than one-half the total amount. Additional, indirect benefits come from purchases through existing Canadian representatives. Furthermore, the developmental nature of much of the work to be done in this country will enhance Canadian capability in these areas.

9. MANPOWER

An estimate of the manpower required to complete the design and to construct and commission MARS is given in Table 3. It should be noted that a substantial part of the engineering, design work, and prototyping, have already been done and that still more will be done by the funding date. The heading of professionals in the table includes the cosigners of this request. Of the 6.5 technical man years listed, one man year for machining the scintillator will be provided by Université Laval, two man years will be funded by a separate NSERC infrastructure grant to support the facility, and 3.5 man years will be provided by AECL.

TABLE 3: MANPOWER REQUIRED FOR CONSTRUCTION AND COMMISSIONING OF THE ARRAY FROM DATE OF FUNDING (man years)

	Professional	Technical	Research Associate/ Student
Chamber and Supports	0.5	1.0	--
Detectors	1.0	2.0	1.0
Electronics and Data Acquisition	1.5	2.5	1.0
Electronics Devel.	1.0	1.0	--
Project Management	0.5	--	--
Total	4.5	6.5	2.0

After the facility is commissioned, the technical effort required to maintain and operate and develop MARS is one full-time mechanical technician and one full-time electronics/firmware technician (see the following section). A large number of physicists, at senior, postdoctoral, and student levels, could productively exploit the chamber and array.

10. OPERATION AND MAINTENANCE FUNDING

As has been discussed, the full operation of the facility will start at the beginning of the third year after funding. The previous two-year period will have allowed the installation of the chamber, construction and testing of the detectors, their mounting in the array, and the process of setting up the electronics. From the third year and on, the two technical man years required per annum (see previous section) and the repair and maintenance expenses will be provided equally by the Universities (NSERC) and AECL. Starting during the construction period, a competent person will be hired and entrusted the task of developing the modus operandi of the coupled detection-acquisition systems by connecting and programming the devices. His salary should be covered by the NSERC infrastructure grant. The mechanical technician required to maintain and upgrade the vacuum chamber and support structures will be provided by AECL. It is also the intention of the University groups to support from their individual operating grants one postdoctoral fellow who would in part assist in development and operation of the facility. Equivalent professional help will be provided by AECL.

The maintenance of the detection system (scintillation material and photomultipliers for replacement and spare parts) and of the

electronics setup (replacement or repair of defective parts, such as cables, connectors or the modules themselves) will also be provided for by the NSERC infrastructure budget. These expenses are estimated as a small fraction of the initial capital costs. However, all complementary detection devices and the supplementary electronics eventually required are not maintenance costs and will be bought at the expense of the users needing the added detectors or ancillary apparatus.

11. OWNERSHIP AND FACILITY MANAGEMENT

Since each of AECL and NSERC would provide half the funding for the facility, ownership would also be shared equally. A fair and sensible way to divide the ownership would be for the Universities to own the detectors and the associated electronics and for AECL to own the permanently installed large scattering chamber with its pumps and mechanical supports. The chamber, once installed, would be difficult to remove without cutting it up or demolishing parts of the building; furthermore, it would by itself form a useful component of the overall TASCC facility. The detectors and electronics are far more portable and could, if needed, be used in other applications or at other laboratories. As discussed in the budget section, the proposed division (NSERC 824.0 K$ + 122.5 K$ contingency, AECL 819.5 K$ + 130.7 K$ contingency) would also be optimum in terms of the economics of purchasing and the skills required for construction.

It is proposed that the facility be managed by a committee of two University and two AECL representatives, with a rotating chairmanship. Initial membership of the committee will be selected

from among the authors of this proposal. While no conflicts are anticipated, such a management structure would provide a mechanism to defuse potential controversies.

As a national facility, the array may attract users not associated with the group initiating this proposal; these users would be completely unfamiliar with the rather complex instrument. In such cases, at least during the initial period of operation, it is suggested that one or more members of the present collaboration participate in the experiment, either in a "support" or a collaborative role.

12. TIMELINESS

Recent accelerator developments have led to the opening of the transitional energy range, and in the past few years a number of first-generation detector systems have been used to produce a tantalizing, but incomplete, picture of the region. A Canadian heavy-ion accelerator, TASCC at Chalk River, is now entering the field. MARS, a second-generation detector array, operational within two years, would ensure that Canada reaps the full scientific benefits of its tremendous accelerator effort. The development of competing arrays elsewhere imparts urgency to the request. Furthermore, there may be an opportunity to begin installation of the bulky chamber during the 1988 accelerator shutdown, which could save some unnecessary duplication of effort and loss of potential experimental time.

PART TWO: SCIENTIFIC JUSTIFICATION

1. INTRODUCTION

For several decades, nuclear physics studies with heavy ions have been performed with an ever-increasing variety of beams, both at a few MeV per nucleon and at relativistic energies. The intermediate energy region, however, between 20 and 200 MeV per nucleon has remained largely unexplored until recently. Only in the last five years have significant amounts of information been obtained with new and upgraded accelerators. Our understanding of this region has therefore evolved through extension of models and theories from the low- and high-energy extremes, namely that dominated by the mean nuclear field and that characterized by the nucleon-nucleon (NN) interaction. Consequently, this is a region of contrasting assumptions. For instance, the mean free path is assumed larger than the nuclear radius for the direct interaction hypothesis within the framework of the mean field, while the hydrodynamics models are based on a mean free path much smaller than the nucleus itself. As recent results are showing, these contrasts can be understood with the realization that the intermediate energy range contains a number of significant changes in nuclear behavior.

A current topic of interest which addresses the "transitional" aspects of this energy range is the equation of state (EOS) describing a large ensemble of nucleons. The thermodynamical properties of nuclear matter such as temperature and entropy can be used as reference variables to study very fundamental issues. Not

only are they useful in the comparison of different theoretical approaches, but they also serve to guide the experimental investigation of the various states of the nuclear matter produced in the laboratory. In terms of these variables, the time evolution of a central collision between two nuclei can be described by an EOS representing the interacting nucleons which are considered to behave as a gas. A calculated equation of state for such a collision is shown in Figure 1 in terms of pressure, P, as a function of density, ρ/ρ_o, and temperature, T[1]. The corresponding phase diagram can be deduced from it, and the possible instability regions and different phase limits identified. Crucial questions concerning the establishment of a correct EOS for nuclear matter remain and constitute a major class of problems to be addressed in studies of central collision phenomena with the instrument proposed here; a more detailed discussion can be found in Section 4.

Peripheral processes, dominated by the quasi-elastic interaction, constitute another class of experiments planned with the facility. Here projectile-like fragments are produced with relatively small amounts of mass and energy transferred between the two colliding nuclei (which consequently preserve their respective identities far better than in a more central collision). This situation contrasts strongly with the formation of a composite system in a central collision, where the target and the projectile can participate equally in the formation of a new final state. In peripheral processes, many mechanisms can contribute, as illustrated in Figure 2. Though several of these mechanisms are already well

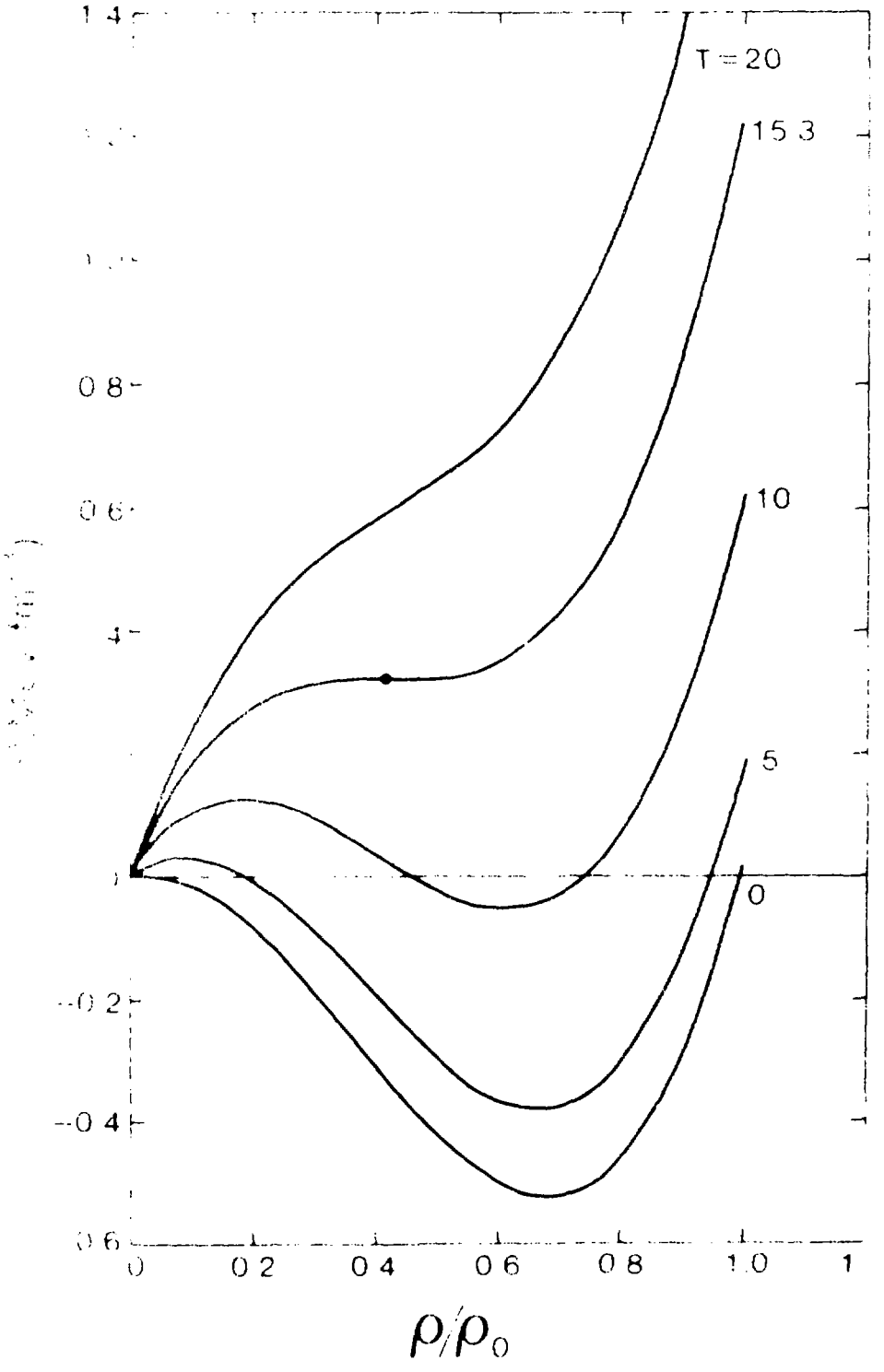

Figure 1. Equation of state predicted for neutral nuclear matter. The temperatures of each isotherm are given in MeV; the critical point is represented by a solid dot. (From ref. 1).

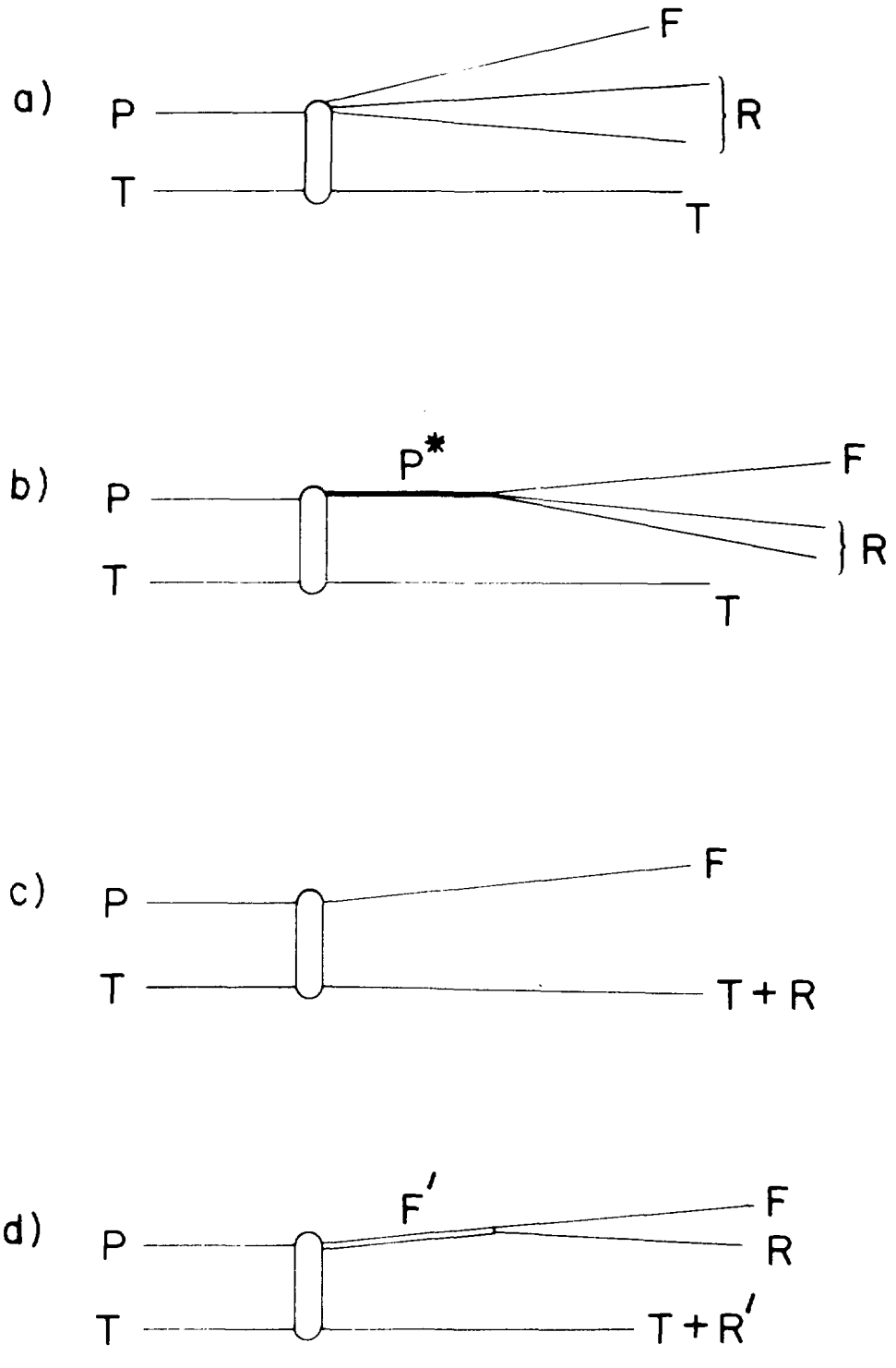

Figure 2. Schematic representation of several mechanisms contributing to the production of observed projectile-like fragments, F, and other unobserved fragments, R. P is the projectile, and T the target. Fig. 2 confuses mechanisms with limitations in the detection system. (From ref. 2).

established, their relative probability and their respective behavior as a function of energy and mass asymmetry are open questions. Moreover, fast fragments with masses far from the projectile mass are also produced. How do these intermediate-mass fragments, originating from a very localized hot source produced by NN collisions, compete with processes based on the mean field? On the other hand, is projectile multifragmentation in the field of the target nucleus an important mechanism in the production of more than one intermediate-mass fragment? A more complete experimental investigation will resolve these problems.

These two general classes of reactions will be reviewed in subsequent sections, with relevant aspects addressed as future experiments for MARS. Topics not well characterized by the limits of small and large impact parameters will be discussed separately.

2. IMPLICATIONS FOR EXPERIMENTS

Two thresholds at about 15-20 and 30-40 MeV per nucleon, corresponding respectively to the sound velocity in the nucleus and the nucleon Fermi kinetic energy, are known to occur in the transitional energy region. Besides reaction channels resulting directly from these thresholds, a number of specific phenomena belong to the region, as is illustrated in Figure 3. In fact, theoretical calculations and model analyses of experimental data have shown that a proper description of the phenomena must often include explicitly the NN collisions, as well as the blocking effect from the Pauli principle and the mean nuclear field[4,5]. Such disparate

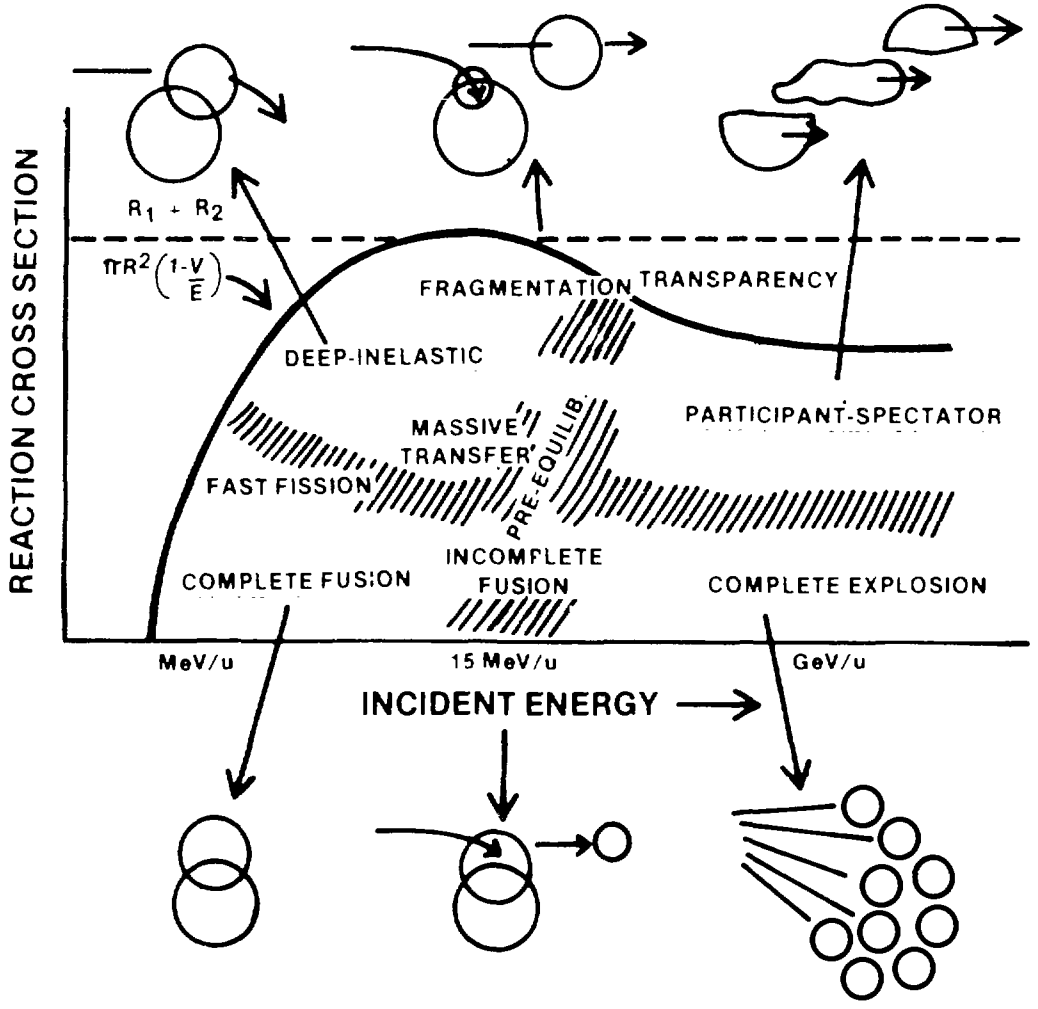

Figure 3. Illustration of different reaction processes that have been observed as a function of bombarding energy and impact parameter. (From ref. 3).

underlying physics concepts lead to an extreme variety of final state observables. It is therefore evident that more sophisticated instrumentation is needed at intermediate energies than at low energy where two-body or quasi-two-body processes dominate. In this energy range, elastic, quasi-elastic, fusion-fission, and other reactions, generally studied at lower energies with a limited number of small detectors[6,7], evolve gradually, with increasing energy, to multibody processes best detected with a high level of coincidence efficiency. Between the simplest inclusive setups and the ideal 4π detector system lie many possible detection configurations that are adequate for specific experiments. For example, a large array of detectors such as MARS may be designed to study certain detailed or global phenomena, either standing alone or in conjunction with complementary detectors. It is indeed imperative that such a system excel at the primary task for which it was designed. However, since there can be but a few such facilities, it should be versatile enough to accommodate other interests and research programs. If it is to have value after current problems are addressed, it must also have the flexibility to accept potential modifications, should future developments require that. In any event, it is clear from what is already known of heavy ion reaction mechanisms at more than 10 MeV per nucleon, that the ability to detect ternary and higher multiplicity events with large dynamic range capability in both mass and energy will remain a common requirement.

3. PERIPHERAL PROCESSES

Peripheral processes are those in which two nuclei collide at large impact parameters. The amount of overlap between the two nuclear volumes is minimal and the collision is a glancing one, with the result that the identities and trajectories of the projectile and target are reasonably well preserved. At low energies these quasielastic collisions are dominated by inelastic scattering and few-nucleon transfer reactions. In the transitional energy range, both of those mechanisms persist, but a number of new processes arise which can lead to the breakup of one or both of the reaction partners. Since the most kinematically focussed and easily observable reaction products are those originating from the beam, the process is, somewhat misleadingly, known as projectile fragmentation. In a very simple picture one might expect that the fragments closest to the original projectile in mass and velocity, known as projectile-like fragments (PLFs), originated from the most peripheral of the collisions, while those far from the projectile's mass and velocity originated from somewhat smaller impact parameters. The latter type, including multifragmentation events, may have their origin in the increasing importance at higher energy of nucleon-nucleon collisions, which permits a much greater energy to be deposited in grazing collisions than does the mean-field interaction.

3.1 Projectile-like Fragments

The earliest observation of projectile fragmentation was with the simplest possible composite projectile, the deuteron. At 95 MeV per nucleon, its breakup was very well described in terms of a

geometrical model.[8] More recently, the approach formulated by Goldhaber[9] for complex projectiles at higher energy has also been quite successful in explaining the observed phenomena. However, the extension of the same description to data at lower bombarding energies, in the intermediate range of 10 to 100 MeV per nucleon, met with limited success. Specifically, the experimental widths of the momentum distributions of the PLFs narrow more rapidly with decreasing beam energy than calculations would predict. This effect is displayed in Figure 4, which plots a comparison of calculated and experimental momentum widths (σ_0) as a function of beam energy.

Several explanations have been proposed (see, for example, ref. 2 and recent reviews given in refs. 10 and 11). In particular, direct nucleon transfer, a dominant process at low energy, continues to compete strongly with other processes at higher energy. [12-14] However, interactions at large or grazing impact parameters are quite complex. Although the reactions are fast and the projectile spends only a short time in the vicinity of the target nucleus, many mechanisms contribute to the PLF yields. Collisions at 20 MeV per nucleon[15] still have many characteristics of deep-inelastic phenomena; an excited PLF can disintegrate by sequential decay in the exit channel[11, 16-18] or in the entrance channel[18], as illustrated by recent work of our group (see Figure 5). Prompt breakup evidently also contributes to the PLF spectra.[20] The recent analysis by Rami et al.[14] in terms of nucleon transfer and projectile fragmentation mechanisms sums these two components in the energy spectrum and yields the reduced widths shown in Figure 6. In fact, even the PLFs with masses very close to the projectile mass are

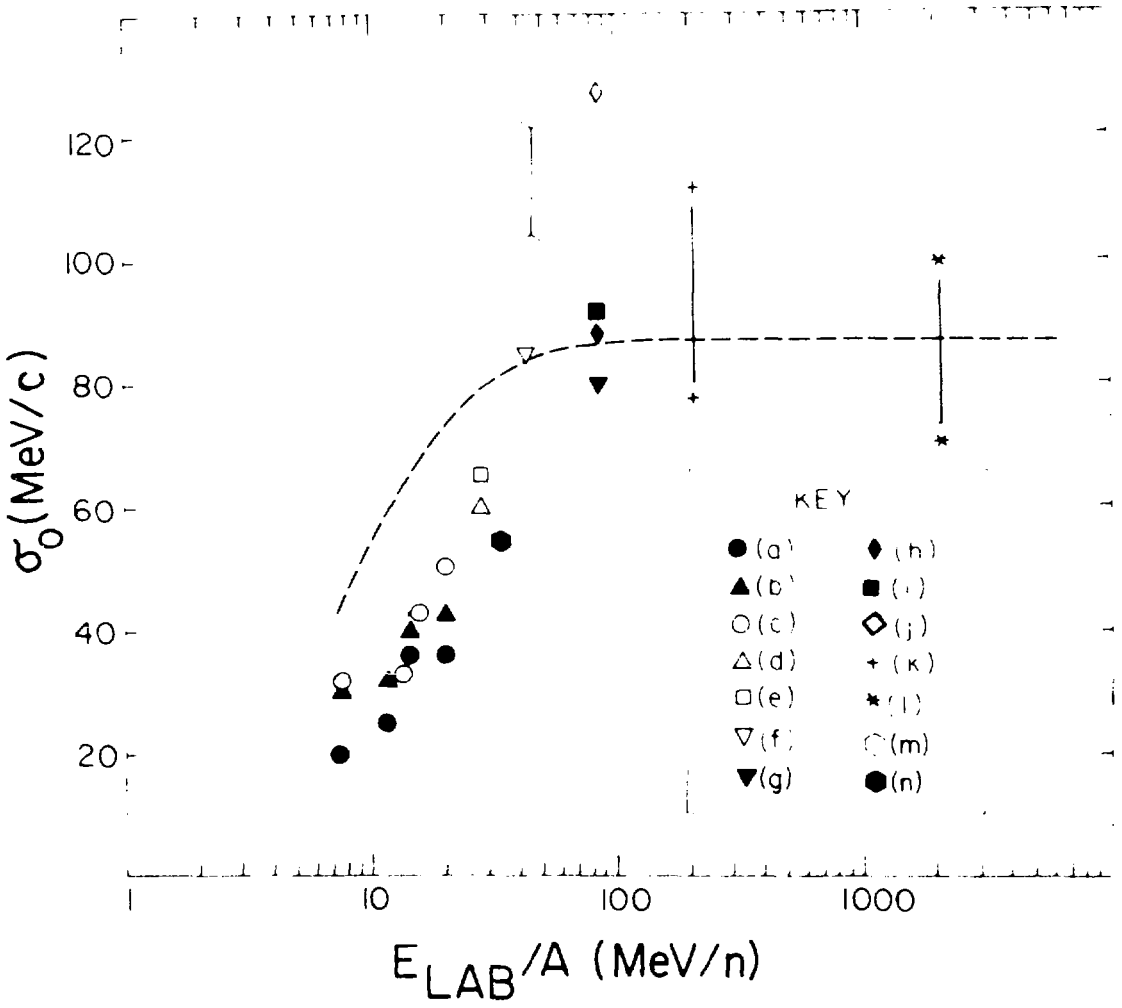

Figure 4. Reduced widths, σ_0, of the PLF linear momentum distributions as a function of projectile energy. The dashed line is a calculation in the peripheral model[24]. Figure from ref.2.

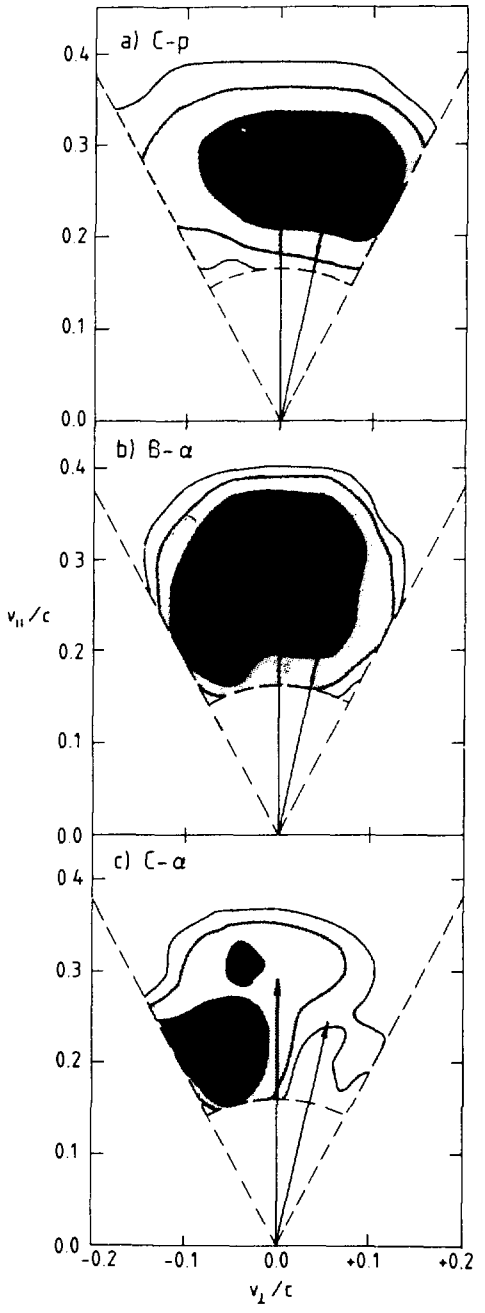

Figure 5. Galilean invariant yields plotted in velocity space for in-plane coincidences between light ions ($-30° < \theta < 30°$) and heavy fragments at $\theta = 12.5°$, in the ^{14}N on gold reaction at 40 MeV per nucleon (refs. 18 and 19). The vertical vector in each panel represents the beam velocity and the vector at $\theta = 12.5°$ is the average heavy-fragment velocity for that channel and angle. Yields for three final states are shown in panels a, b, and c. The beam-like velocity vector for the α particles in the B-α channel suggests an entrance-channel breakup of the ^{14}N projectile, and the fragment-like vector for the protons suggests a sequential decay of the projectile in the exit channel.

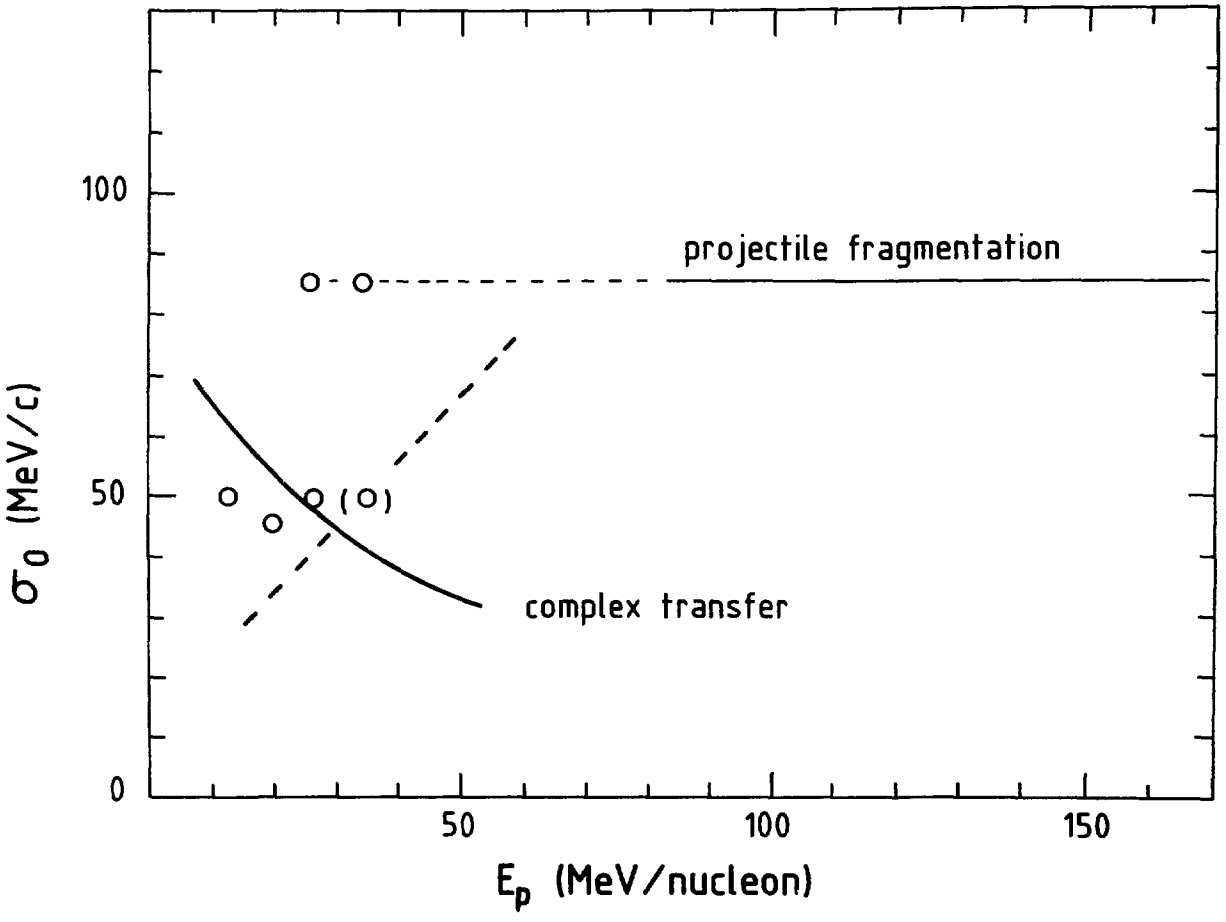

Figure 6. Reduced widths, σ_0, of the PLF momentum distributions as a function of bombarding energy. The solid dots and open circles represent the projectile fragmentation and nucleon transfer reactions, respectively, in the ^{40}Ar + ^{68}Zn reaction by, Rami et al.[21]. The solid curve is a complex transfer calculation, the straight (solid and dotted) horizontal line shows the trend of the experimental data and the dashed line displays the σ_0 tendency from the experimental data found in the literature in the 10 to 50 MeV/nucleon range. The figure illustrates the superposition of several reaction mechanisms to give the σ_0 observed in inclusive measurements.

part of a very complex picture.[10,21] A common remark from recent papers is that several aspects show a strong resemblance to low energy processes, while others are reminiscent of the projectile fragmentation at relativistic energy. The Coulomb final state interaction has an important effect at intermediate energies[21], but its inclusion does not provide the successful explanation that Coulomb corrections achieved between 100 and 200 MeV per nucleon. Some anomalies (see ref. 11 for a review and a discussion) can be explained by the inclusion in the analysis of more constraints, such as the Pauli blocking effect[22], the Fermi gas nature of the nucleus,[23] or Coulomb effects.[24]

Nevertheless, rather basic questions remain unanswered. Some, such as the dependence of the reaction dynamics upon beam energy and projectile-target mass asymmetry, can be explored by the systematic study of a large number of reactions. In this class lies the evolution from the phenomena of the transitional energy range to the participant-spectator model, which is so successful at high energy.[25,26] Others, questions like the validity of new models joining the nucleon-nucleon and mean field effects (see refs. 27 and 28 , for example), require "new experiments as exclusive as possible".[11] Specifically, this issue is best addressed through the reaction trajectory, as determined from source velocities, geometric and shadowing effects, and correlated fragment emission.

A new generation of multicoincidence detection systems has been developed with such experiments in mind.[29] MARS is particularly well suited to the task. Its angular range when positioned 2 m from

the target covers most of the phase space of the PLF; at half that distance, it permits one to follow the trends of processes that extend still further in angle or that start to take place when the forward peaked mechanisms vanish. Furthermore, the challenging study of decay properties of highly excited fragments produced at the lower end[15] of the transitional energy region can also be accommodated with a setup composed of gas detectors at large angle in coincidence with the multidetector array. Consequently, the array will allow investigation of several competing processes for projectile fragmentation, each in its respective dynamical range.

3.2 Fragments With Masses Far From The Projectile Mass

Fragments with masses very different from that of the projectile or target have sometimes been called intermediate-mass fragments. Clearly, at least one of the reaction partners must have broken up to produce such a fragment. Beyond that simple criterion, however, the name becomes ambiguous. Some can originate largely from a heavy projectile[30] while others may be produced in reactions with lighter projectiles.[31,32] The latter type appear to emanate from sources with velocities much less than that of the beam: they have been the basis for a variety of experiments, e.g. as triggers for extensive light-particle studies[33] and linear momentum transfer measurements[31] and in a study of the coexistence of equilibrated and unequilibrated sources.[32] Central collisions also appear to emit "intermediate-mass" fragments.

In this section, however, we are more concerned with the type originating from the projectile[30] containing a fast component.

This can be seen from Figure 7 as a function of the beam velocity, or from Figure 8, as a separate component of the different velocity-Z distributions. The two figures come from a study[30] of the reaction Kr on Au at 35 and 44 MeV per nucleon. In this recent experiment, correlated fragments with Z=8 to 36 were detected in the angular range 3°-30°. The study concluded that the coexistence of two different mechanisms was needed to explain the two types of correlated fragments. In one mechanism, both fragments came from a very slow, excited projectile produced in a pick-up reaction. The other shows a near-beam velocity fragment in coincidence with a slower fragment emitted either by the target after a stripping reaction or by a hot zone common to the projectile and the target. The latter hypothesis supports a potential explanation already discussed[21] which could be tested by experiment.

Such experimental tests can be achieved with the proposed multidetector array which has a rather complete coverage of forward solid angle. For a wider dynamic range in mass, gas detectors added at about 90° to the beam region would allow the simultaneous study of light-particles and intermediate-mass-fragment correlations. This would provide a much higher level of exclusivity for the type of multiple-source analysis performed in the past.[33,34] Such an analysis is complementary to alternative approaches probing the early stage of the collision. The early stages and the subsequent evolution towards equilibrium are usually considered either in terms of exciton, Fermi-jet or hot-spot models.[35]

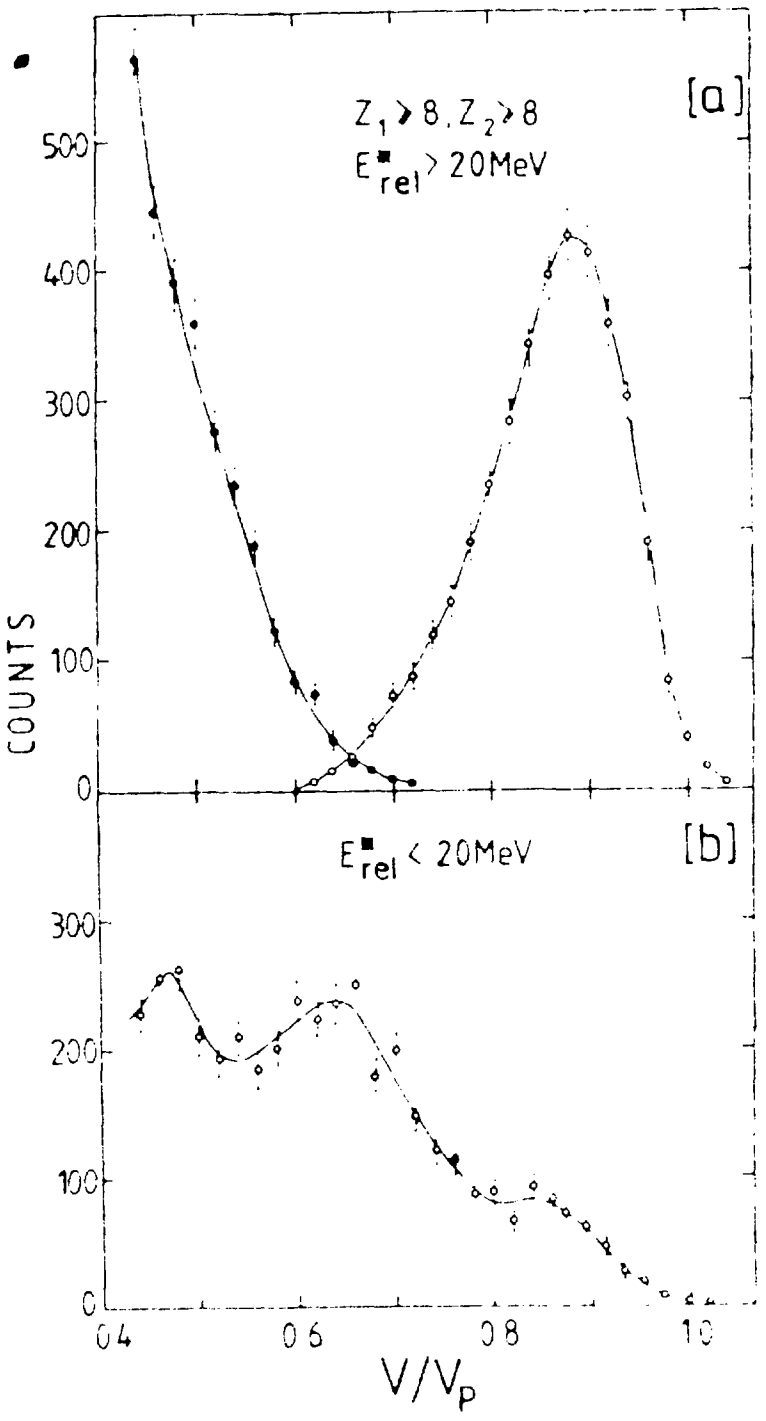

Figure 7. Coincident fragment yield for two different ranges of E^*_{rel} as a function of the ratio between the fragment velocity and the projectile velocity. The reaction is $^{84}Kr + ^{197}Au$ at 44 MeV per nucleon (ref. 30). E^*_{rel} is the difference between the total kinetic energy of two coincident fragments (in their cm system) and their Coulomb repulsion energy. In part a, the black and open dots are the fragments in coincidence with a fast ($v/v_p > 0.67$) and slow ($v/v_p < 0.67$) particle, respectively. The bottom spectrum is the sum of both types of coincident fragments.

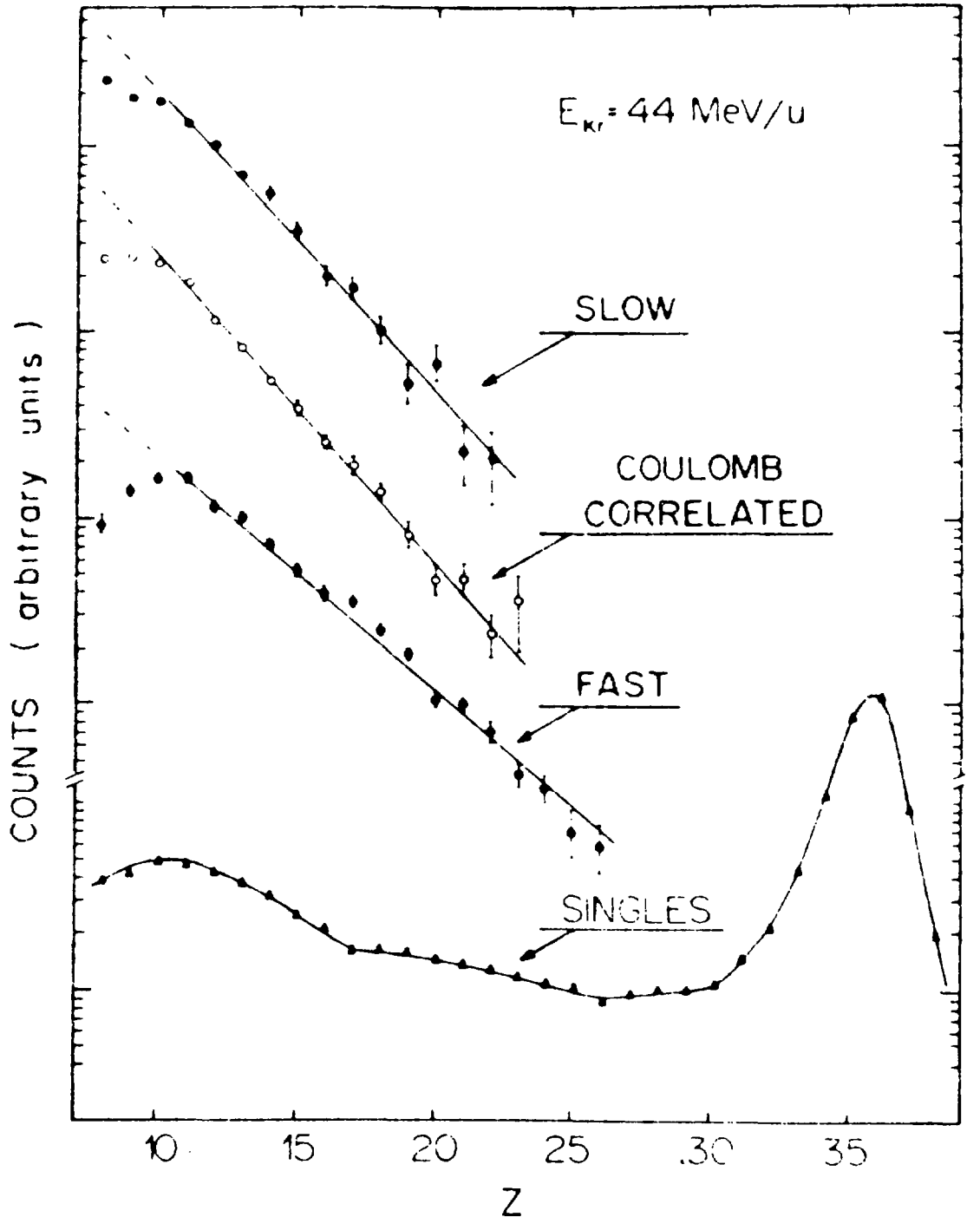

Figure 8. The Z distributions corresponding to the slow, Coulomb-correlated, and fast components from the reaction of ^{84}Kr with ^{197}Au at 44 MeV per nucleon. The singles spectrum is for events integrated over all energies and angles. (From ref. 30).

Exclusive data are quite sparse for heavy fragments. Inclusive measurements were performed at 22 and 35 MeV per nucleon.[37] While the low-energy results were interpreted in terms of a process combining features of the participant-spectator model and the deep-inelastic interaction, fragments observed to be strongly energy-relaxed have remained without explanation. This apparent overlap of various mechanisms rooted in both low and intermediate energies certainly calls for a study of their energy dependence and a better understanding of their respective contribution to the reaction yields. In the case of Kr on Au (ref. 30), the identification of the two distinct mechanisms has revealed a new process, strongly energy dependent from 35 to 44 MeV/nucleon, but not observed in the ^{35}Cl + Ta study at 20 MeV/nucleon.[38]

The need for new high-quality exclusive measurements is well established by the complex picture emerging of the intermediate energy range, which is clearly a region of transition for the various production processes of intermediate-mass fragments.

3.3 Multifragmentation of the Projectile

The previous topic is apparently quite similar to that of the present heading. As it may be recalled from Section 3.1, the excitation of the projectile, either via nucleon transfer processes or via inelastic scattering is a dominant mechanism leading to projectile fragmentation in peripheral collisions. The critical quantity is the degree of excitation of the primary fragment which may then decay through various paths, giving the PLF. The discussion is here purely restricted to the potential emergence of three or more

nuclei after a peripheral interaction in the field of the target. The target plays a rather instrumental role, largely as an interaction center. A crucial question is whether projectile multifragmentation can occur, directly by a prompt multibody breakup of the projectile, or by subsequent sequential decays. Recent theoretical models,[39] formulated with a transport equation which includes NN collision terms, have given clues regarding the role of the incoming nucleons (they are practically all inherent participants in all but the most peripheral collisions). A comprehensive study of collisions at the extreme nuclear periphery may therefore be an essential starting point for understanding the onset of projectile multifragmentation. Furthermore, as it has been pointed out in a recent investigation[40] of the ^{40}Ar on Au reaction at 60 MeV per nucleon, the participant-spectator picture describing the colliding ensemble may be an oversimplification at that energy.

The primary excitation energies are expected to be sufficient to allow the occurrence of projectile multifragmentation in intermediate energy collisions, with an appreciable probability relative to two-body channels. In fact, discrete states are excited in the primary fragments.[41] Since direct nucleon-nucleus and nucleon-nucleon interactions might become an important excitation mechanism, discrete states can be formed after a first interaction has taken place. Some evidence of direct multifragmentation of a projectile has been seen at 30 MeV per nucleon.[42] A multiplicity analysis[19] of the reaction of a 40 MeV/u ^{14}N beam with a gold target has revealed a significant number of events involving three or more particles.

A recent experiment[43] performed in part by Laval University members of the MARS collaboration was done at 32.5 MeV per nucleon with a variety of beams and targets to investigate the role of the entrance channel reaction partners, in particular how the threshold Q value of a given projectile can differentiate one case from another. This class of experiments, when investigated with a large number of detectors, will create a bridge between a purely peripheral collision, with all its two- and multi-body processes, and the mechanisms dominating at decreasing impact parameters. MARS, which provides 128 detectors within a cone of 38° offers enough granularity to measure the characteristics of these multi-fragment events.

To understand the onset of several mechanisms evolving, like those discussed so far, in angle, mass and energy, and to unambiguously identify and follow their trends, a flexible setup is essential; the proposed array would allow accurate studies of these mechanisms. Experiments with PLF, detected in coincidence with other fast fragments or light particles, would allow a complete event reconstruction. This should be adequate to describe precisely that class of peripheral collisions and its trends with impact parameter.

3.4 Lifetime of Excited Fragments

The measurement of compound nuclear lifetimes by crystal blocking techniques has provided valuable insight into the time evolution of nuclei decaying by particle emission. For such decay modes the lifetime, τ is $< 10^{-15}$s.

Considerable effort has been made to study the fission decay of compound nuclei produced in heavy-ion reactions[44-47]. In these measurements, many of which have been performed at Chalk River, beams of C to Ne were used to bombard crystal targets of Ta, W, Au and U. Figure 9 shows a two-dimensional blocking pattern for 40 MeV ^{16}O ions elastically scattered from a Ta crystal along a <111> direction. The axial and planar minima stand out clearly in the two-dimensional pattern. A plot of intensity in the y-direction through the center of the axial dip, for the position indicated by the dot on the x-axis, is shown in the lower half of the figure. The lifetime results, when combined with total fission cross section measurements and fission fragment angular distributions, have permitted severe restriction of parameters in the statistical model describing the decay.

With very heavy, high energy beams it is possible to extend these measurements to shorter lifetimes by using low Z crystals e.g. ^{127}I bombardment of a Ge crystal. The resulting compound nucleus recoil velocity is then increased by about an order of magnitude over that achieved in the earlier measurements with a corresponding increase in the lifetime sensitivity.

The crystal blocking lifetime technique has also been used to measure nuclear deexcitation times down to 10^{-19}s by bombarding a diamond crystal with an ^{16}O beam and measuring blocking patterns for evaporation residues[48]. In this work the time delay associated with the production of evaporation residues with Z values from 6 to 12 were measured and found to be in the range 5×10^{-18}s to 5×10^{-17}s.

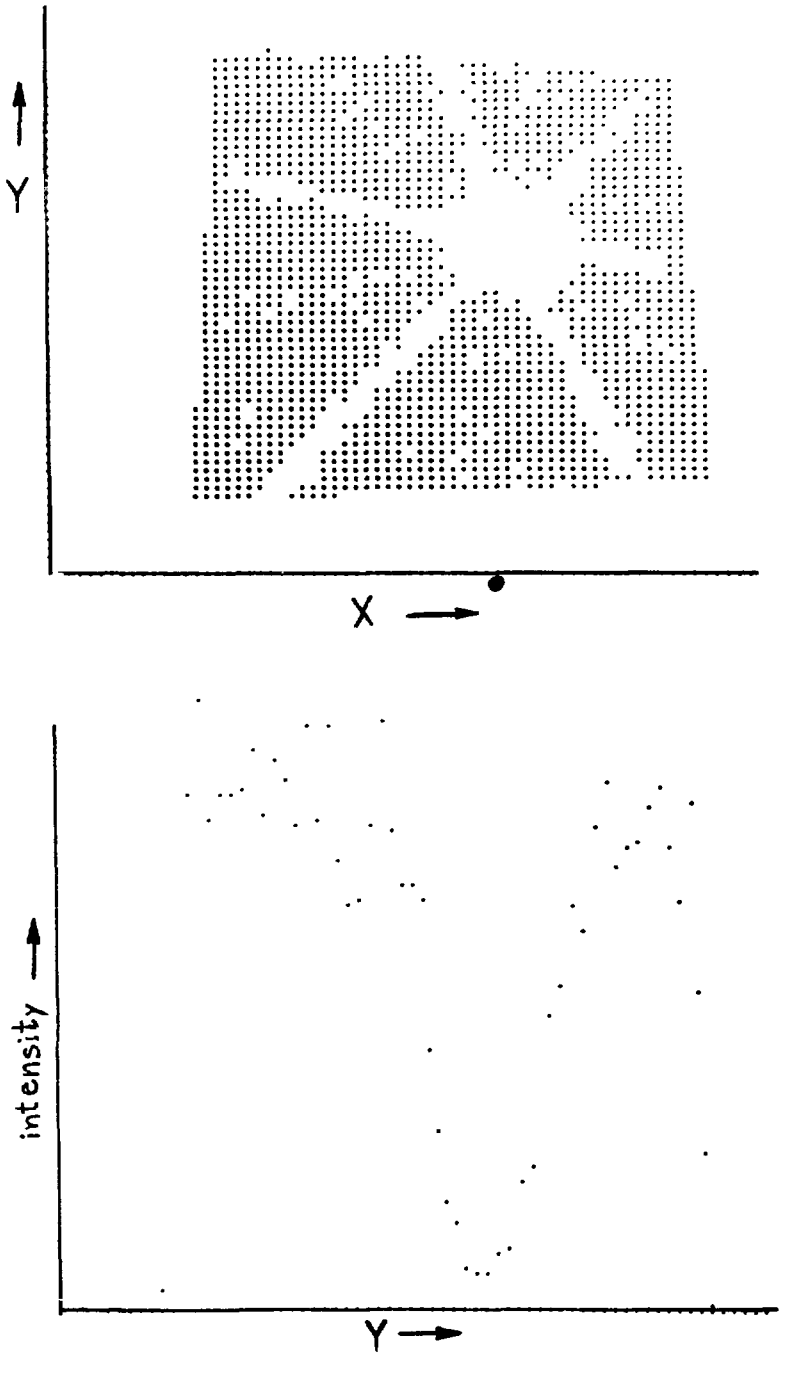

Figure 9. Display of a blocking pattern recorded in the elastic scattering of ^{16}O on W (orientation < 111 >) at 40 MeV (ref. 45). The black dots in the upper 2-D spectrum correspond to (x, y) channels containing more counts than a pre-selected minimum value. A y-scan through the center of the axial blocking dip is shown in the lower half of the figure. The black dot on the x-axis indicates the x value for the scan.

In all of the measurements described above, the beam particles are assumed to fuse with a target nucleus resulting in a compound nucleus with a well-defined recoil velocity ; also, the distribution of decaying particles covers a wide angular range. A straightforward determination of the lifetime value can then be made by a comparison of blocking dips measured at different angles, since the displacement of the compound nucleus from the lattice site perpendicular to the axis along which the blocking pattern is measured is just $v\tau \sin \vartheta$ where v is the compound nucleus velocity, τ the mean lifetime of the compound nucleus and ϑ is the angle between the velocity vector and the crystal axis.

More recently, the technique has been used in an attempt to measure time delays of projectile-like fragments in heavy-ion reactions, in particular ^{40}Ar + Ge at 44 MeV/nucleon[49]. In this reaction, primary fragments, which are highly excited, are produced at the lattice site on a very short time scale. They subsequently decay by light particle emission to produce the secondary fragment measured in the detector and it is the time delay between primary and secondary fragments which is determined by the crystal blocking technique.

The data analysis is now considerably more complicated because, in a single measurement, the primary fragment is unknown: e.g. a detected Si nucleus could have resulted from α-decay of a S primary fragment, from n-decay of Si, p-decay of P, etc. Also, the recoil direction of the primary fragment is no longer unique and assumptions about it must be made. The comparison of blocking dips for different angles of measurement is also no longer straightforward. However, a

large forward array, which could detect the decay particles of the primary fragment, would help resolve many of the difficulties associated with such measurements. The results could provide detailed information on the time evolution of heavy ion reactions at intermediate energies which is unobtainable by any other known technique. Members of the collaboration have been active in blocking lifetime measurements (e.g. refs 45-47) for over fifteen years and are capable of making significant contributions with the blocking technique to heavy-ion reaction studies.

4. CENTRAL PROCESSES

The highest temperatures and densities are achieved in central collisions. Such collisions are therefore selected in experimental investigations of the behavior of nuclear matter, its equation of state and thermodynamical properties. The studies may take the form of a search for the onset of multifragmentation, of finding the limiting momentum or excitation energy which can be imparted to a nuclear system, or of probing localized sources for their extent, velocity, and temperature.

4.1 Equation of State and Thermodynamical Properties

Nuclear matter formed in central nucleus-nucleus collisions may display temperatures ranging from a few MeV up to several tens of MeV. One can attempt to describe the system by an EOS such as the one shown in Figure 1. The corresponding phase diagram[1)] is displayed in Figure 10, with limits and characteristic curves indicated on the graph. An essential reference value deduced from those calculations is the critical temperature for breakup, T_c. In the calculation of reference 1, based on a zero-range Skyrme interaction, a critical temperature of 15.3 MeV is obtained. A much

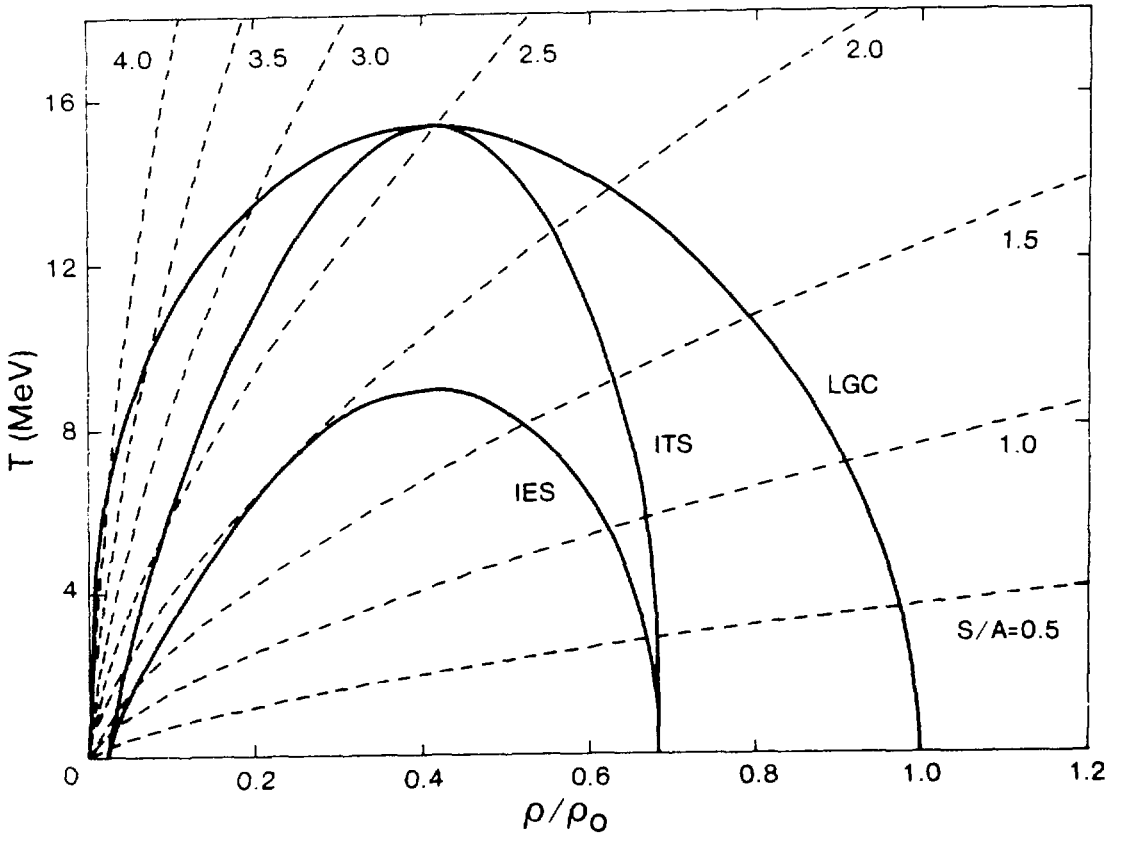

Figure 10. Phase diagram for neutral nuclear matter corresponding to the EOS of Figure 1 (ref. 1). Isentropes for different values of S, entropy, are indicated by dashed curves. The boundary of liquid-gas coexistence (LGC) and the curves of constant pressure (isothermal, ITS, and isentropic, IES) are shown with solid lines.

lower value is calculated when a Coulomb interaction is incorporated into the calculations,[50] thus describing a system which should disintegrate at a much lower temperature than that for neutral nuclear matter.[1,51] A mechanical instability region,[1,52] which defines the points for onset of multifragmentation influences the reaction time evolution; although experimental identification of this point has remained elusive, a clear energy dependence should appear[51] in two-fragment correlations such as those displayed in Figures 11 and 12. Several different formulations exist for the EOS, but similar properties for nuclear matter in phase transition are found[53] in each of them. This type of computer simulation[51] provides a basis for testing the EOS and its instability region.

A supplementary measurement concerning the EOS is the determination of the entropy, which increases through the predicted mechancial instability region.[1] The isotope-yield ratios for intermediate mass fragments, as reported recently[55] and shown in Figure 13, reflect the temperature and density at breakup, thus providing a measure of the entropy. Since the entire target is involved in the central collisions observed here, event detection must be as complete as possible. This has been pointed out in ref. 56, in an entropy determination from complex-fragment yields without isotope resolution. The apparent power-law behavior of the mass yields (Figure 14) has been interpreted[57] in terms of the nuclear liquid-vapor phase transition.

MARS is well suited to central collision experiments; when it is operated in "close geometry" mode, 1 m from the target, it intercepts up to 75% of the light ions emitted from an intermediate-velocity

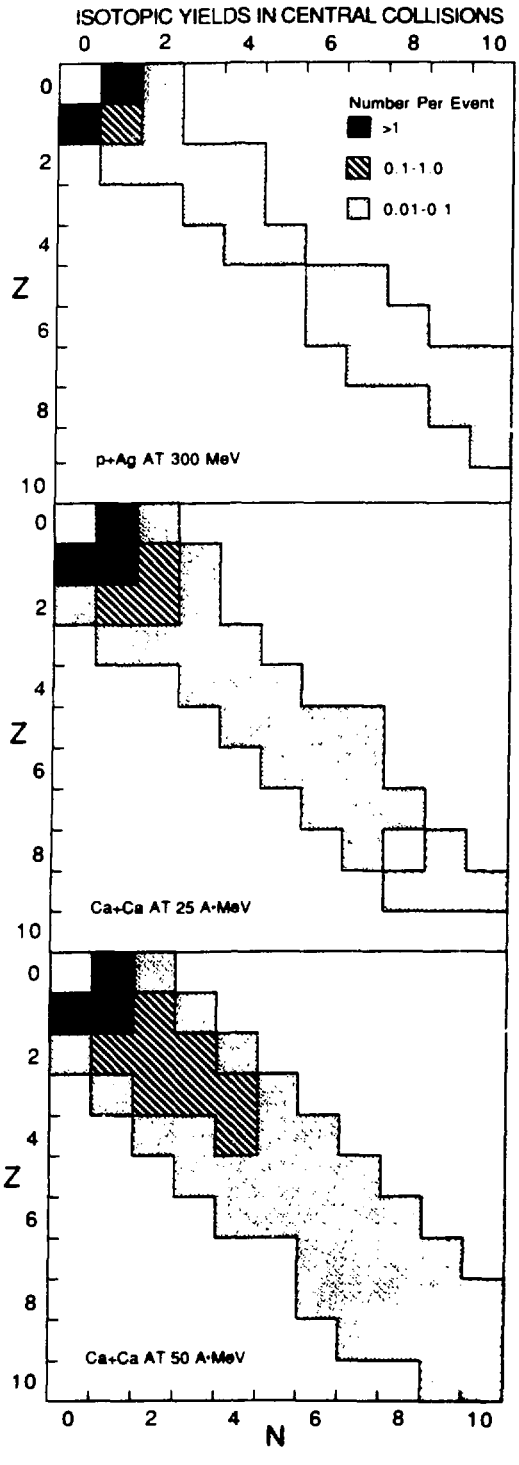

Figure 11. Isotopic yields obtained in different simulated reactions (ref. 51). The yields are represented as the number of fragments of a given Z, N pair.

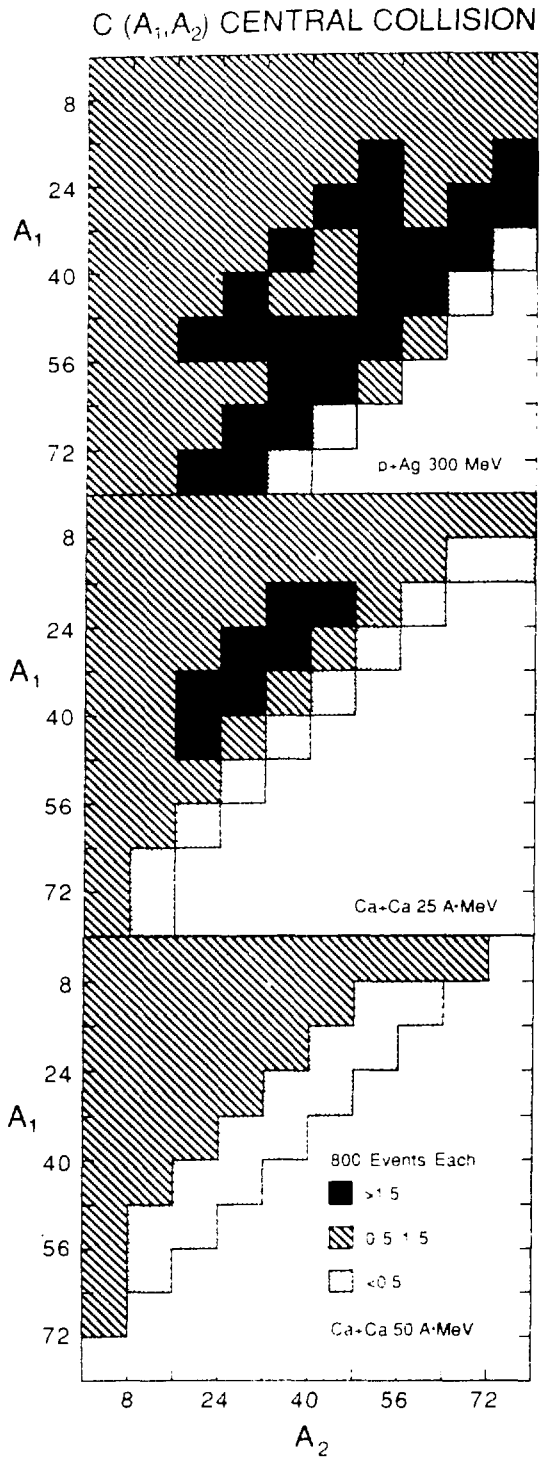

Figure 12. Mass-mass correlation yields for the indicated simulated reactions (ref. 51). Each bin represents eight units of mass.

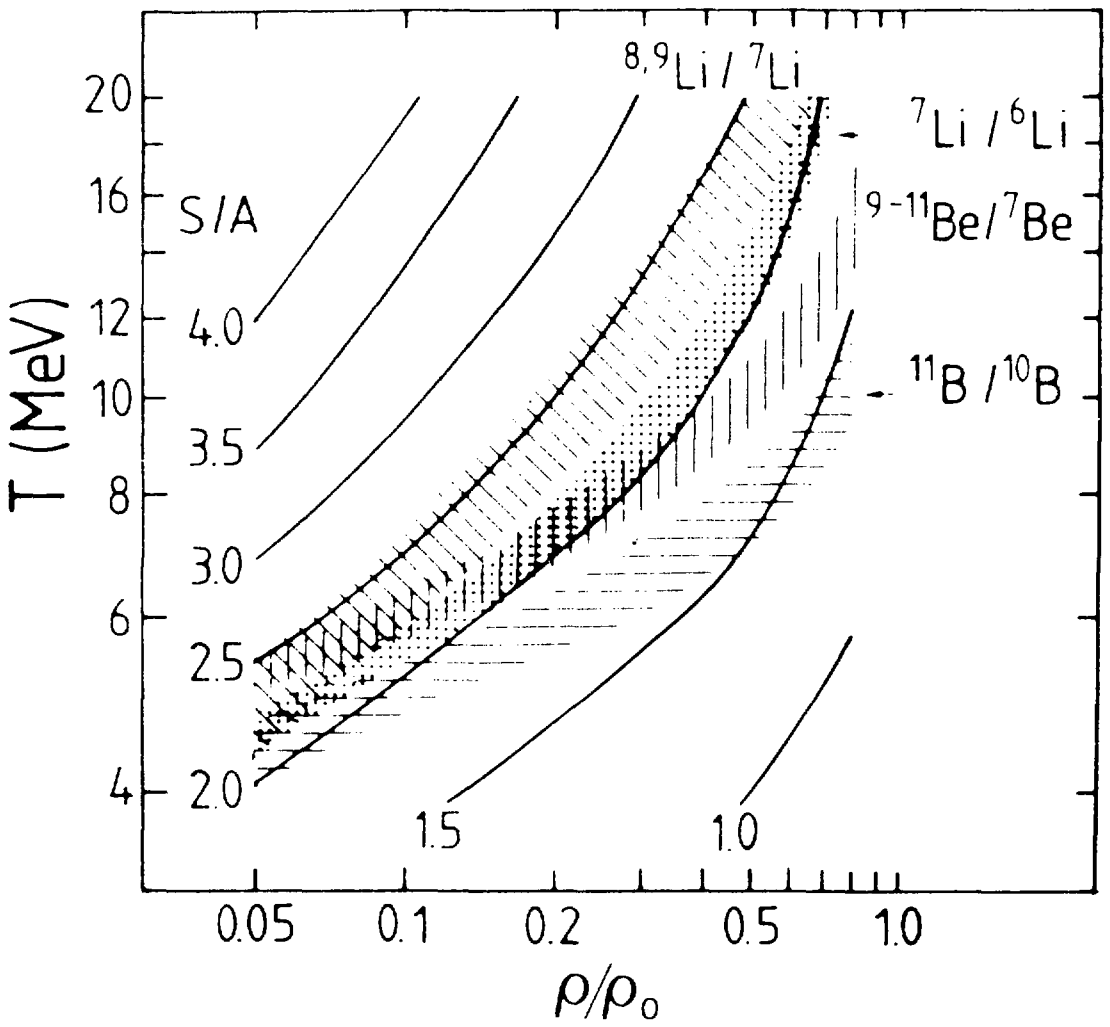

Figure 13. Comparison between calculations from a quantum statistical model and experimental data for the ^{12}C + ^{197}Au system at 84 MeV per nucleon (ref. 55). The isentropes are shown with solid lines and the regions of agreement between the calculated and measured isotopic-yield ratios are indicated by shaded areas.

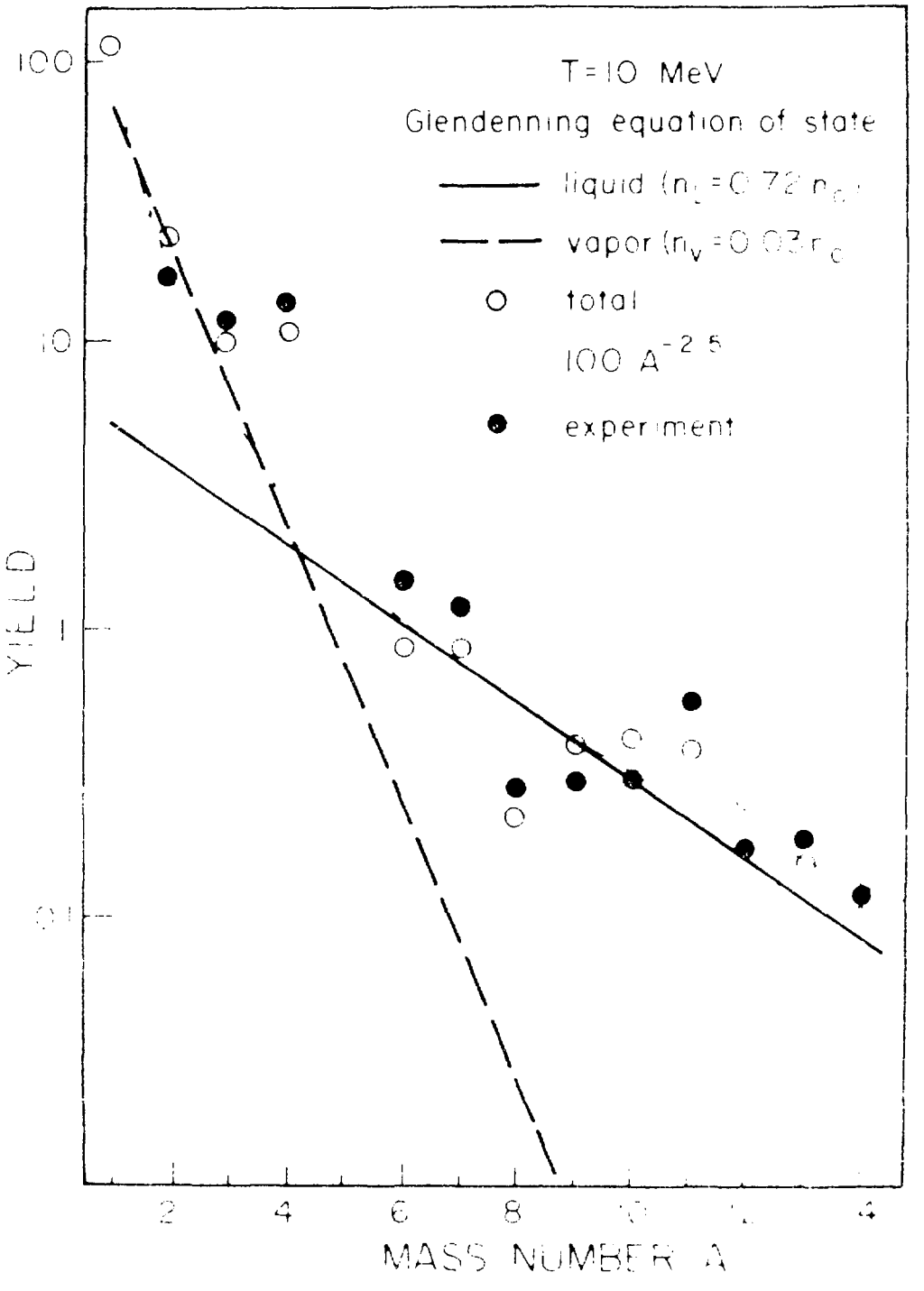

Figure 14. Exponential distributions resulting from fitting functions to the fragment yields obtained from the disassembly of the liquid and vapor phases (ref. 57). The experimental results are from the reaction ^{40}Ar on gold at 42 MeV per nucleon (ref. 56).

source. This gives a useful multiplicity trigger for central collisions. Additional filtration of peripheral events is obtained by requiring an absence of projectile-like fragments near and forward of the grazing angle. Two-fragment correlations between fairly light ions ($Z \leq 8$) can be performed with the array itself; auxiliary large-area detector telescopes can extend the measurement to heavier elements.

Addition of a few high resolution telescopes permits measurement of isotopic yield ratios. With the event type determined by the array, estimates of entropy production gain a more specific meaning.

4.2 Onset of Multifragmentation

Another approach to the disintegration of hot nuclei into many fragments, formulated from a statistical liquid-drop model,[58] also provides a clear blueprint for possible experimental verification. Different systems have been studied[58,59] from this perspective; Figures 15 and 16, show Monte Carlo simulations of the average temperature and the average multiplicity, respectively, plotted as a function of the excitation energy per nucleon. The multifragmentation sets in at a well-identified point called the "crack temperature", (ca. 6 MeV in Figure 15) above which the compound nucleus loses its cohesiveness. The corresponding multiplicity (Figure 16) increases rapidly with excitation energy. The temperature remains at a plateau until the system reaches the free gas limit. Calculated fragment mass distributions are presented in Figure 17 for three different excitation energies. Like the theoretical predictions in Figure 15, the experimental data in Figure

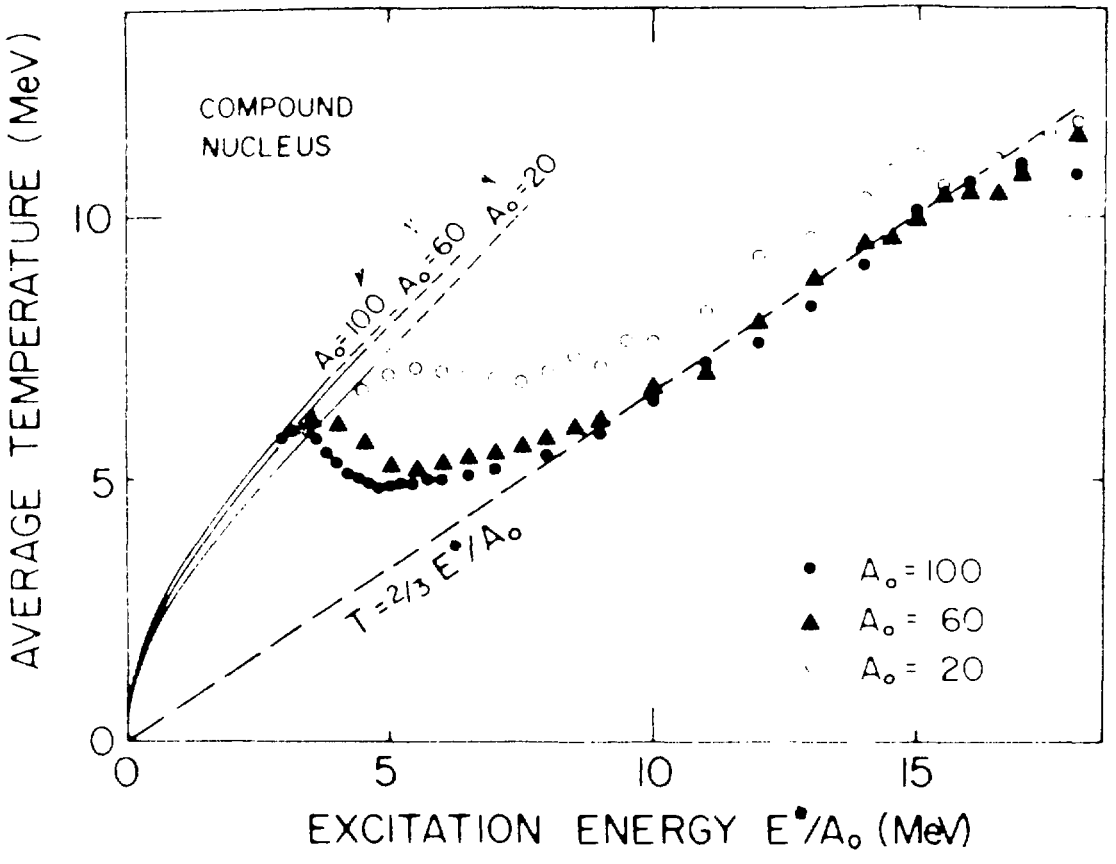

Figure 15. Monte Carlo simulations of the average temperature T as a function of the excitation energy for different values of A_0, the total mass. The dashed line is the free gas limit (refs. 58 and 59).

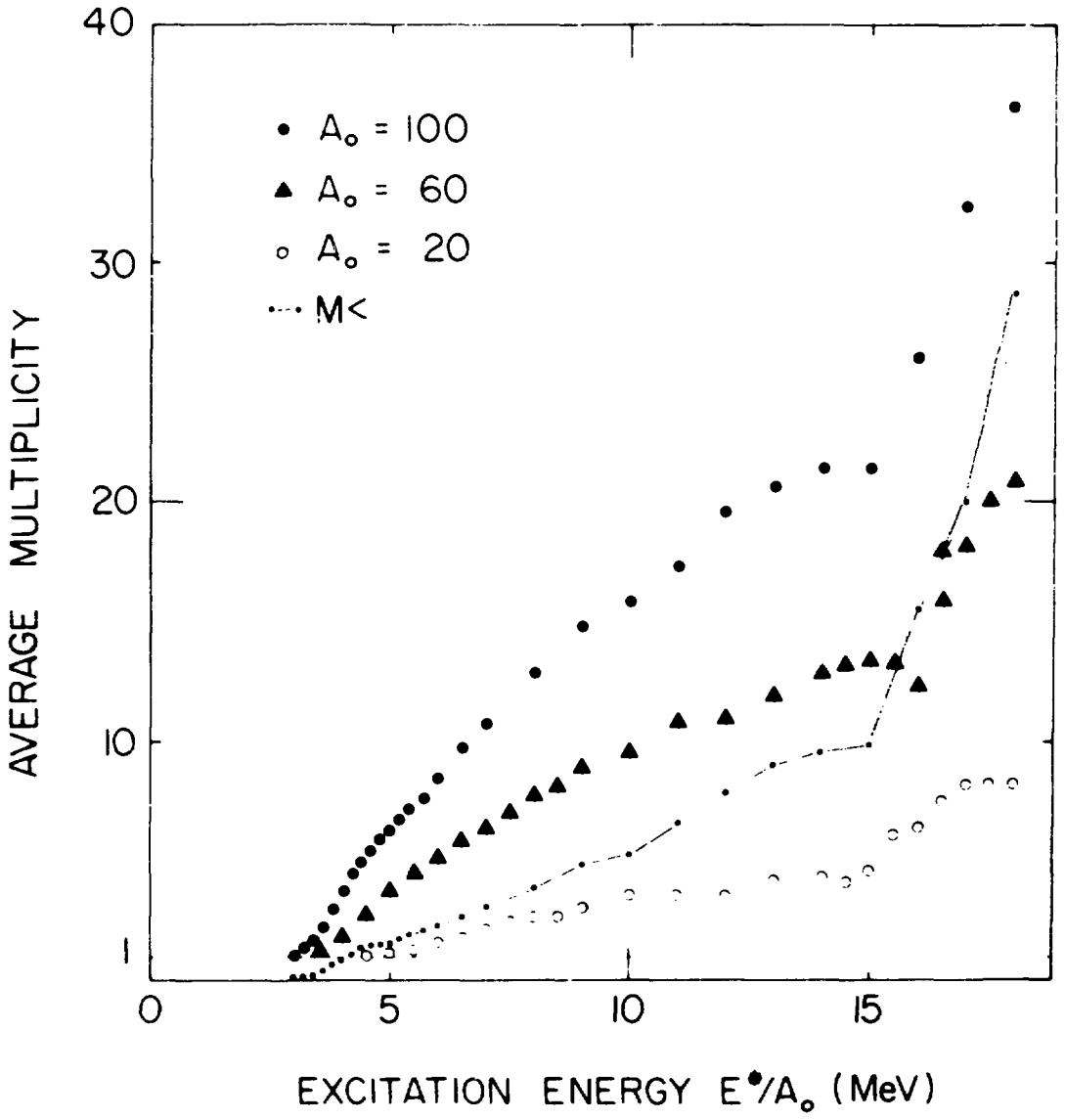

Figure 16. Monte Carlo simulations of the average multiplicity M as a function of the excitation energy for different systems of total mass A_0. The solid line is the result for A_0 = 100 considering only clusters of A < 4 (refs. 58 and 59).

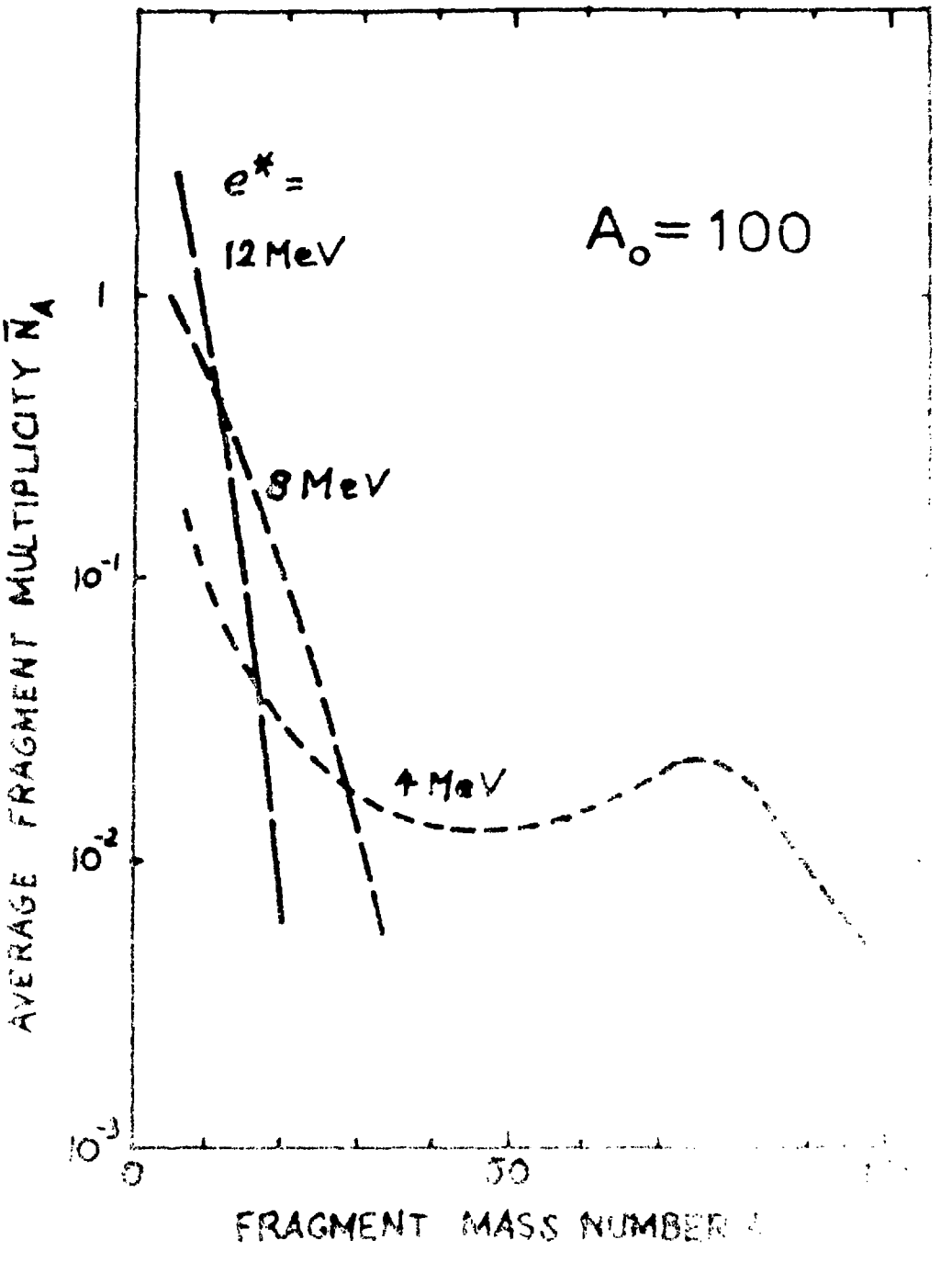

Figure 17. Calculated average mass distributions for various excitation energies $e^* = E^*/A_0$ in the system with a total mass of $A_0 = 100$.

18 give nuclear temperature as a function of source excitation per nucleon. A striking similarity between the two figures, namely a plateau in temperature for excitations per nucleon between 3 and 10 MeV, has been noted.[60] However, as pointed out by Borderie,[61] the apparent velocities extracted from intermediate-velocity source data do not permit the corresponding excitation energies to be attributed to the whole system, and without a knowledge of the excitation energies, the results are inconclusive.

Additional experimental verifications of theoretical predictions are proposed in an extension made recently[62] to the Boltzmann-Uehling-Uhlenbeck model.[63] Mass distributions have been calculated for the ^{20}Ne on ^{20}Ne and ^{40}Ca on ^{40}Ca systems in the energy range 50 to 100 MeV per nucleon. Figure 19 shows such distributions for the case Ca on Ca at 72 MeV per nucleon.

Previous attempts to determine the excitation energy corresponding to the onset of multifragmentation or to the saturation of apparent temperature parameters have to date shared a common ambiguity. Without assurance that a central collision has occurred, without an estimate of the source velocity, and with no event-by-event measurement of the multiplicity, all observed quantities are averaged over impact parameter, reaction channel, and kinematic origin. The proposed array can both reject events with projectile-like components and perform a multiplicity cut quickly enough to serve as an on-line trigger; for high multiplicity events, an off-line estimate can be made of the source velocity. The consequence is profound: a determination can be made of the limiting point beyond which multifragmentation sets in.

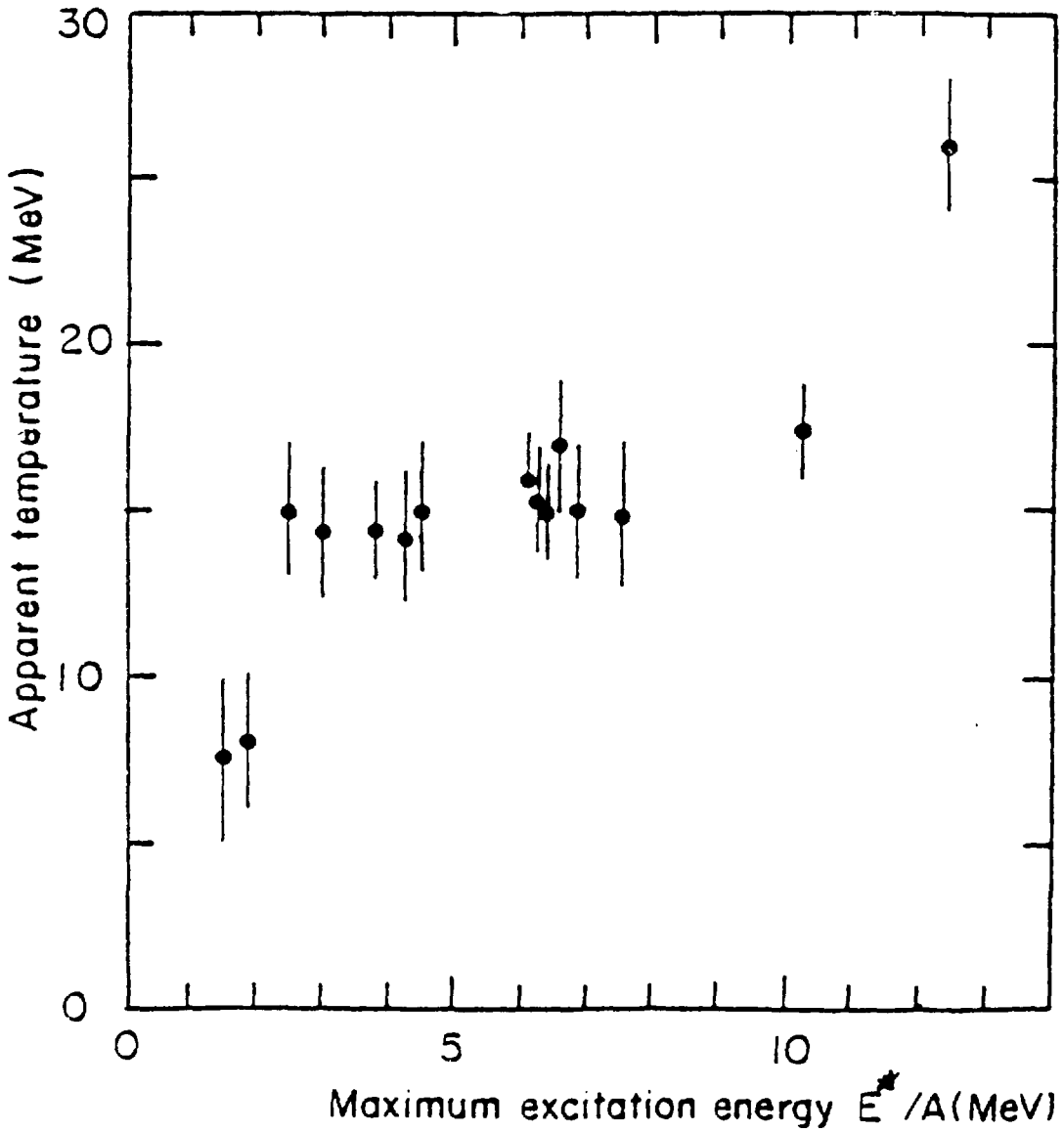

Figure 18. Average apparent temperature of the intermediate velocity source (determined from fitted slopes of experimental energy spectra) as a function of the maximum possible excitation energy deposited in the center of mass. The list of references for the data is given in ref. 61.

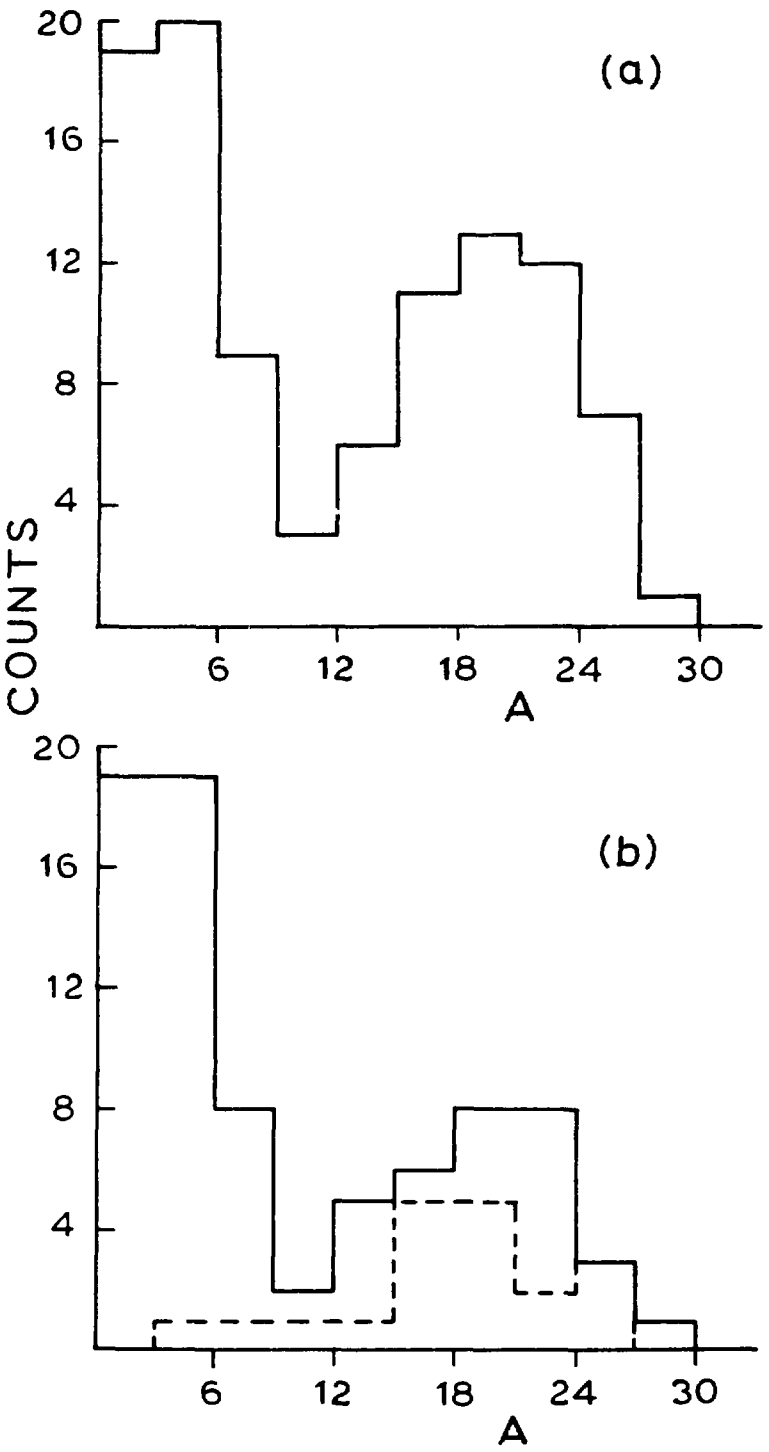

Figure 19. Calculated mass distributions for Ca on Ca at 72 MeV per nucleon. All clusters are included in the top curve, while separate contributions from participants (solid line) and spectators (dashed line) are displayed in the bottom section of the figure (ref. 62).

4.3 Linear Momentum Transfer and Maximum Excitation Energy

What is the maximum excitation energy that a composite system can hold before it disintegrates? How can the deviations from complete fusion be interpreted correctly? Several recent works have provided new insight into the early stages of collisions at different energies and a review[64] of the subject raises crucial questions. Incomplete fusion processes represent a broad range of pre-equilibrium mechanisms having different properties depending upon the bombarding energy or the projectile-target system under study. Cluster emission is proposed as a possibility at 16 MeV per nucleon[65] while a study[66] at 20 and 35 MeV per nucleon suggests that the latter value represents the limit to the energy that a composite system can sustain before it disintegrates into light fragments. Another exploration[67] of the 24-40 MeV per nucleon range establishes a limit for composite nucleus formation just above 27 MeV. Figure 20 gives a global picture of the deposited excitation energy as function of the mass of the composite systems studied. A more systematic view is presented in Figure 21 in terms of the most probable values of linear momentum transferred from the projectile to the composite system.

The ideas outlined above reflect quite a complex situation of overlapping effects as the limits to fusion are reached. Pre-equilibrium effects are not completely ruled out, but a temperature limit is tentatively assigned to the composite system[67] although several questions remain open[64]. The threshold temperature predicted for disintegration[50] could therefore represent the same limit of excitation energy as that deduced from

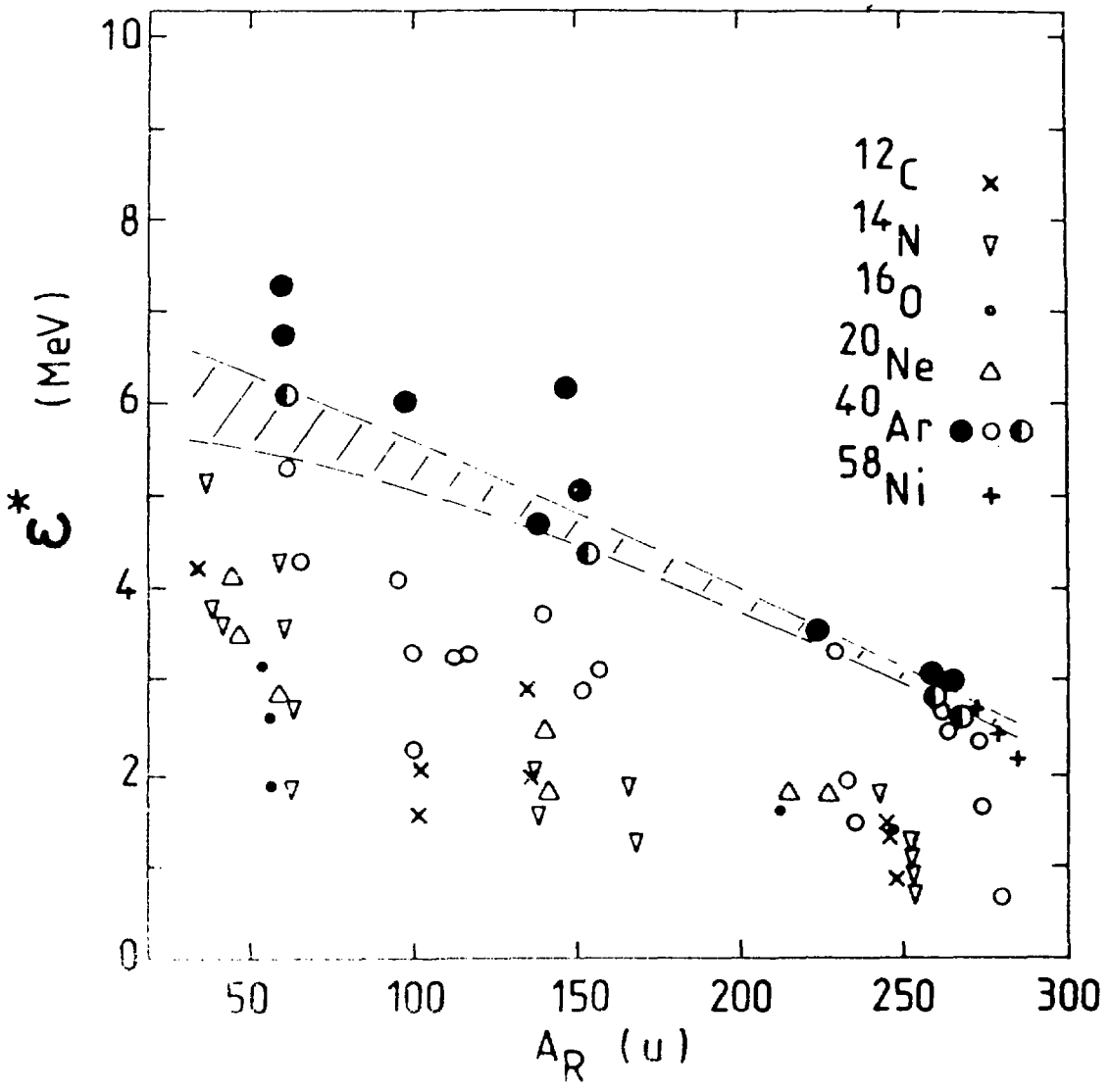

Figure 20. Excitation energy per nucleon deposited in the composite system as a function of the mass A_r of that composite system. Filled circles are systems with no fusion (175 MeV/c assumed for p_t/A) and half-filled ones represent systems for which fusion begins to disappear. The references are given in ref. 64. The excitation energy seems to reach its limiting value in the dashed region.

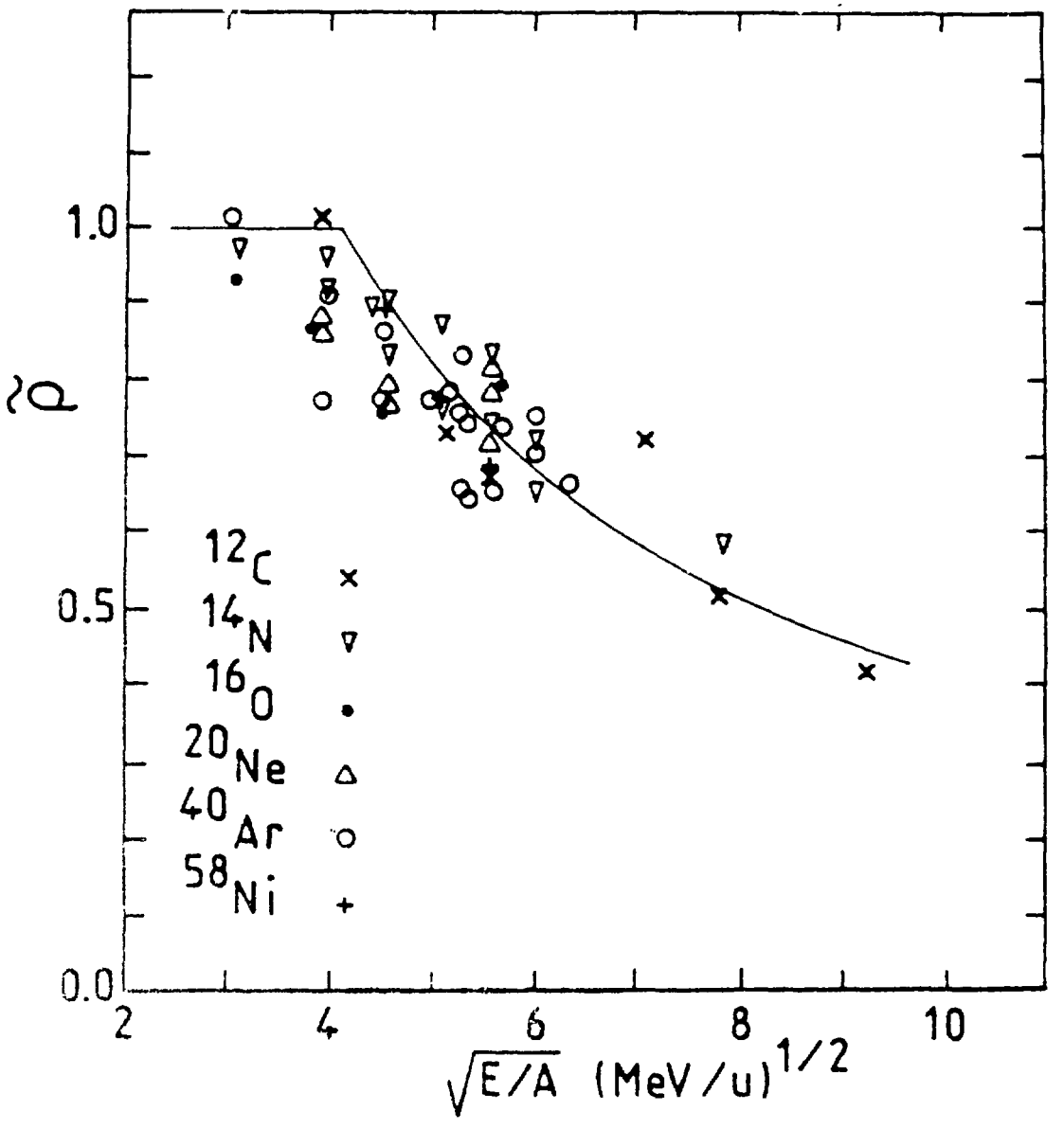

Figure 21. Most probable value of the linear momentum transferred p as a function of $(E/A)^{1/2}$ for the composite system A. The solid line has been drawn by assuming a limiting value of 175 MeV/c for p_t/A and is a rather good fit to the data (see ref. 64 for a list of references to data).

the momentum transfer data.[67] As suggested from missing momentum studies,[31] the energy deposition in central collisions depends primarily on the velocity and mass of the projectile and less on the total energy. This result supports the suggestion[67] that the limiting temperature could best be measured in symmetric collisions. The beam energies required to reach the critical breakup temperature of a composite system of mass A formed with C and Ar projectiles is shown in Figure 22. The lower limit for the production of nuclei at the predicted critical temperature in symmetric collisions is also shown. From this figure it is evident that symmetric collision e.g. Ca on Ca are ideally suited to test the hypothesized breakup temperature.

This perspective on central collisions differs only slightly from that of the multifragmentation view. Here we seek to observe the disappearance of few-body final states rather than the appearance of many-body states. Consequently large-area heavy-fragment detectors, such as avalanche counters or gas ΔE detectors are required. However, experiments at this level have already been done. The contribution of MARS will be to allow one to ascertain the amount of projectile-like component present as the limits to fusion are approached, i.e. how much of the "missing" momentum can be attributed to causes other than incomplete fusion.

4.4 Nuclear Interferometry and Localized Sources of Excitation

Two-particle correlation techniques[68] have provided information on the time and space localization of reactions and on the temperature of the emitting source. A localized region of high

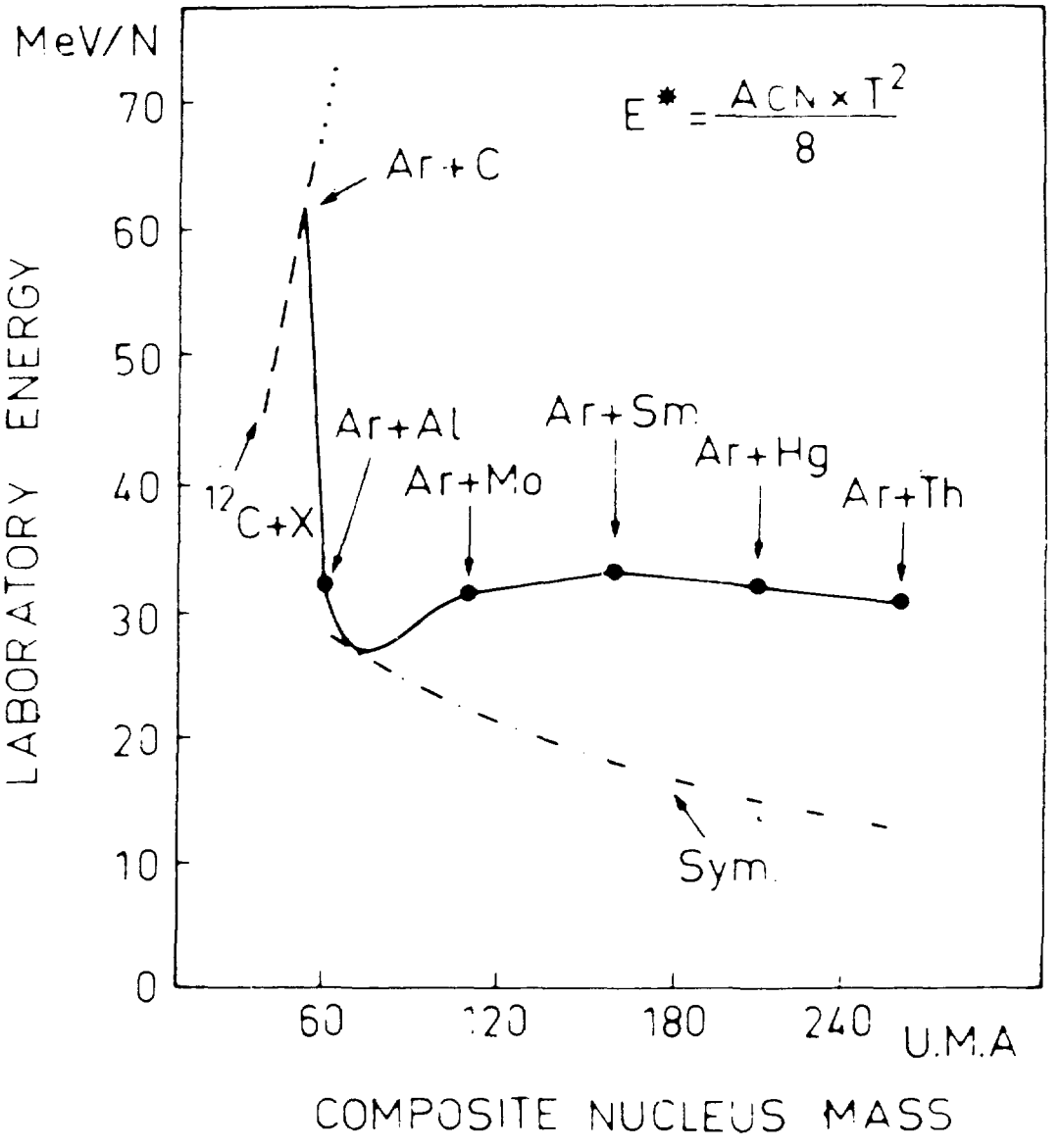

Figure 22. Laboratory beam energies required to reach the critical temperature for breakup of a composite system of mass A formed with Ar (solid line) and C (dashed line) projectiles. The symmetric cases lie on the dot-dashed line which sets a lower limit in energy required for the production of the predicted critical temperature conditions. The figure is from ref. 67.

excitation has been identified with p-p correlations in reactions at 25 MeV per nucleon;[69] information has been extracted as to the space-time extent of the emitting region as has been done at relativistic energies in studies of the nuclear fireball. At intermediate energies source radii can be extracted from correlations between protons and other light fragments, and a time scale associated with the source. An assessment of the number of participant nucleons can also be made.[70] However, a recent paper[71] on ^{14}N-induced reactions at 35 MeV per nucleon, analysed with the two-particle correlation technique, addresses several new questions; their answers will require a considerable amount of experimental and theoretical work.

The "interferometry" field is evidently still expanding, and more sophisticated experiments could be designed to use the technique at its full potential. Already, multiplicity-tagged correlation functions have been reported.[71] Used with a small close packed array of high resolution telescopes for the correlation measurements, the large array will offer a considerable improvement over present measurements by performing high-level event selection (e.g. by particle type or velocity distribution). The University of Toronto group is developing such a prototype lattice of CsI/plastic telescopes. Use of this lattice in coincidence with the large array will remove from the correlation functions undesired contributions coming from sequential mechanisms or other sources (e.g. projectile-like or target-like) unrelated to the central events of interest.

5 OTHER TOPICS

5.1 Subthreshold Pion Production

In recent years, the collective nature of pion production mechanisms at subthreshold energies has been clearly established by many experiments.[72-74] Those results have fostered various theories to describe possible subthreshold production mechanisms, including nucleon-nucleon single collisions,[75] statistical and thermal models,[76-81] bremsstrahlung models[82-84] and a time-dependent Hartree-Fock (TDHF) model.[85] However, the details of the processes are still uncertain because the experiments, so far, were aimed mostly at establishing the total production cross section and because the different theoretical models already mentioned generally manage to reproduce the gross features of the total production cross section. The typical results presented in Figure 23 were obtained by members of our collaboration.[76] Although these different models all reproduce more or less the pion production cross section, they are nevertheless very different from one another; these differences should manifest themselves in the reaction products that are coincident with the pion.

The experiments needed at this stage in order to lift this ambiguity must be designed to detect not only the pions but also the particles and fragments produced with them. One way to achieve that will be to have one or more pion detectors in conjunction with a finely segmented array of detectors. The latter should provide the broadest detection range possible in mass and energy while covering as much as possible of the reaction phase space. The pion detector

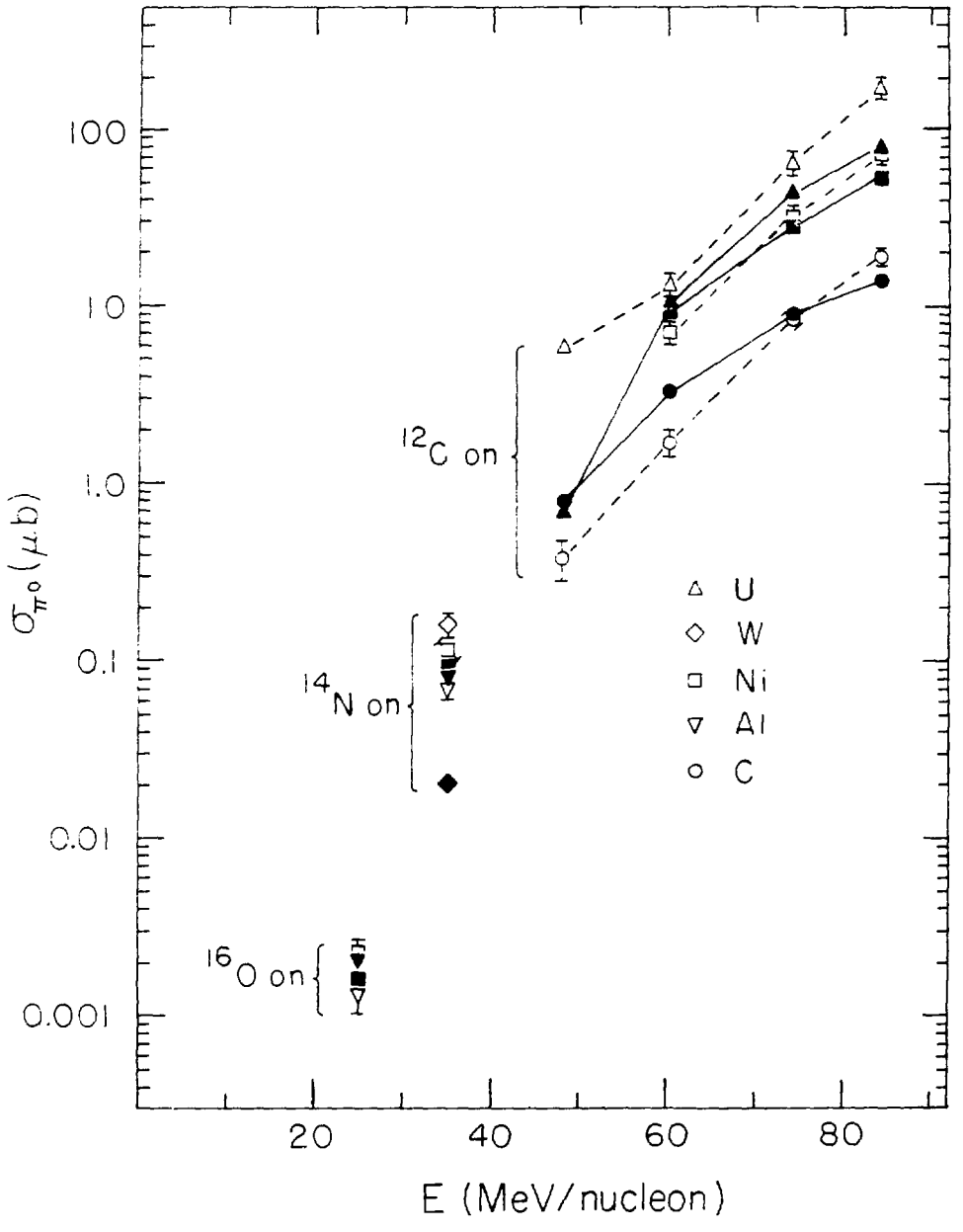

Figure 23. Experimental and calculated subthreshold pion production total cross sections, σ_π, for beams of ^{12}C, ^{14}N and ^{16}O on different targets, as a function of energy. The open symbols are used for the experimental data (refs. 72-74) and the calculated yields (ref. 76) are shown by solid symbols. In the case of ^{12}C beams, the values are linked

could be of the type used at GANIL in an experiment with a 94 MeV per nucleon ^{16}O beam.[86] This detector is a particle telescope made of thirteen layers of plastic scintillator for a total thickness of 27 cm. The role of the detector array can be filled by the proposed array, complemented if necessary by other modules to increase the detection solid angle for fragments and particles other than the pions.

5.2 Total and Reaction Cross Sections

One of the most fundamental questions in intermediate and high energy heavy-ion physics is to what degree a nucleus-nucleus collision proceeds through a series of incoherent nucleon-nucleon interactions. That is, to what degree do incoherent quasi-free interactions dominate the nucleus-nucleus collision process? If indeed the reaction cross sections are dominated by such incoherent interactions, then it is important to choose carefully experiments which enhance the probability of observing regions of highly compressed and excited nuclear matter relative to the quasi-free scattering (QFS) background.

Recently work at TRIUMF by a University of Toronto group has shown the remarkable ability of microscopic theoretical calculations to predict nucleon-nucleus scattering cross sections and polarization parameters, as well as reaction cross sections.[87] Indeed, Faessler's group has extended these parameter-free microscopic calculations to heavy-ion collisions, where they have demonstrated that, at higher energies (>50 MeV/u), the heavy-ion reaction cross sections are dominated by QFS. On the other hand at low energies the

reaction cross sections are dominated by the excitation of the nuclear surface and fusion. The calculations have for example, predicted the energy dependence of the ^{12}C-^{12}C reaction cross section, as well as the elastic scattering cross section and the scattering cross sections to low-lying excited states of ^{12}C.[88]

Very few data exist in the literature, and a group from the University of Toronto, which participates in the MARS collaboration, has built apparatus for total and reaction cross section measurements in heavy-ion collisions, to be used with the Chalk River TASCC facility. They are also constructing a detector to measure the elastic and inelastic differential cross sections for the same reactions. These detectors are being tested at Chalk River (in the autumn of 1987), and the first experiment is planned with the TASCC ^{40}Ca beams. Such measurements will be greatly improved with the construction of the equipment proposed here. The availability of better time-of-flight information will permit rejection of recoil events and the large solid angle of the array will provide enhanced anticoincidence capabilities. Further, the scale of the vacuum vessel allows greater angular precision in setting up detectors.

REFERENCES FOR PART II

1. D.H. Boal and A.L. Goodman, Phys. Rev. C33 (1986) 1690.

2. R.G. Stokstad, Comm. Nucl. Part. Phys. 13 (1984) 231.

3. D.K. Scott, Nucl. Phys. A354 (1981) 375C.

4. S. Nagamiya and M. Gyulassy, Advances in Nuclear Physics (Plenum, New York, 1984) Vol. 13, p. 201.

5. R. Stock, Phys. Reports 135 (1986) 259.

6. R. Bass, Nuclear Reactions with Heavy Ions (Springer-Verlog, 1980).

7. Heavy Ion Collisions, R. Bock, ed. (North-Holland, Amsterdam, 1980) Vol. 2.

8. R. Serber, Phys. Rev. 72 (1947) 1008.

9. A.S. Goldhaber, Phys. Lett. 53B (1974) 306.

10. R. Dayras, J. de Physique, C4 (1986) 13.

11. G. Bizard, ibidem, p. 35.

12. M.C. Mermaz, J. Barrette, and H.E. Wegner, Phys. Rev. C24 (1981) 1948; M.C. Mermaz, F. Auger, and B. Fernandez, ibidem, C28 (1983) 1587 and Y. Blumenfeld, Ph. Chomaz, N. Frascaria, J.P. Garron, J.C. Jacmart, J.C. Roynette, D. Ardonin, and W. Mittiz, Nucl. Phys. A455 (1986) 357.

13. G. Bizard, R. Brou, H. Doubre, A. Drouet, F. Guilbault, F. Hanappe, J.M. Harasse, J.L. Naville, C. Lebrun, A. Oubahadou, J.P Patry, J. Peter, G. Ployart, J.C. Steckmeyer, and B. Tamain, Phys. Lett. B172 (1986) 301.

14. F. Rami, A. Fahli, J.P. Collin, G. Guillaume, B. Heusch, F. Jundt, P. Wagner, P. Fintz, S. Kox, Y. Schutz, and M.C. Mermaz, Z. Phys. A327 (1987) 207.

15. S. Gralla, J. Albinski, R. Bock, A. Gobbi, N. Herrmann, K.D. Hildenbrand, J. Kuzminski, W.F.J. Müller, M. Petrovicci, H. Stelzer, J. Toke, H.J.W. Wollersheim, A. Olmi, P.R. Maurenzig, and A.A. Stefanini, Phys. Rev. Lett. 54 (1985) 1898 and references therein.

16. J. Barrette, J. de Physique C4 (1986) 141; S. Wald, S.B. Gazes, C.R. Albiston, Y. Chan, B.G. Harvey, M.J. Murphy, I. Tserruya, R.G. Stokstad, P.J. Countryman, K. Van Bibber, and H. Homeyer, Phys. Rev. C32 (1985) 894.

17. D. Horn, G.C. Ball, R. Bougault, D. Cebra, D. Fox, E. Hagberg, L. Potvin, C. Pruneau, R. Roy, C. St-Pierre, and G.D. Westfall, J. de Physique C4 (1986) 83.

18. D. Horn, G.C. Ball, R. Bougault, E. Hagberg, L. Potvin, C. Pruneau, R. Roy, C. St-Pierre, D. Cebra, D. Fox, and G.D. Westfall, Preprint TASCC-P-87-9.

19. C. Pruneau, Ph.D. Thesis (Université Laval, Sainte-Foy, 1987).

20. R. Ost, A. Gamp, S. Kox, C. Perrin, N. Longequeue, and F. Merchez, Phys. Rev. C32 (1985) 1927.

21. R. Dayras, A. Pagano, J. Barrette, B. Berthier, D.M. de Castro Rizzo, E. Chavez, O. Cisse, R. Legrain, M.C. Mermaz, E.C. Pollaco, H. Delagrange, W. Mittig, B. Heusch, R. Coniglione, G. Lanzano, and A. Palmeri, Nucl. Phys. A460 (1986) 299.

22. G. Bertsch, Phys. Rev. Lett. 46 (1981) 47.

23. M.J. Murphy, Phys. Lett. 135B (1984) 25.

24. W.A. Friedman, Phys. Rev. C27 (1983) 569.

25. J. Hüfner, K. Schäfer, and B. Schürmann, Phys. Rev. C12 (1975) 1888.

26. L.F. Oliveira, R. Donangelo, and J.D. Rasmussen, Phys. Rev. C19 (1979) 826.

27. C. Grégoire, 24th Inter. Winter Meeting on Nucl. Phys. (Bormio, Italy, 1986).

28. J. Aichelin and H. Stöcker, Phys. Lett. 163B (1985) 59; J. Aichelin and G. Bertsch, Phys. Rev. C31 (1985) 1730; J. Aichelin, J. de Physique C4 (1986) 63.

29. G. Bizard, A. Drouet, F. Lefebvres, J.P. Patry, B. Tamain, F. Guilbault, and C. Lebrun, Nucl. Inst. Meth. in Phys. Res. A244 (1986) 483.

30. G. Rudolf, J.C. Adloff, A. Kamili, F. Scheibling, B. Boishu, A. Genoux-Lubain, C. Le Brun, J.F. Lecolley, F. Lefebvres, M. Louvel, R. Regimbart, O. Granier, S. Leray, R. Lucas, C. Mazur, C. Ngô, M. Ribrag, and E. Tomasi, Phys. Rev. Lett. 57 (1986) 2905.

31. M. Fatyga, K. Kwiatkowski, V.C. Viola, W.G. Wilson, M.B. Tsang, J. Pochodzalla, W.G. Lynch, C.K. Gelbke, D.J. Fields, C.B. Chitwood, Z. Chen, and T. Nayak, Phys. Rev. Lett. 58 (1987) 2527 and R. Bougault, D. Horn, C.B. Chitwood, D.J. Fields, C.K. Gelbke, D.R. Klesch, W.G. Lynch, M.B. Tsang, and K. Kwiatkowski, Phys. Rev. C36 (1987).

32. K. Kwiatkowski, J. Bashkin, H. Karwowski, M. Fatyga, and V.E. Viola, Phys. Lett. 171 B (1986) 41.

33. B.E. Hasselquist, G.M. Crawley, B.V. Jacak, Z.M. Koenig, G.D. Westfall, J.E. Yurkon, R.S. Tickle, J.P. Dufour, and T.J.M. Symons, Phys. Rev. C32 (1985) 145.

34. M. Korolija, N. Cindro, R. Caplar, R.L. Auble, J.B. Ball, and R.L. Robinson, Z. Phys. A327 (1987) 237 and references therein.

35. See D. Boal, Advances in Nuclear Physics (Plemun, New York, 1985) Vol. 15, p. 85, for a comprehensive list of references.

36. D. Dalili, M. Berlanger, S. Leray, R. Lucas, C. Mazur, C. Ngô, M. Ribrag, T. Suomijarvi, C. Cerruti, S. Chiodelli, A. Demeyer, D. Guinet, A. Genoux Lubin, C. Lebrun, J.F. Lecolley, F. Lefebvres, and M. Lauvel, Z. Phys. A 320 (1985) 349.

37. D. Dalili, P. Lhenoret, R. Lucas, C. Mazur, C, Ngô, M. Ribrag, T. Suomijarvi, E. Tomasi, B. Boishu, A. Genoux Lubin, C. Lebrun, J.F. Lecolley, F. Lefebvres, M. Louvel, R. Regimbart, J.C. Adloff, A. Kamili, G. Rudolf, and F. Scheibling, Z. Phys. A316 (1984) 371, and J.C. Adloff et al., in Proc. of the Workshop on Nuclear Dynamics, V.E. Viola ed. (Indiana University, Bloomington, 1984) p. 109.

38. M.J. Murphy, S. Gil, M.N. Harakeh, A. Ray, A.G. Seamster, R. Vandenbosch, and T.C. Awes, Phys. Rev. Lett. 53 (1984) 1543 and M.J. Murphy, D. Leach, A. Ray, A. Seamster, and R. Vandenbosch, Phys. Rev. C33 (1986) 165.

39. J. Aichelin, Phys. Rev. C33 (1986) 537; C. Grégoire et al., in Phase Space Approach to Nuclear Dynamics, ed. M. di Toro (World Scientific, Singapore, 1980) and J. Aichelin, and G. Bertsch, Phys. Rev. C31 (1985) 1730.

40. A. Kyanowski, F. Saint-Laurent, D. Ardonin, H. Delagrange, H. Doubre, C. Grégoire, W. Mittig, A. Peghavre, J. Peter, Y.P. Viyogi, B. Zwieglinski, J. Québert, G. Bizard, F. Lefebvres, B. Tamain, J. Pochodzalla, C.K. Gelbke, W. Lynch, and M. Maier, Phys. Lett. 181B (1986) 43.

41. See for example J. Wilczynski, K. Siwek-Wilczynska, Y. Chan, E. Chavez, S.B. Gazes, and R.G. Stokstad, Phys. Lett. 181B (1986) 229 and references therein.

42. D. Guinet, R. Billerey, C. Cerruti, S. Chiodelli, and A. Demeyer, Phys. Lett. 137B (1984) 318.

43. R. Stokstad, Y.D. Chan, A. Dacal, A. Harmon, M.E. Ortiz, E. Plonol, J. Pouliot, N.C. Britt, D.J. Fields, G. Sangster, M. Webb, R. Roy, and L. Potvin, LBL 88-Inch Cyclotron Proposal, January 1987.

44. Yu. V. Melikov, Y.D. Otstavnov, and A.F. Tulinov, Zh. Eksp. Teor. Fiz. 56 (1969); Sov. Phys. JETP 29 (1969) 969; Yad. Fiz. (1970) 50, Sov. J. Nucl. Phys. 12 (1971) 27.

45. J.U. Andersen, A.S. Jensen, K. Jorgensen, E. Laegsgaard, K.O. Nielsen, J.S. Forster, I.V. Mitchell, D. Ward, W.M. Gibson, and J.J. Cuomo, Mat. Fys. Medd. Dan. Vid. Selsk. 40 (1980) no. 7.

46. J.U. Andersen, A.S. Jensen, E. Laegsgaard, K.O. Nielsen, J.S. Forster, I.V. Mitchell, D. Ward, and W.M. Gibson, Int. Symp. on Phys. and Chem. of Fission, IAEA-Sm/241-C7 (1979 IAEA: Jülich).

47. J.S. Forster, I.V. Mitchell, J.U. Andersen, A.S. Jensen, E. Laegsgaard, W.M. Gibson, and K. Reichelt, Nucl. Phys. A464 (1987) 497.

48. J. Gomez del Campo, D. Shapira, J.A. Biggerstaff, C.D. Moak, P.D. Miller, N. Neskovic, R.W. Fearick, and J.P.P. Sellschop, Phys. Rev. Lett. 51 (1983) 451.

49. C. Cohen in Relativistic Channeling, R.A. Carrigan Jr., and J.A. Ellison, Ed. (Plenum, New York) to be published.

50. P. Bonche, S. Levit, and D. Vautherin, Nucl. Phys. A436 (1985) 265 and S. Levit and P. Bonche, Nucl. Phys. A437 (1985) 426.

51. G.E. Beauvais, D.H. Boal, and J. Glosli, to appear in Nucl. Phys. A, and G.E. Beaunais, D.H. Boal, and J.C.K. Wong, Phys. Rev. C35 (1987) 545.

52. D.H. Boal, J. de Physique C4 (1986) 409.

53. See refs. 1, 50 and 54 for discussions and references.

54. C.K. Gelbke and D.H. Boal, Preprint MSUCL-584 (December 1986).

55. R. Wada, K.D. Hildenbrand, U. Lynen, W.F.J. Müller, H.J. Rabi, H. Sann, H. Stelzer, W. Trautmann, R. Trockel, N. Brummund, R. Glasow, K.H. Kampert, R. Santo, E. Eckert, J. Pochodzalla, I. Bock, and D. Pelte, Phys. Rev. Lett. 58 (1987) 1829.

56. B.V. Jacak, G.D. Westfall, C.K. Gelbke, L.H. Harwood, W.G. Lynch, D.K. Scott, H. Stöcker, M.B. Tsang, and T.J.M. Symons, Phys. Rev. Lett. B1 (1983) 1846.

57. G. Fai, L.P. Csernai, J. Randrup, and H. Stöcker, Phys. Lett. 164B (1985) 265.

58. J.P. Bondorf, J. de Physique C4 (1986) 263 and references therein.

59. J.P. Bondorf, R. Donangelo, H. Schulz, and K. Sneppen, Phys. Lett. 162B (1985) 30.

60. H.W. Barz, J.P. Bondorf, and H. Schulz, Phys. Lett. 184B (1987) 125.

61. B. Borderie, J. de Physique, C4 (1986) 251.

62. H.H. Gan, S.J. Lee, and S. Das Gupta, preprint.

63. G.F. Bertsch, H. Kruse, and S. Das Gupta, Phys. Rev. C29 (1984) 673 and H. Kruse, B.V. Jacak, and H. Stöcker, Phys. Rev. Lett. 54 (1985) 289.

64. S. Leray, J. de Physique, C4 (1986) 280.

65. H.-J. Keim, B. Kohlmeyer, H. Stege, H.A. Bösser, F. Pühlhofer, and W.F.W. Schneider, A. Phys. A327 (1987) 101.

66. Y. Patin, S. Leray, E. Tomasi, O. Granier, C. Cerruti, J.L. Charvet, S. Chiodelli, A. Demeyer, D. Guinet, C. Humeau, P. Lhenoret, J.P. Lochard, R. Lucas, C. Mazur, M. Morjean, C. Ngô, A. Peghaire, M. Ribrag, L. Sinopoli, T. Suomijärvi, J. Uzureau, and L. Vagneron, Nucl. Phys. A457 (1986) 146.

67. G. Auger, E. Plaguol, D. Jouan, C. Guet, D. Heuer, M. Maurel, H. Nifenecker, C. Ristori, F. Schussler, H. Doubre, and C. Grégoire, Phys. Lett. 169B (1986) 161.

68. W.G. Lynch, J. de Physique C4 (1986) 51, and references therein. A review is presented in ref. 54.

69. W.G. Lynch, C.B. Chitwood, M.B. Tsang, D.J. Fields, D.R. Klesch, C.K. Gelbke, G.R. Young, T.C. Awes, R.L. Ferguson, F.E. Obenshain, F. Plasil, R.L. Robinson, and A.d. Panagiotou, Phys. Rev. Lett. 51 (1983) 549.

70. D.H. Boal and J.C. Shillcock, Phys. Rev. C33 (1986) 549.

71. J. Pochodzalla, C.B. Chitwood, D.J. Fields, C.K. Gelbke, W.G. Lynch, M.B. Tsang, D.H. Boal, and J.C. Shillcock, Phys. Lett. 174B (1986) 36.
R.A. Dayras, Proc. Workshop on Heavy-Ion Reaction Dynamics studied with Large Counter Arrays, U. of Toronto (1987 March 26-27) p. 105.

72. J. Stachel, P. Braun-Munzinger, R.H. Freifelder, P. Paul, S. Sen, P. DeYoung, P.H. Zhang, T.C. Awes, F.E. Obenshain, F. Plasil, G.R. Young, R. Fox, and R. Ronningen, Phys. Rev. C33 (1986) 1420, and references therein.

73. H. Noll, E. Grosse, P. Braun-Munzinger, H. Dabrowski, H. Heckwolf, O. Klepper, C. Michel, W.F.J. Mueller, H. Stelzer, C. Brendel, and W. Rosch, Phys. Rev. Lett. 52 (1984) 1284, and references therein.

74. H. Heckwolf, E. Grosse, H. Dabrowski, O. Klepper, C, Michel, W.F.J. Mueller, H. Noll, C. Brendel, W. Rosch, J. Julien, G.S. Pappalardo, G, Bizard, J.L. Laville, A.C. Mueller, and J. Peter, Z. Phys. A315 (1984) 243, and references therein.

75. G. Bertsch, Phys. Rev. C15 (1977) 713.

76. L. Potvin, R. Roy, C. St-Pierre, and D. Horn, to be published.

77. J. Aichelin and G.F. Bertsch, Phys. Lett. B138 (1984) 350.

78. C. Gale and S. Das Gupta, Phys. Rev. C30 (1984) 414.

79. R. Shyam and J. Knoll, Nucl. Phys. A426 (1984) 606.

80. R. Shyam and J. Knoll, Nucl. Phys. A459 (1986) 732.

81. M. Prakash, P. Braun-Munzinger, and J. Stachel, Phys. Rev. C33 (1986) 937.

82. H.J. Pirner, Phys. Rev. C22 (1980) 1962.

83. D. Vasak, H. Stocker, B. Muller, and W. Greiner, Phys. Lett. 93B (1980) 243.

84. J.W. Norbury, F.A. Cucinotta, P.A. Deutchman, and L.W. Townsend, Phys. Rev. Lett. 55 (1985) 681.

85. M. Tohyama, R. Kaps, D. Masak, and U. Mosel, Nucl. Phys. A437 (1985) 739.

86. Nouvelles de Ganil, PE.10a Avril (1986).

87. L. Lee, T.E. Drake, D. Frekers, S.S.M. Wong, L. Buchnann, A. Galindo-Uribarri, R. Schubank, H.V. von Geramb, to be published in Phys. Lett. B.
C.A. Miller, A. Scott, R. Abegg, R. Helmer, K.P. Jackson, M. Whiten, S. Yeu, L. Lee, T.E. Drake, D. Frekers, S.S.M. Wong, R.E. Azuma, L. Buchnann, A. Galindo-Uribarri, J.D. King, R. Schubank, R. Dymarz, H.V. von Geramb, C.J. Horowitz, Phys. Lett. 169B (1986) 166.

R. Dymarz, Phys. Lett. 155B (1985) 5.
L. Rikus and H.V. von Geramb, Nucl. Phys. A426 (1984) 496.
F. Brieva and J. Rook, Nucl. Phys. A291 (1977) 299, 317 and Nucl. Phys. A297 (1978) 206.
D. Murdock and C. Horowitz, Phys. Rev. C35 (1987) 1442.

88. M. Trefz, A. Faessler and W.H. Dickhoff, Phys. Lett. 149B (1984) 459, and Nucl. Phys. A443 (1985) 499.

PART THREE: DESIGN AND PERFORMANCE

1. DESIGN GOALS

The Multidetector Array for Reaction Studies consists of a large vacuum vessel, a forward array of ΔE-E telescopes, and the attendant electronics and controls. The forward array is a complete, stand-alone spectrometer; however it may also be used in conjunction with other detector assemblies in the vacuum chamber. The array is readily removable for stand-alone operation of the chamber. The main performance criteria considered in the design of the array are:

- Efficiency (for detecting products from both peripheral and central collisions).
- Granularity (to avoid double hits in high-multiplicity events and to maximize event rate by reducing pileup).
- Detector response (thresholds, ion identification, energy resolution, and neutron response).
- Flight path (for time-of-flight resolution).
- Fast decision capability (when the array is used as an event tag).

It is also considered important that the facility be simple in construction, operation, and maintenance, and that it be compatible with coincidence experiments with large gas-filled detectors and provide scope for additional counter arrays.

Detailed discussions of these criteria can be found in subsequent sections of the proposal. Their optimization depends on the importance attached to the various types of experiments. Our highest priorities are the exclusive measurement of projectile multifragmentation and the characterization of central collisions by measuring the majority of the fragments emitted in each event. For this purpose, the efficiency and granularity of the array are the prime concerns, leading us to propose a total of 128 detectors, together covering a cone of about 38° half-angle. The types and sizes of the individual detectors, their distance from the target, and consequently the size of the vacuum vessel can then be determined from the performance criteria as discussed in the following sections. The most important design and performance specifications for the array and chamber are summarized in Table 1.

2. EFFICIENCY OF THE ARRAY

Since a major design criterion for the array is its efficiency for charged particle detection, this topic will be addressed in some detail. Plastic scintillator is essentially 100% efficient for detecting charged particles. In a practical calculation of array efficiency, however, this figure is reduced by many effects. The extent or solid angle of the array, the inactive area between modules, its low-energy threshold (punch-through energy for ΔE detectors), and its high energy cut off (punch-through energy for E detectors) all contribute to the array's efficiency factor in ways

TABLE 1: DESIGN AND PERFORMANCE SPECIFICATIONS FOR MARS

ARRAY

Geometry	"bull's eye" 8 rings, 16 segments each
Distance to target	variable, maximum 2 m
Inner (2°-4.5° @ 2 m) detectors	32 ΔE (only) fast plastic 0.5 mm thick
Outer (4.5°-38° @ 2 m) detectors	96 ΔE-E tapered phoswich, Fast/slow plastic 0.23 and 75 mm

Typical effective solid angles for light ions from collisions induced by a beam of 40 MeV/u heavy ions.

Laboratory frame	11% of sphere
Projectile-velocity source	92% of sphere
Intermed. velocity source	75% of sphere

CHAMBER

Geometry	Horizontal axis cylinder
Size	3 m (diameter) x 3.7 m
Material	Stainless steel
Operating pressure	1×10^{-6} Torr
Detector supports	Steel table set on 6 "hard points" supported independently of chamber walls.

that depend heavily on the reaction mechanisms producing the particles. These are considered in the first of the following subsections, which describes the geometrical aspects of the array's efficiency. The subsequent loss or mismeasurement of ions which do have the right trajectory and energy for detection is discussed in the second subsection.

2.1 Geometrical Efficiency

The array can operate at its normal distance of 2 meters from the target, or at a reduced distance, chosen in the following estimates to be 1 meter. In the former configuration the tapered detectors' sides point directly at the target; this configuration is ideal for the energetic, long-range light fragments emitted in projectile fragmentation events; the "dead" sections between detectors in this mode comprise less than 1% of the array solid angle. In the second configuration, the solid angle is greatly increased, making the array suitable for detection of ions from intermediate velocity sources. These ions generally have a shorter range, and thus a modest amount of masking (<2%) on the outer perimeter of each ring of detectors will serve to eliminate events which could be misidentified due to the incorrect detector taper at this distance. These minor losses for the two operating modes are neglected in the following discussion of the effective array efficiency for specific reaction types.

When light ions are emitted from a moving frame of reference, the fraction that is focussed into a forward cone of half-angle θ can be obtained by integrating the moving-source formulae[1] over the

cone angle and the lower and upper energy thresholds of the detector array to obtain the probability of particle emission.

Let us consider an array centered on the beam axis that detects particles emitted from a source moving in the direction of the beam. Then, in the laboratory frame, the non-relativistic energy spectra for particles emitted by this process may be obtained from the expression:

$$\frac{d^2\sigma}{d\Omega\, dE} = \begin{cases} N\sqrt{E-E_c}\, \exp\left(-\left[E - E_c + E_s - 2\sqrt{E_s}\,(E-E_c)\cos\theta\right]/T\right) & E>E_c \\ 0 & E\leq E_c \end{cases}$$

where E_c represents the Coulomb repulsion from the target, E_s is the laboratory kinetic energy of the particle at rest in the moving frame, T is the source temperature, θ is the detection angle defined from the beam axis, E is the energy of the detected particle and N is a normalization constant.

The fraction that is focussed into a forward cone of half-angle θ_M can therefore be obtained from:

$$P_c(\theta_m, \theta_M) = \frac{\int_{E_m}^{E_M}\int_{\theta_m}^{\theta_M} \frac{d^2\sigma}{d\Omega\, dE}\, \sin\theta\, dE\, d\theta\, d\phi}{\int_0^{\infty}\int_0^{\pi}\int_0^{2\pi} \frac{d^2\sigma}{d\Omega\, dE}\, \sin\theta\, dE\, d\theta\, d\phi}$$

where E_m and E_M represent respectively the low and high-energy cut-off of the detector for the particle considered, θ_m is related to the empty central cone of the array, and ϕ is the azimuthal angle. The parameters E_s and T are dependent on the reaction type:

1) Emission from an intermediate-velocity source

The parameters pertaining to evaporation from a mid-rapidity source are fairly well known. For example, the system $^{16}O + ^{197}Au$ has been extensively studied[4] and the results indicate that the source temperature can be calculated by

$$T = [2\, m_o\, v_s^2\, E_f/\pi^2]^{1/2}$$

where E_f is the Fermi Energy, m_o is the nucleon mass, and v_s is the velocity of the source, assumed to be half the beam velocity. For calculations of the typical efficiencies we chose $E_c = 10\ Z_f$ MeV to be the Coulomb repulsion from the target for the detected fragment having atomic number Z_f.

The results of the calculation are presented in Fig. 1 for protons, deuterons, tritons, and alpha particles emitted by the source. This calculation is for the system $^{16}O + ^{197}Au$ but the results are fairly independent of which system is chosen. The numerical integration was carried out for the angular cone of 4° to 65° that will be covered by the array when it is placed one meter away from the target. The calculated efficiencies range from 75% for protons to 90% for alphas.

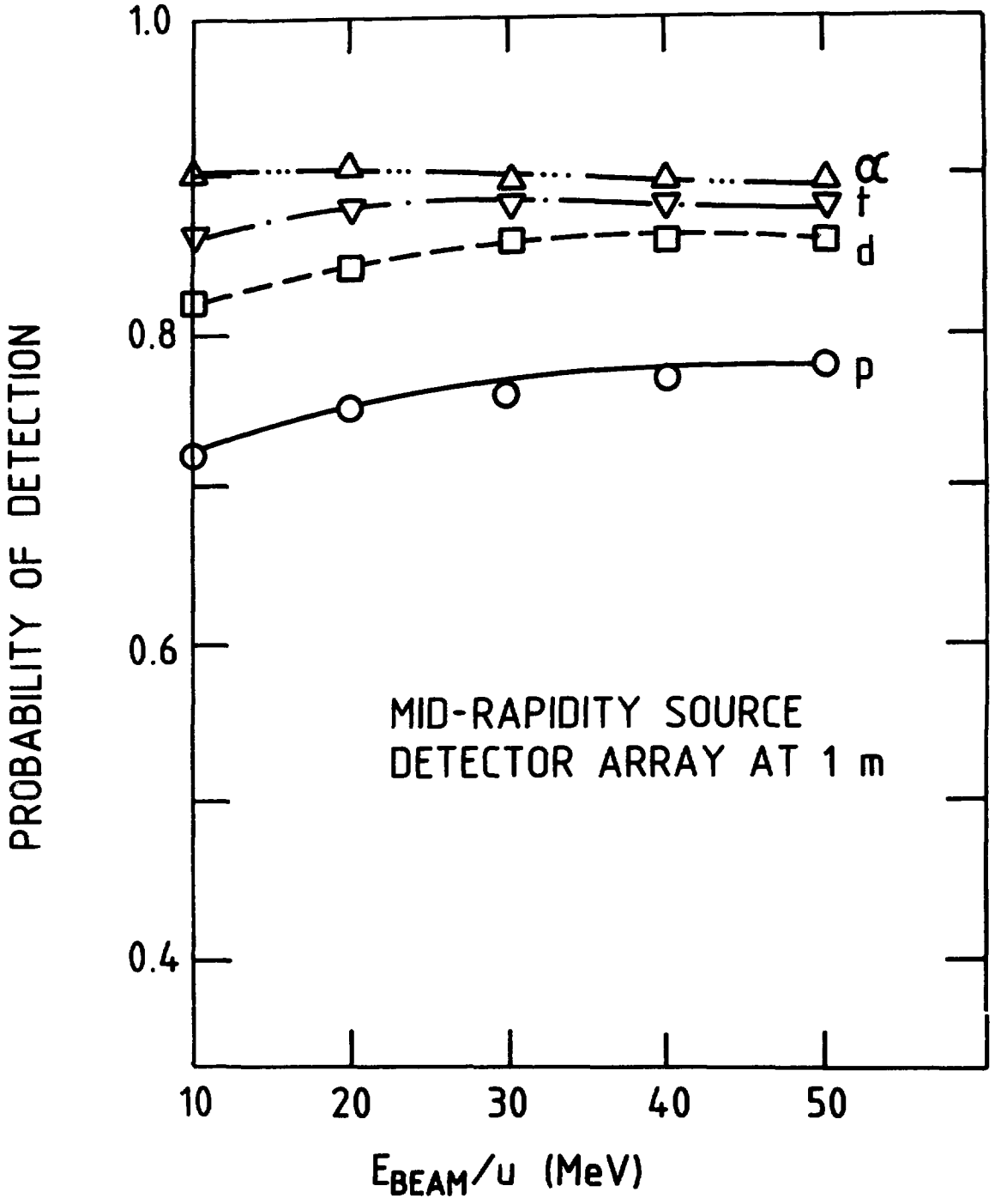

Figure 1. Calculated probability of detection as a function of beam energy for protons (p), deuterons (d), tritons (t), and alpha particles (α) emitted by a mid-rapidity source when the array is positioned 1 m from the target.

b) Projectile-like fragments

For this process the fragment velocity is ≈90% of the projectile velocity. Thus $E_s \simeq 0.8E \cdot M_f/A_{projectile}$ when E is the total beam energy and M_f is fragment mass. Also the temperature can to first approximation be scaled as $T \propto (E^*/A)^{1/2}$ for excitation energy E*.

For calculations of typical efficiencies shown in Fig. 2, we assumed E_c=0, and $T = 0.59\sqrt{E/u}$, which gives 4.1 MeV for E=48 MeV/u beam energy. The forward-angle cone from 2° to 38° will be covered when the array is placed 2 meters from the target. The low and high energy thresholds applicable to a 0.23 mm ΔE and 7.6 cm E plastic were determined from range-energy calculations and are given in Table 2. For beam energy between 15 and 50 MeV/u, the geometrical efficiency for detection of light ions from a projectile fragmentation process event is 85-95%.

2.2 Losses

The geometric efficiency discussed above gives only the probability that a particle will enter a detector. In order to give the full energy pulse height, the ion must spend all its kinetic energy stopping in the detector medium. Inelastic nuclear reactions of the particle with the nuclei of the detector and Coulomb scattering to trajectories that exit the detector are two processes that give a reduced energy signal. This is not only detrimental to the overall energy resolution, but may also cause misidentification of the particle or loss of the event. One must therefore know the magnitude of these two effects and minimize them wherever possible.

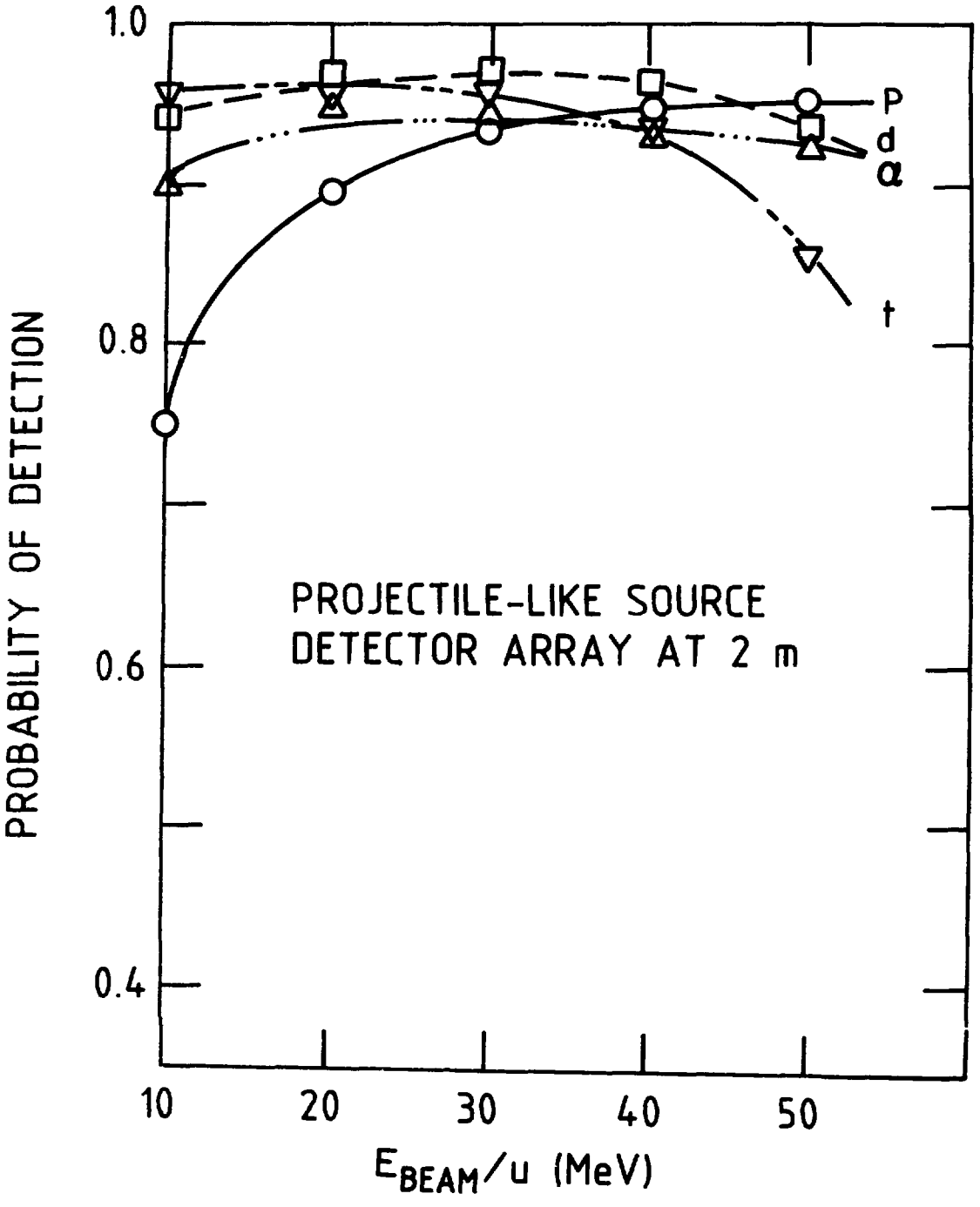

Figure 2. Calculated probability of detection as a function of beam energy for protons (p), deuterons (d), tritons (t), and alpha particles (α) emitted by a projectile-like source when the array is positioned 2 m from the target.

TABLE 2: ENERGY THRESHOLDS FOR 0.23 mm ΔE DETECTOR THICKNESS AND 76 mm E DETECTOR THICKNESS

Particle	Lower Threshold (MeV)	Upper Cut off (MeV)
p	4	105
d	5	140
t	6	170
^{4}He	16	420

"Reaction losses" result from the collision of the ion to be detected with a nucleus of the detector medium. In such a collision the ion's incident energy goes into Q-value, γ-rays, neutrons, or charged particles, thereby producing a reduced amount of scintillation. We have performed a calculation[3] for the ratio of reduced energy (tail) to full energy (peak) scintillation pulses. The calculation follows the method of Measday and Richard-Serre[4], dividing the particle range into cells of 0.1 g/cm^2 in length and obtaining the fraction of inelastic events by summing the reaction probabilities, p_i, in each cell. The fraction of reduced energy or "tail" events is then

$$f = [1 - \exp(-\Sigma p_i)].$$

Reaction cross sections were taken from the model of Karol[5], Coulomb-corrected for lower energies. The tail-to-peak ratio, $f/(1-f)$ as a function of energy, is plotted in Figure 3 for protons, deuterons, tritons, ^{3}He, and alpha particles in plastic. For example, at 50 MeV per nucleon, 8% of alpha particles and 4% of protons do not show full energy; for the two heavy hydrogen isotopes, the fraction is higher, though most "tail" events will not result in misidentification of the ion.

The multiple Coulomb scattering of ions by nuclei in the detector can cause ions to escape through the side of the detector. A calculation for a much smaller detector module has already been performed in reference 3. The projected angle, $\theta_{1/e}$ in radians was given by the equation

$$\theta_{1/e} = \frac{17.5 \text{ MeV/c}}{p\beta\sqrt{2}} \; Z_p \sqrt{\frac{T}{T_R}} \left[1 + 0.125 \log_{10}\left(\frac{T}{0.1\ T_R}\right)\right],$$

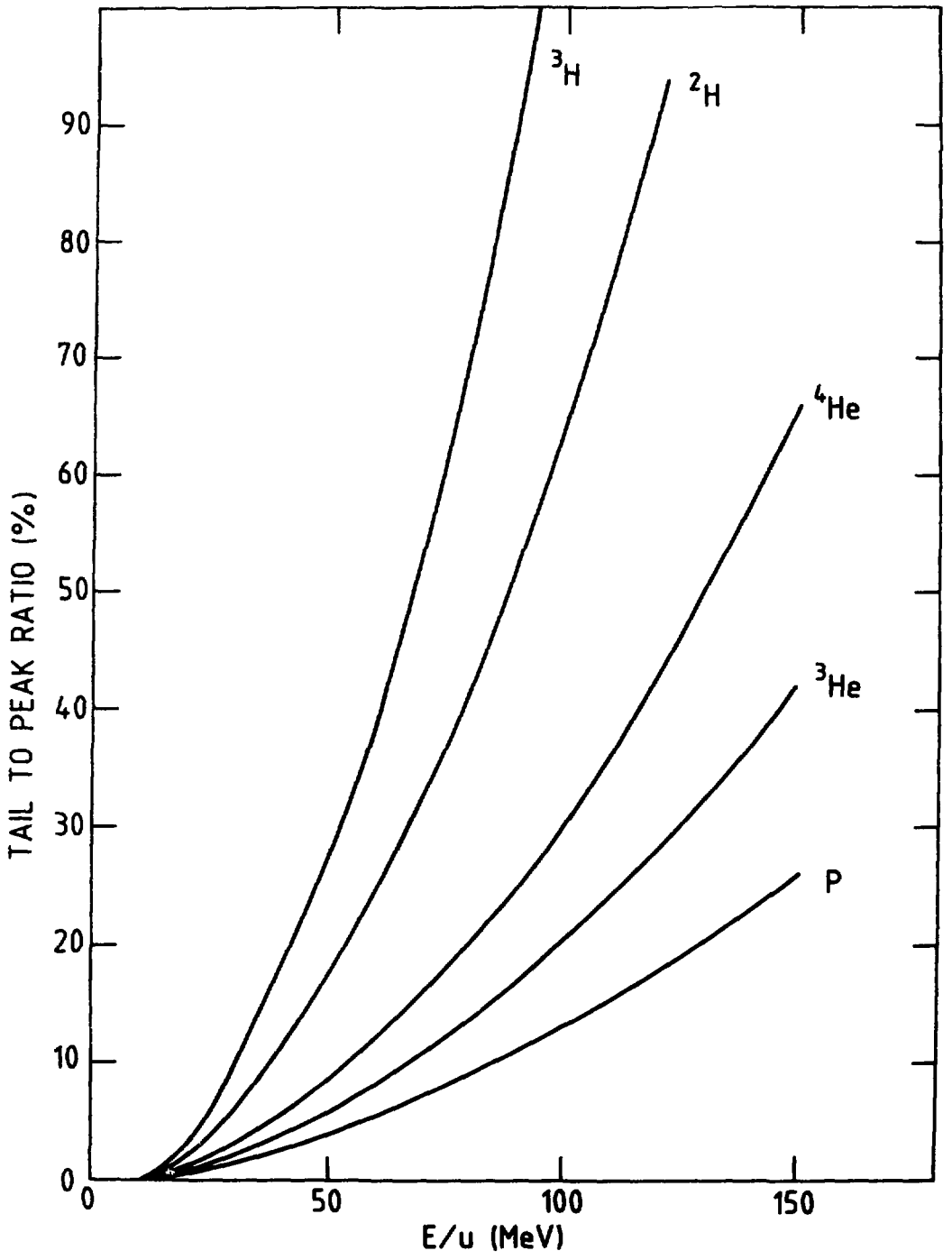

Figure 3. Particles lost (i.e. detected incompletely) due to inelastic reactions in the plastic scintillator, plotted as a function of the particle's energy. The loss of particles is expressed as a tail-to-peak ratio defined as f/(1-f), where f is the fraction of particles that undergo inelastic reactions.

where p, β, and Z_p are the momentum, velocity (v/c) and charge number of the incident particle, and T/T_R is the thickness in radiation lengths of the medium. A Monte Carlo simulation was then made of the scattering in a conically tapered detector with an active area of 5.4 cm^2. To first order, the number of particles that scatter out of the detector scales as the ratio of perimeter to active area for the detector. We have therefore chosen as a "worst case" to scale the calculations of reference 3 for our smallest phoswich detectors. They have a perimeter-to-area ratio more favorable by a factor of three. The result, again plotted as a ratio of tail events to full energy events, is shown in Figure 4. Even in this worst case, a triton of 50 MeV/u has a tail-to-peak ratio of less than 2%. We can therefore neglect this efficiency correction in most applications of the array. It is interesting to note that if the granularity of this detector ring had instead been obtained by placing smaller phoswiches of the same 1.5 millisteradian solid angle at a distance of 40 cm from the target, the corresponding number would have been 10%.

3. ARRAY RESPONSE TO HIGH-MULTIPLICITY EVENTS

3.1 Granularity

In both central and peripheral collisions one needs to characterize, as completely as possible, each collision on an event-by-event basis. The array efficiency discussed in the previous section is a prerequisite for such a characterization. Equally important is the granularity of the array; a very coarse-grained array would clearly be susceptible to a large number of double hits, i.e. cases in which two fragments from the same event strike one detector. Furthermore a coarse-grained array would have a very high

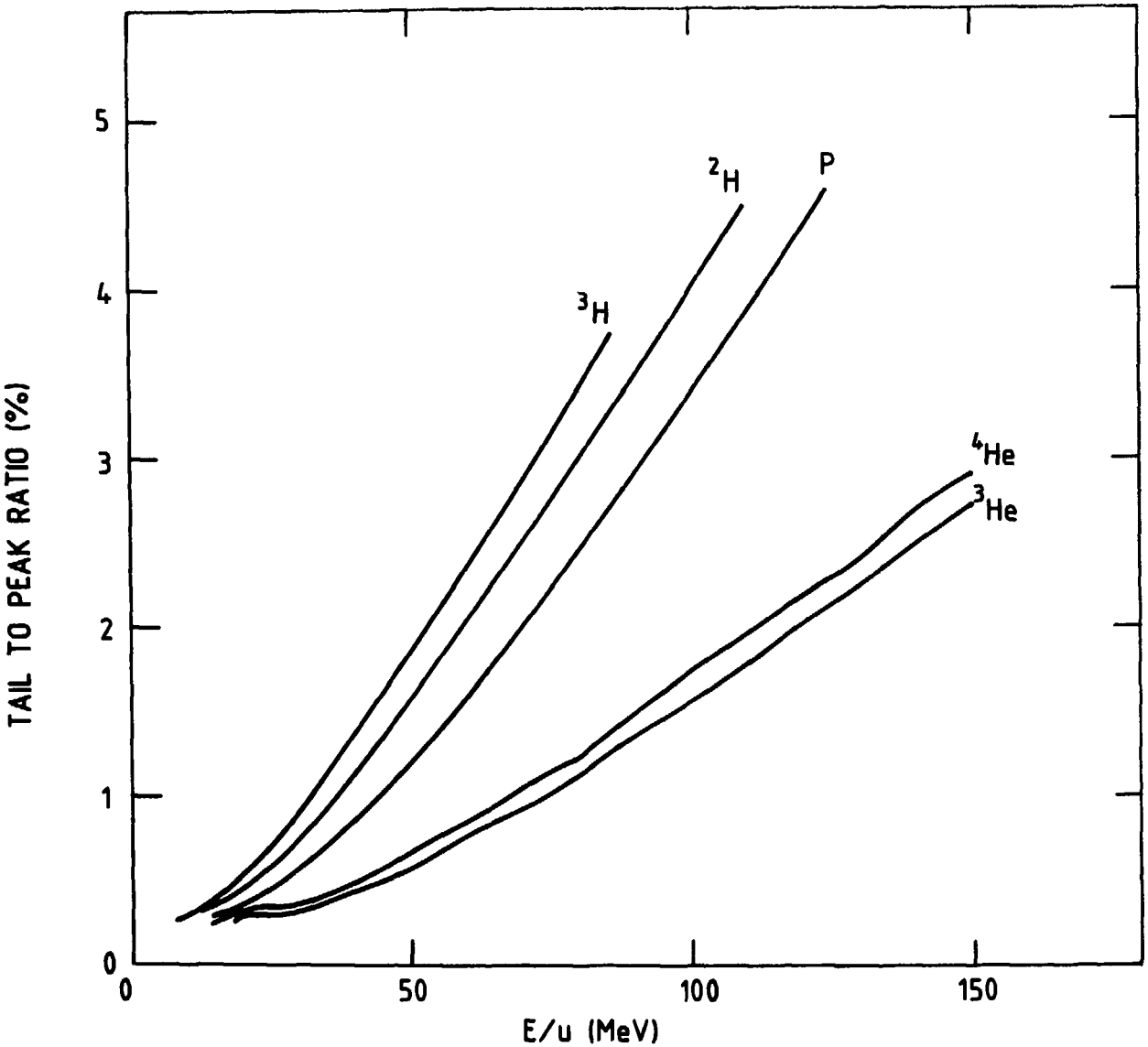

Figure 4. Loss of particles by multiple Coulomb scattering plotted as a function of the particles' energy. The amount of scattering out of the detector is expressed as a tail-to-peak ratio defined as in Figure 3. The fraction f of particles scattered out is calculated in a Monte Carlo simulation.

count rate in each detector element, thereby limiting the overall event rate by pileup considerations. On the other hand, a very fine-grained array would be impractical and uneconomical, both because of the large number of readout channels, and because the scattering-out losses discussed earlier would be severe. Solving the latter problem would require the detectors to have a large area but to be placed many meters from the target, necessitating an overly large scattering chamber. The questions of immunity to double hits and of multiplicity resolution must therefore be addressed in a quantitative and consistent fashion, and the array granularity optimized for the most important types of experiments.

Quantitative calculations of response to high-multiplicity events are best performed by Monte Carlo simulations. A computer program originally written to calculate gamma ray detector response has been modified for this purpose[6]. Given values of source temperature, source velocity, fragment multiplicity, and detector granularity, the program provides distributions of fragment energies in the moving frame, fragment angular distributions in the moving and laboratory frames, and distributions of the events in terms of "fold" or number of separate detectors triggered. Unit efficiency, 4π steradian solid angle, and constant laboratory frame detector granularity are assumed. Since realistic source parameters are needed, we have used the results of Brummond et. al.[7], who measured the velocities and "temperatures" (or energy spectrum slope parameters) for the three moving sources in the reaction of 48 MeV/u ^{20}Ne on a gold target.

3.2 Performance in Peripheral Collision Experiments

In a projectile multifragmentation experiment, it is important to collect all projectile-like components, to permit reconstruction of the primary fragment. This constitutes a more stringent requirement on the granularity than does event-by-event extraction of an approximate ($\pm$ 1) multiplicity. Therefore the multiplicity response should not be taken as an end in itself, but rather as a benchmark indicating how well we avoid double hits. We use the moving source parameters v = 0.29 c and T =4.1 MeV. We also assume that one seldom encounters projectile fragment multiplicities greater than 5. (In the data of figure 5 from the reaction of 40 MeV/u ^{14}N on a gold target [8] one sees that the fourfold events are a factor of 200 less intense than the twofold events. This is partly because the small array used did not cover the full solid angle for fragmentation; nevertheless the rapid falloff for higher K is evident.)

Figure 6 shows the results of the Monte Carlo simulation for 500 projectile fragmentation events at a number of values of detector granularity, which is expressed in terms of detector half-angle, $\theta_{1/2}$ (i.e. one-half the angle subtended by a circular detector). One sees from panel a) of the figure, that for detectors with an average half angle, $\theta_{1/2} \approx 3°$, about 90% of the events are free of double hits. From the angular distribution in panel b) of the figure it is apparent that most of this double hit probability comes from the region $\theta_{lab} \lesssim 20°$ where the number of particles per solid angle is the greatest. These results have been coupled with a desire to spread the high counting rate from elastic scattering over many

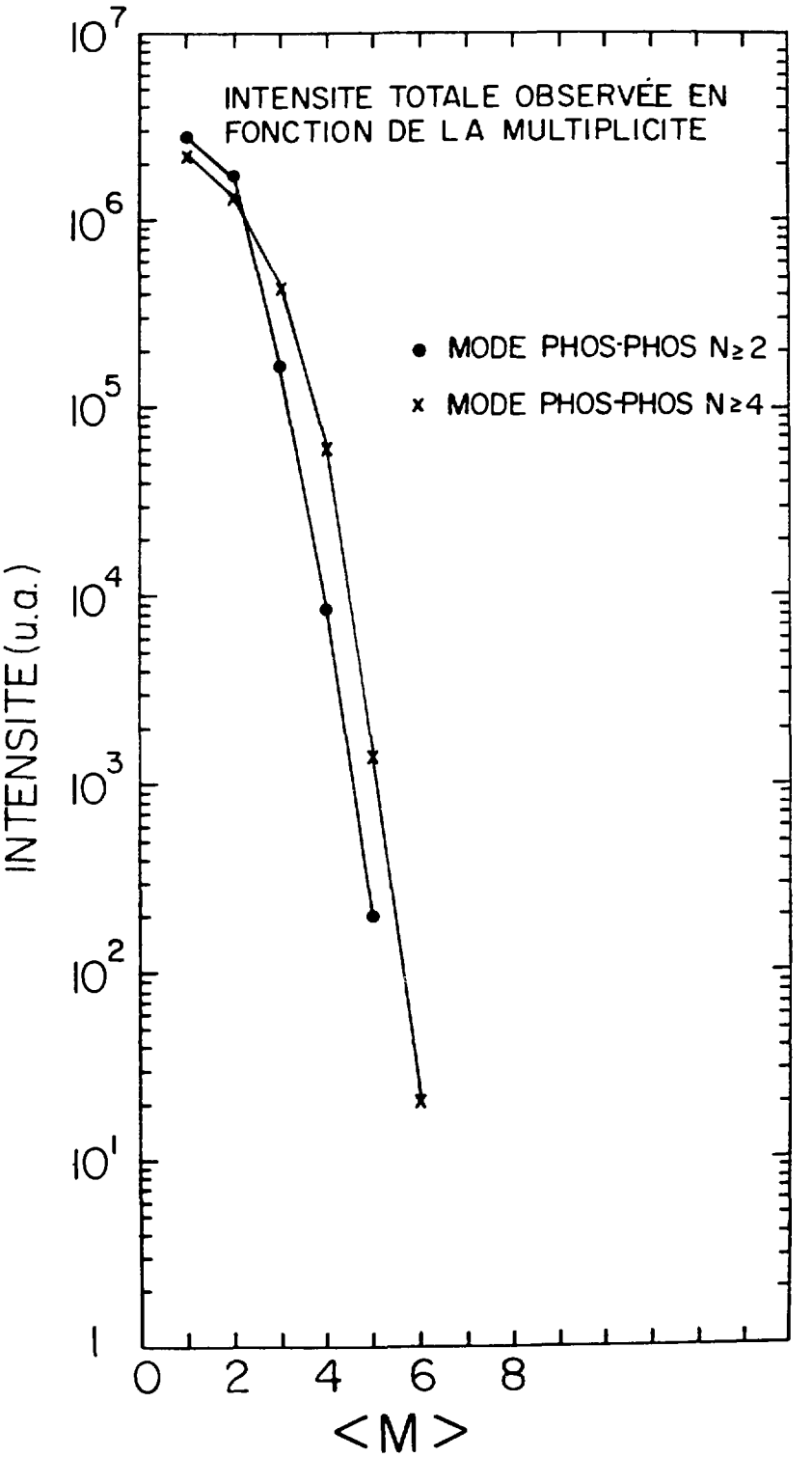

Figure 5. Multiplicity spectrum for the reaction of 40 MeV/u ^{14}N with a gold target. The fragments ($1 < Z < 7$) were detected in an array of 32 phoswich detectors covering a solid angle of 0.214 sr. and centered at 12.5° with respect to the beam direction.

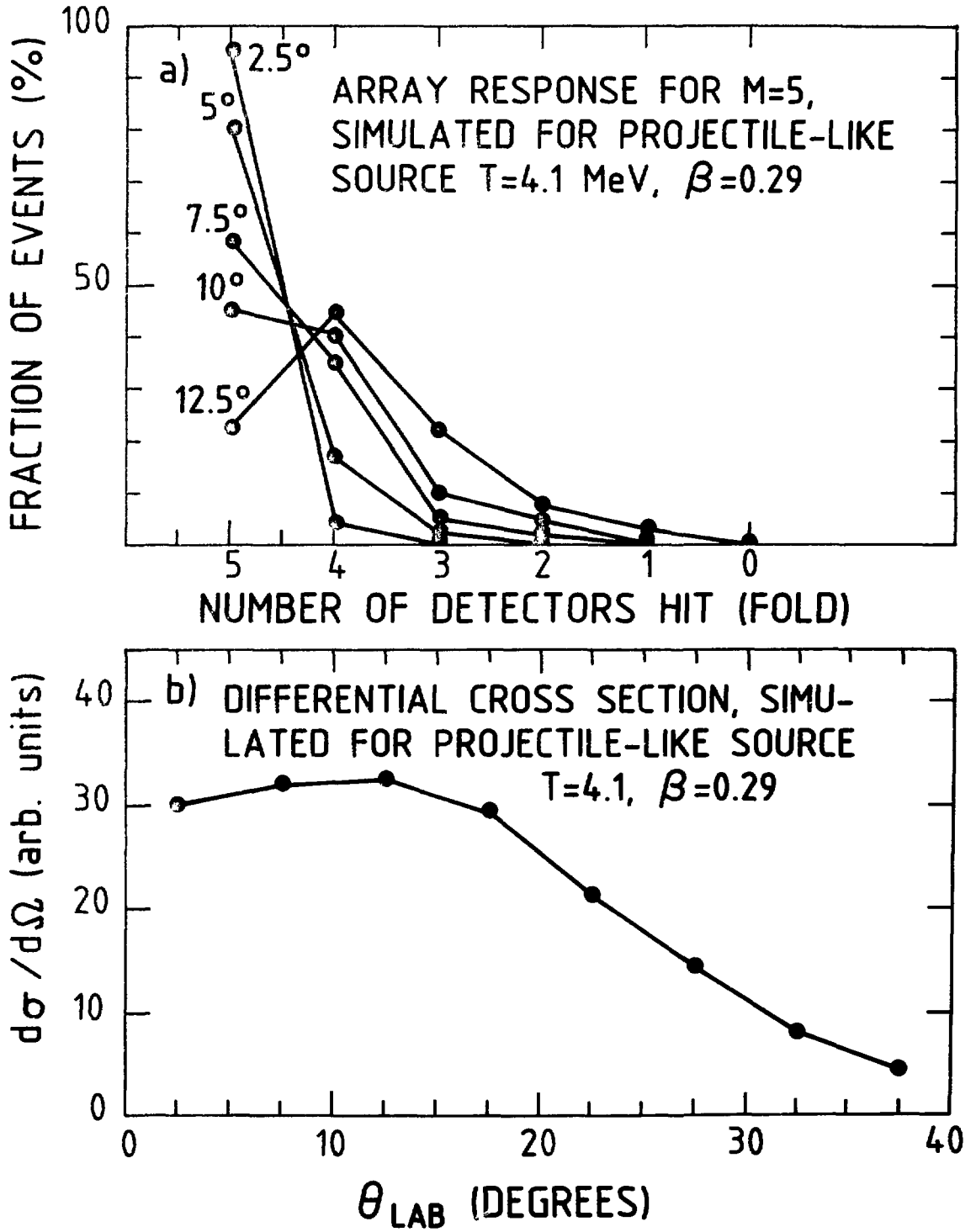

Figure 6. Simulation of projectile-like source events:

a) Monte Carlo simulation of the number of detectors hit by a typical projectile fragmentation event of multiplicity 5. The response of the array is shown as a function of the individual detector half-angle.

b) Differential cross section for the particles emitted from a projectile-like source at a temperature of 4.1 MeV and a velocity of 0.29 C.

detectors inside the grazing angle (typically 5-10°) and, consequently, detector solid angles increase with θ_{lab}. Other considerations include azimuthal symmetry and the efficiency of light collection from the scintillators. The latter requirement favors detectors with widths comparable to their lengths. An array geometry consisting of 8 concentric rings, each divided into 16 segments of 22.5° each satisfies the above needs. The dimensions are listed in Table 3. As may be seen from the table, $\theta_{1/2}$ for MARS detectors increases with θ_{lab}, ranging from less than one degree at very forward angles to about 4 degrees for the outermost ring.

3.3 Performance in Central Collision Experiments

The study of central collisions requires selection of high-multiplicity events having no projectile-like component. The latter condition can be assured with a forward array by requiring an anticoincidence with beam-velocity particles near the grazing angle; the former is more difficult. The array has been optimized for projectile fragmentation experiments. Nevertheless, Monte Carlo simulations demonstrate that it is also possible to characterize central collisions on an event-by-event basis by taking advantage of the "close geometry" option of the array. With a 1-m distance to the target, the detector granularity and the time-of-flight mass resolution degrade by a factor of four. On the other hand, compared with a projectile fragmentation experiment, a source moving with one-half the beam velocity has less stringent requirements in these quantities. We look now at an intermediate-velocity source (v = 0.19 c and T = 11.9 MeV, taken from ref. 7). The efficiency

TABLE 3: ARRAY GEOMETRY: 8 RINGS OF 16 SEGMENTS EACH

Ring No.	Angular Range (deg.at 2 m)	Solid Angle per Detector Ring (sr.)	Detector Type
1	2 - 3	0.0049	ΔE only (fast plastic)
2	3 - 4.5	0.0108	
3	4.5 - 6.75	0.0242	ΔE/E phoswich (fast/slow plastic)
4	6.75 - 10	0.0519	
5	10 - 15	0.1186	
6	15 - 22.75	0.2747	
7	22.75 - 30.5	0.3806	
8	30.5 - 38.25	0.4795	

factors for the array located one meter from the target were discussed in section 2; the multiplicity response to 500 simulated events, each with M = 10, is shown in figure 7a). Again, unit efficiency and 4 π steradian solid angle is assumed in the calculation. In fact, we see from the angular distribution that about 75% of the emitted fragments are within the 65° covered by the array. The differential cross sections (panel b), multiplied by the detector solid angle, give a relatively uniform counting rate for $20° \leq \theta \leq 65°$. The simulated rate for $\theta \leq 20°$ drops rapidly with decreasing values of θ. The limiting case for multiplicity response at 1 σ is therefore taken at $\theta \approx 40°$, where the detector half-angle is 7.5°. It is possible to estimate analytically the effect of a 75% efficiency factor on a multiplicity response curve such as that for 7.5° in panel a) of the figure. The result is the dashed curve, peaked at "fold" K = 7.5, with a full width at half maximum corresponding to ± 25% in multiplicity. Thus, one can obtain, on an event-by-event basis, an approximate value of the particle multiplicity to use as a trigger in a central collision experiment. (Clearly a measurement of the average multiplicity summed over many events, namely <M>, could be obtained with much greater precision by simply deconvoluting a high-statistics multiplicity spectrum). Combining the forward-angle anticoincidence with a multiplicity trigger and adequate space to mount gas-filled detectors for intermediate-mass fragments provides a powerful central collision facility, matched only at MSU and GANIL; of those laboratories, GANIL relies exclusively on ΔE measurements, and MSU lacks a forward array.

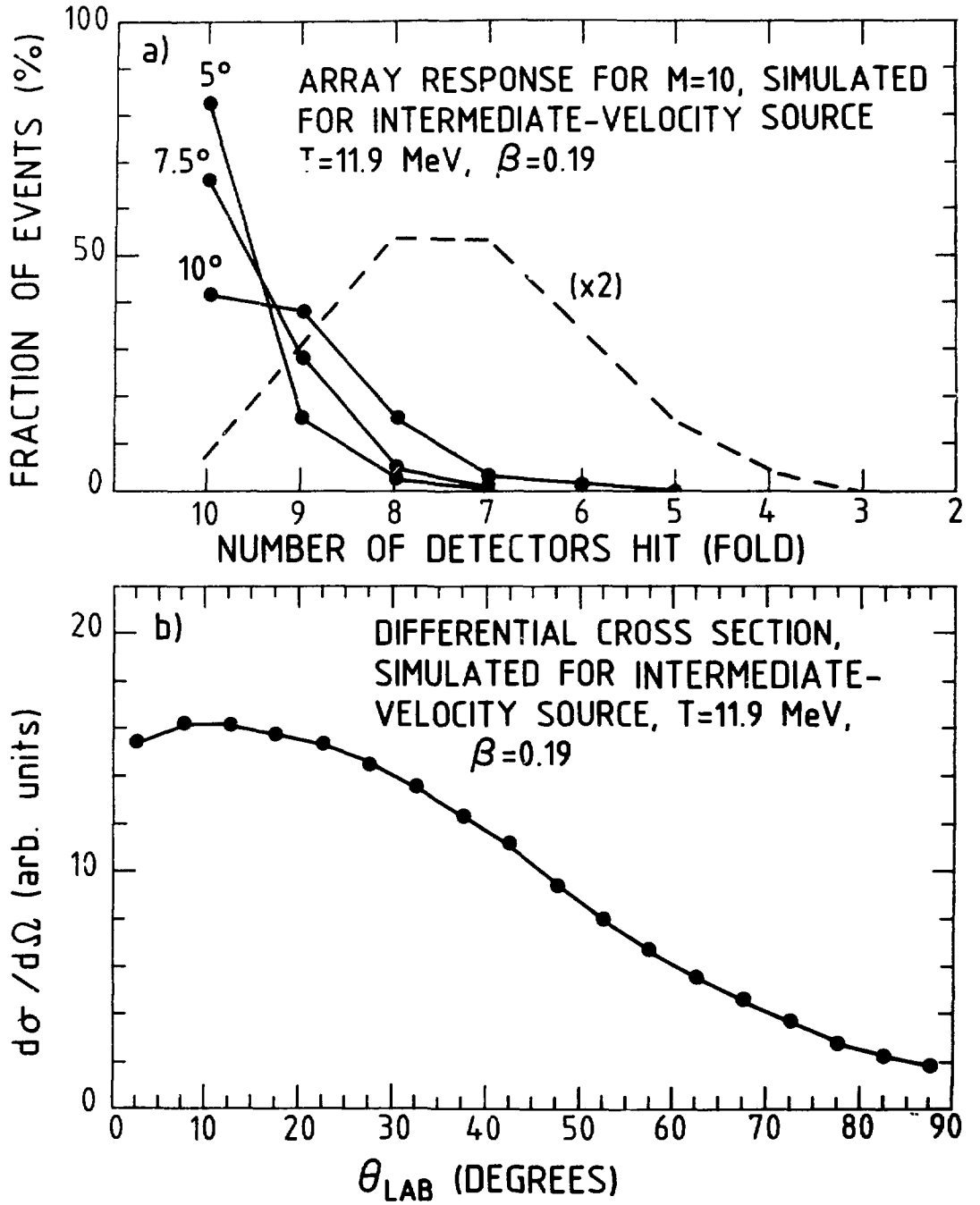

Figure 7. Simulation of intermediate-velocity source events:

a) Monte Carlo simulations showing the number of detectors hit by a typical intermediate-velocity source event of multiplicity 10. The response of the array is shown as a function of the individual detector half-angle. The dashed curve indicates the multiplicity response when the geometrical efficiency of the array, evaluated at 75%, for this reaction is taken into account.

b) Differential cross section of the particles emitted from an intermediate-velocity source at a temperature of 11.9 MeV and a velocity of 0.19 c.

4. THE DETECTORS

This section discusses the design of an individual detector module, its resolution in E, Z, and A, its neutron response, and its stabilization system.

4.1 Design

Each detector module located between the angles of 4.5 and 38 degrees is a ΔE-E telescope consisting of two plastic scintillators. The ΔE component is a "fast" plastic such as NE-102A or BC-400, and the E detector is a "slow" plastic such as NE-115 or BC-444, which have decay times on the order of 2.4 ns and 200 ns, respectively. The two scintillators are viewed through a lucite light guide by a single photomultiplier tube in a phoswich arrangement similar to that pioneered by the Berkeley Plastic Ball group.[9] A schematic illustration of a typical detector module is shown in Figure 8, along with an indication of how a single photomultiplier pulse can be integrated over two different time windows to obtain values proportional to both E and ΔE. The detector pictured is from the annulus which covers 10 to 15 degrees; note that its sides taper slightly to focus at a 2-m target distance. Phoswiches for the rings forward of 10° are being manufactured independently of this proposal.

The detectors of the two innermost rings, from 2 to 4.5 degrees are not phoswich detectors. These are ΔE detectors only, made of fast plastic scintillator, 0.5 mm in thickness. Because of total particle dose and count rate considerations, this detector type has been chosen for the most forward angles. Specific reasons include the reduction in pileup for fast plastic relative to slow plastic

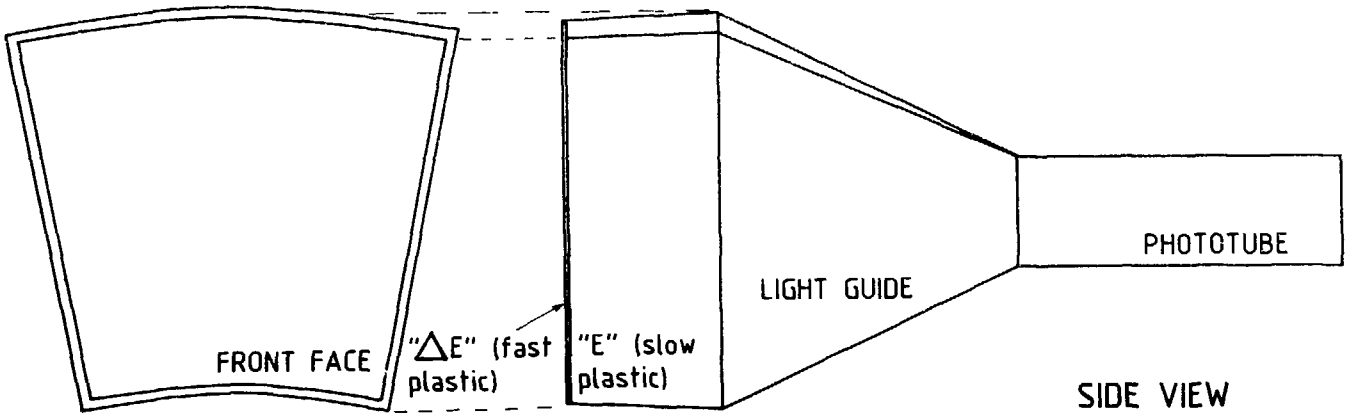

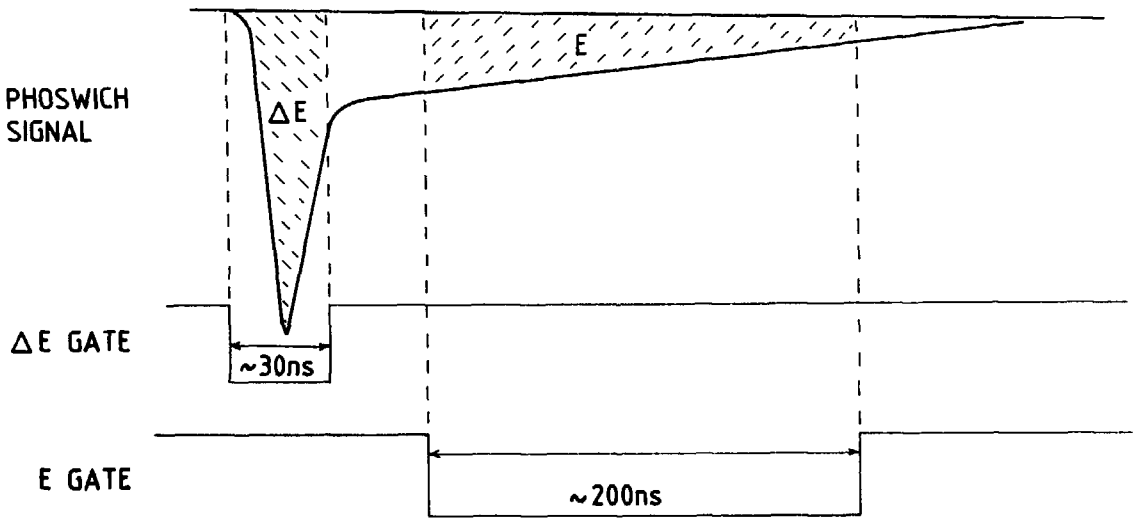

Figure 8. Schematic illustration of a typical phoswich detector module of the array. The lower portion of the figure shows the extraction of E and ΔE from the phoswich signal with independent time windows. Alternatively, the "E" gate may be long (≈700 ns) and encompass the total E+ΔE analog signal.

and the reduction in radiation damage when particles are allowed to exit the back of the detector without stopping.

4.2 Resolution

The response of phoswich detectors to radiation has been detailed in a number of publications.[10] Our prime concerns include the detection threshold, determined by the thickness of the ΔE element, the Z resolution, which is also largely determined by the ΔE thickness (but conflicts with the desire for a low threshold), the energy resolution which is strongly influenced by light collection, and the mass resolution, which depends on a combination of timing and energy resolution.

The detection threshold for light ions should fall below 5 MeV per nucleon. This is necessary if we wish to observe a significant number of light ions emitted by a mid-rapidity source from a 20 MeV/u collision. Figure 9 shows the energy losses calculated for a variety of ions and energies in a 0.23-mm ΔE scintillator followed by a 75-mm E scintillator. The black dots indicate the points at which the particle's range exceeds the thickness of the detector telescope; for protons and alpha particles this occurs at about 100 MeV per nucleon. The detection thresholds for protons and alpha particles are at 3 and 4 MeV per nucleon, respectively. Equally important is the array's ability to detect projectile fragments. For ^{9}Be, ^{16}O, ^{40}Ca and ^{79}Br, the thresholds are 5, 8, 11, and 12 MeV per nucleon, respectively. It should be noted that unit resolution in element number for a heavy ion like ^{79}Br will not be obtained due both to saturation effects and dynamic range problems. Phoswich spectra showing the uniformity possible with four matched detectors are

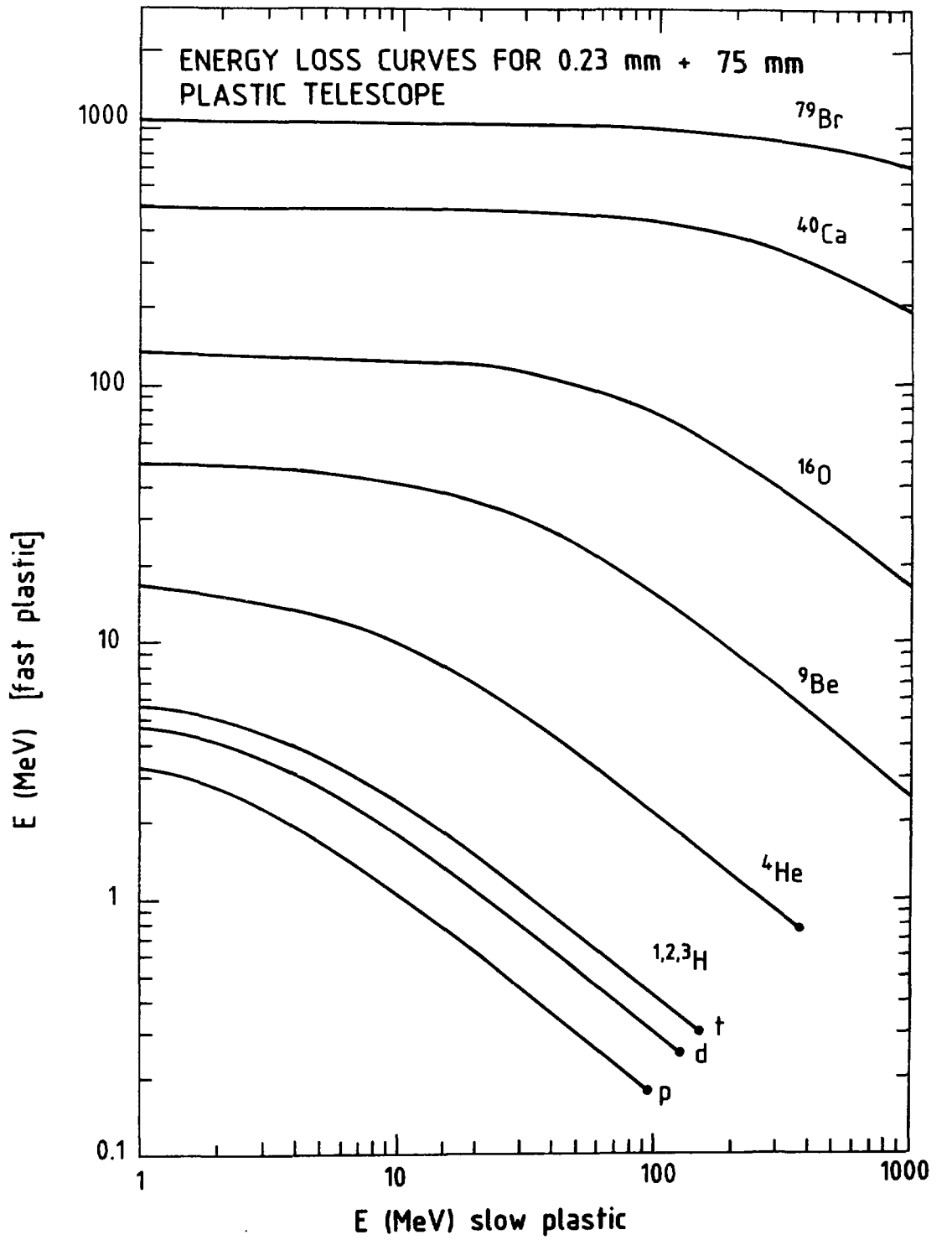

Figure 9. Energy loss in the fast plastic scintillator (thickness 0.23 mm) vs energy loss in the slow plastic scintillator (thickness 75 mm) for various ions.

displayed in Figure 10. The data are taken from trials of a zero-degree fast/slow phoswich test module built by members of the MARS collaboration as a four-segment annulus (1.5 mm ΔE, 76 mm E), analogous to the 16-segment rings proposed here. A 5 MeV/u ^{28}Si beam on an aluminum target produced the light ion spectra shown in the figure. The clear isotope resolution for hydrogen seen in the figure will not be found in the production array modules because of their thinner ΔE. However, even for a ΔE detector thinner[11] than those for MARS, unit Z resolution is obtained for elements heavier than aluminum. In fact, a ΔE detector of only 0.1 mm[12] gives satisfactory Z resolution in most cases (see Figure 11). We then have the option, when complete light-ion identification is needed, to use the energy information in conjunction with the flight time to obtain the mass.

The energy resolution of the detectors is a weighted combination of $\sigma_{\Delta E}/\Delta E$ and $\delta E/E$. The former term, which is the worse of the two at typical values[9,10] of 10-15% for low-amplitude signals, only contributes significantly to the overall resolution near the detector threshold. The major component of the energy resolution comes from the thick plastic scintillator and depends chiefly on the light collection efficiency. Typical resolution values range from 2 to 5% for light ions of 10-100 MeV/u. Figure 12 shows our measurements[3] of the deuteron energy spectrum from the reaction ^{2}H(^{14}N, ^{2}H)^{14}N at 6.6 MeV/u. The detector was a phoswich with a 2-inch RCA 4856 phototube. The elastic peak, labeled (A), corresponds to 39-MeV deuterons and has a full width at half maximum of $\delta E/E$ = 3.6%. Peaks (B), (C), and (D) represent excitations of 2.3, 4.0, and 5.0 MeV in ^{14}N. An energy resolution of 5% is specified for protons and alpha particles at 50 MeV/u in this proposal.

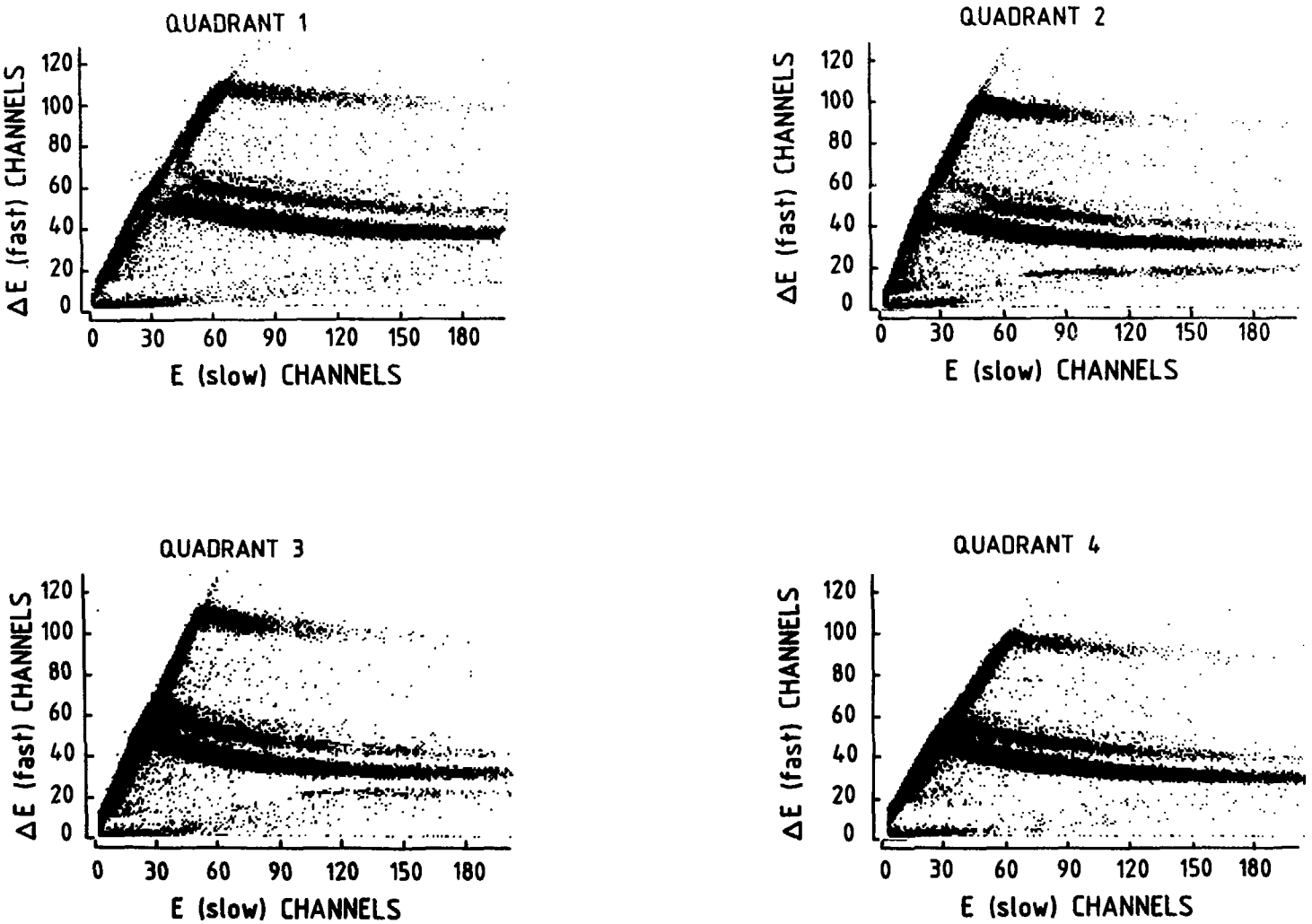

Figure 10. ΔE – E phoswich spectra obtained with our fast/slow phoswich test module built as a four-segment annulus. The three closely spaced bands are H isotopes. The top band is due to He.

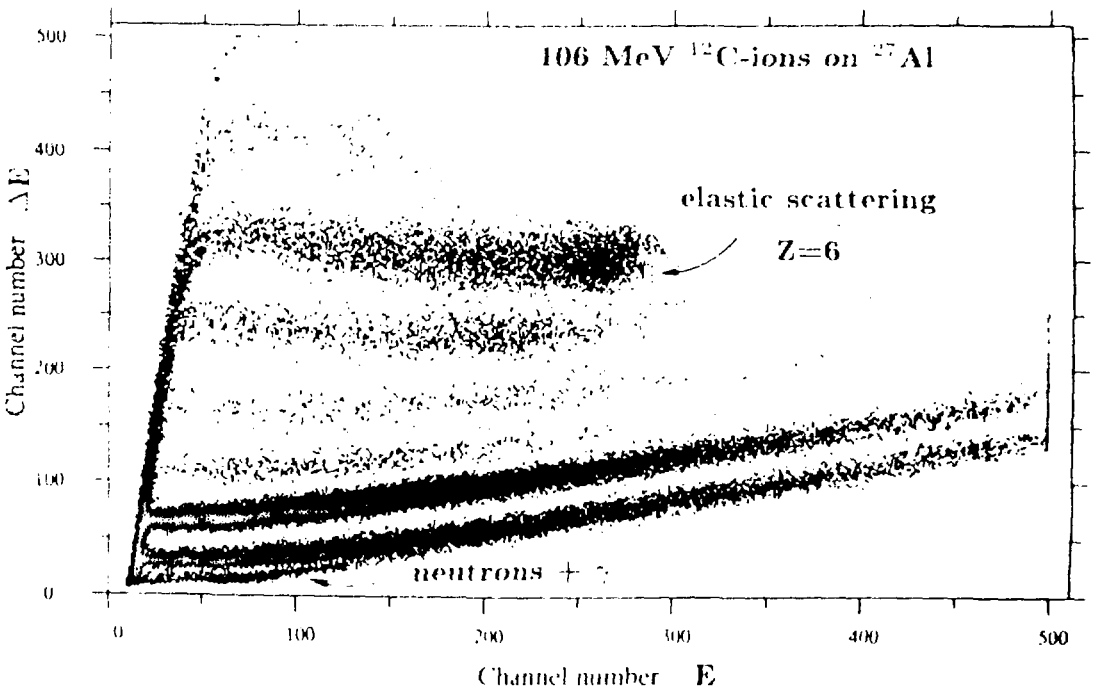

Figure 11. ΔE - E phoswich spectra obtained with a thin ΔE detector (0.1 mm) (from ref. 11).

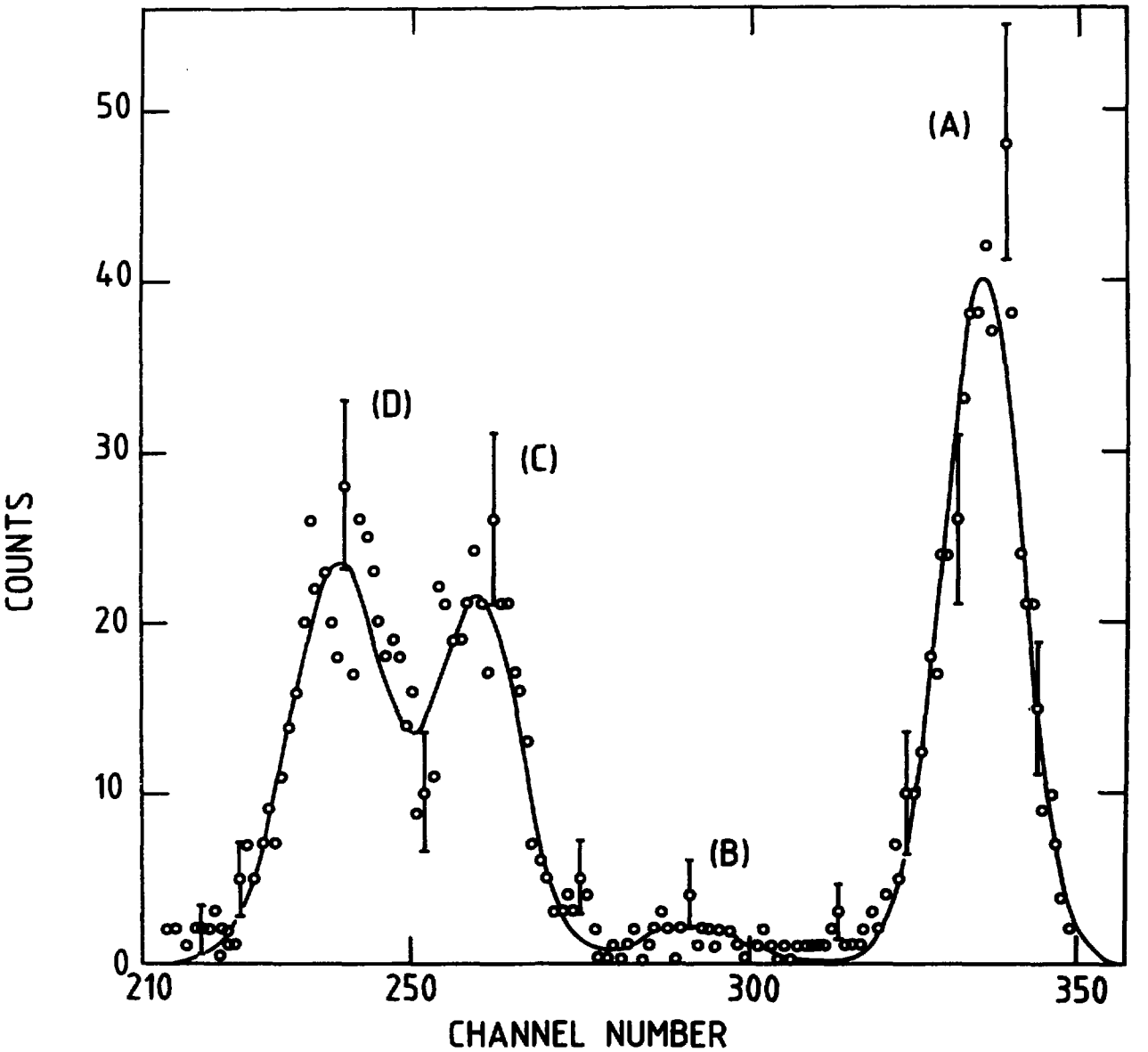

Figure 12. Deuteron energy spectrum from the reaction ^{2}H (^{14}N, ^{2}H)^{14}N at 6.6 MeV/u obtained with a slow/fast phoswich. Peaks (a), (b), (c), and (d) correspond respectively to deuterons of 39 MeV (elastic peak), 36.7 MeV, 35 MeV, and 34 MeV.

If the energy and time resolution are adequate, a time-of-flight determination may be made of the particle's mass. The mass of an ion is proportional to its energy multiplied by the square of its flight time for a fixed distance. Neglecting minor differences in flight distance, this leads to an expression for mass resolution,

$$\delta A/A = [(\delta E/E)^2 + (2\ \delta T/T)^2]^{1/2} \quad ;$$

our flight distance is two meters under normal operation and one meter in "close geometry" mode, used mostly in reactions for which one would expect somewhat slower fragments. The specified energy resolution is 5% and the duration of cyclotron beam bursts at our target location, specifically chosen for its good timing and focus properties, should fall between 0.25 and 0.5 ns, depending on the specific beam type and energy. The phoswich detector timing should ordinarily be better than 1 ns. Table 4 lists the various values of $\delta A/A$ attainable in the large chamber with the phoswich array for three values of overall time resolution. Clearly there is no problem separating the isotopes of light ions under any circumstances. The mass resolution for medium-mass fragments at projectile velocity (2-m flight path) and intermediate velocity (1-m path) depends mainly on the detector timing. Isotopic identification for ions in the oxygen region is attainable with sub-nanosecond timing. If mass resolution of heavier ions is needed, specialized detectors can be inserted to take advantage of the long flight path permitted by the chamber. High-resolution counters, e.g. individual start and stop detectors for timing and Si(Li) detectors or ion chambers for energy could be introduced. For example, a system with 0.25 ns overall time resolution and 0.5% energy resolution will give isotopic identification for a 5-MeV/u A=100 fragment.

TABLE 4: MASS RESOLUTION BY TIME-OF-FLIGHT ASSUMING δE/E = 5% FOR 1- AND 2-METER FLIGHT PATHS

FRAGMENT E/n (MeV)	FLIGHT TIME (ns)	MASS RESOLUTION, ΔA/A, in percent for various assumed values of time resolution: Δt = 0.5 ns	Δt = 1.0 ns	Δt = 2.5 ns
1-m FLIGHT PATH:				
1	73	5.2	5.7	8.6
5	32	5.9	8.0	14.8
20	16	8.0	13.5	31.6
50	11	10.4	18.9	45.7
2-m FLIGHT PATH:				
1	144	5.0	5.2	6.1
5	64	5.2	5.9	9.3
20	32	5.9	8.0	16.4
50	21	6.9	10.8	24.3

4.3 Neutron Response

Though the main purpose of the array is to detect charged particles, not neutrons, there may be occasions when detection of coincident neutrons is not only useful, but also feasible with the array proposed here. Spectroscopy of neutrons provides information on the properties of an emitting source, unperturbed by final-state Coulomb interactions.

The organic scintillator used for the E detector in the phoswich modules is thick enough to have a reasonable probability for intercepting neutrons. Information about the neutron signals would permit evaluation of neutron emission itself or in some cases assessment of the neutron contamination in the proton spectra. Particularly at higher energies, because of the very thin ΔE scintillator the neutron and proton lines are closely spaced in ΔE-E spectra. Consequently it is desirable to understand the response of the phoswich to neutrons and investigate the available techniques for identification of neutron signals. Since a neutron has no charge, its detection results from the ionization produced by the charged products of its nuclear interactions. In organic scintillators these interactions nearly always occur with hydrogen and carbon nuclei, producing protons, alpha particles, heavier ions, and possibly secondary neutrons, which may interact again if the scintillator size is larger than or comparable to the neutron mean free path. Figure 13 shows typical values of the neutron detection efficiency calculated from the total light generated in the scintillator. The efficiency is defined as the probability that the total light produced in a 10 cm thick BC 444 scintillator is greater than the trigger threshold. The neutron interaction probability in the thin fast ΔE scintillator is negligible.

The physical dimensions of the phoswich modules (0.23 mm fast ΔE and 75 mm slow E scintillators) and the planned mode of operation with multiparameter time-of-flight (TOF)and pulse-height recording would enable us to explore three complementary techniques for particle identification of neutrons:

- The ΔE-E signal correlation will distinquish between the charged particles and neutrons or gamma-rays. In the case of neutrons there will be no signal from ΔE due to the negligible probability of interaction in the thin plastic. The proton recoils for the E detector will not travel backwards. However, some alpha particles from the C(n, 3α) reaction may produce detectable ΔE signal at higher neutron energies. Also, practical requirements of a finite signal threshold to offset electronic noise will limit the range of applicability of this technique.
- The TOF technique will provide identification between particles of different masses and energies. The only degeneracy would be between protons and neutrons. The 1 and 2 meter flight paths will give adequate TOF separation between gammas and neutrons. The TOF resolution has been discussed earlier in this section. The practical limitation of this technique will be the time resolution of neutron pulses that come predominantly from the slower E scintillator. Furthermore the TOF information above will not identify a neutron from a proton of the same energy.

- The pulse height - TOF correlation will provide excellent separation between the signals from protons and neutrons. The protons will lose almost all their energy in the E scintillator giving a total energy pulse height amplitude of finite resolution that will be correlated with the TOF amplitude. However for neutrons, the probability of complete energy transfer to the recoiling charged particle responsible for the scintillation is low. Consequently the observed pulse heights will be much smaller than those for a proton of an equivalent TOF.

Any combination of the above complementary techniques could be used, either on-line or during off-line analyses, to provide identification of the neutron signals.

For experiments that require information on neutron energy spectra it may be feasible to replace some of the fast/slow phoswich modules with slow/fast modules of equivalent dimensions. This would improve the TOF resolution of neutron events.

The overall neutron detection efficiency then depends on the scintillator dimensions and on the threshold setting of the electronics that is necessary to avoid random triggering on noise. The practical threshold setting will depend on the background environment, the beam intensity and, to some extent, the range of the particle energies. This threshold will also determine the attainable TOF resolution. From experience one expects to be able to establish conditions permitting thresholds as low as 0.25 MeV electron energy equivalent.

The Monte Carlo simulations of the efficiencies were made with the Kent State University Code[13] modified at CRNL for a point source with isotropic angular distributions. This code is widely used and gives excellent results for neutron energies up to 400 MeV. Comparison of the calculated efficiencies with our previously measured (Lone et. al.[14]) efficiencies of a 13.2 cm^3 stilbene detector showed agreement to within 5%. Figure 13 shows the calculated efficiencies for a 100 mm thick scintillator as a function of neutron energy for various threshold settings. For high energy neutrons, the efficiency of a 75 mm thick plastic will be about three quarters of those shown in Figure 13. Thus, with a reasonable threshold setting of about 0.3 MeV electron energy equivalent, the 75-mm thick E scintillator would give a 25% efficiency for neutrons of energy between 2 and 40 MeV.

For neutron detection, special considerations will have to be given to the possibility of an increase in the cross talk between the adjacent detectors due to the production of secondary neutrons from inelastic scattering. The probability of these neutrons generating a detectable signal in a neighbouring detector will depend on the assembly and can be studied in detail with Monte Carlo simulations. In the present setup, because of the relatively small thickness, 75 mm, of the detectors, large flight paths and high neutron energies, the cross talk is not expected to be severe. In any case, the data analysis will provide a mechanism to veto any signal having an adjacent detector triggering for elimination of the potential cross talk events.

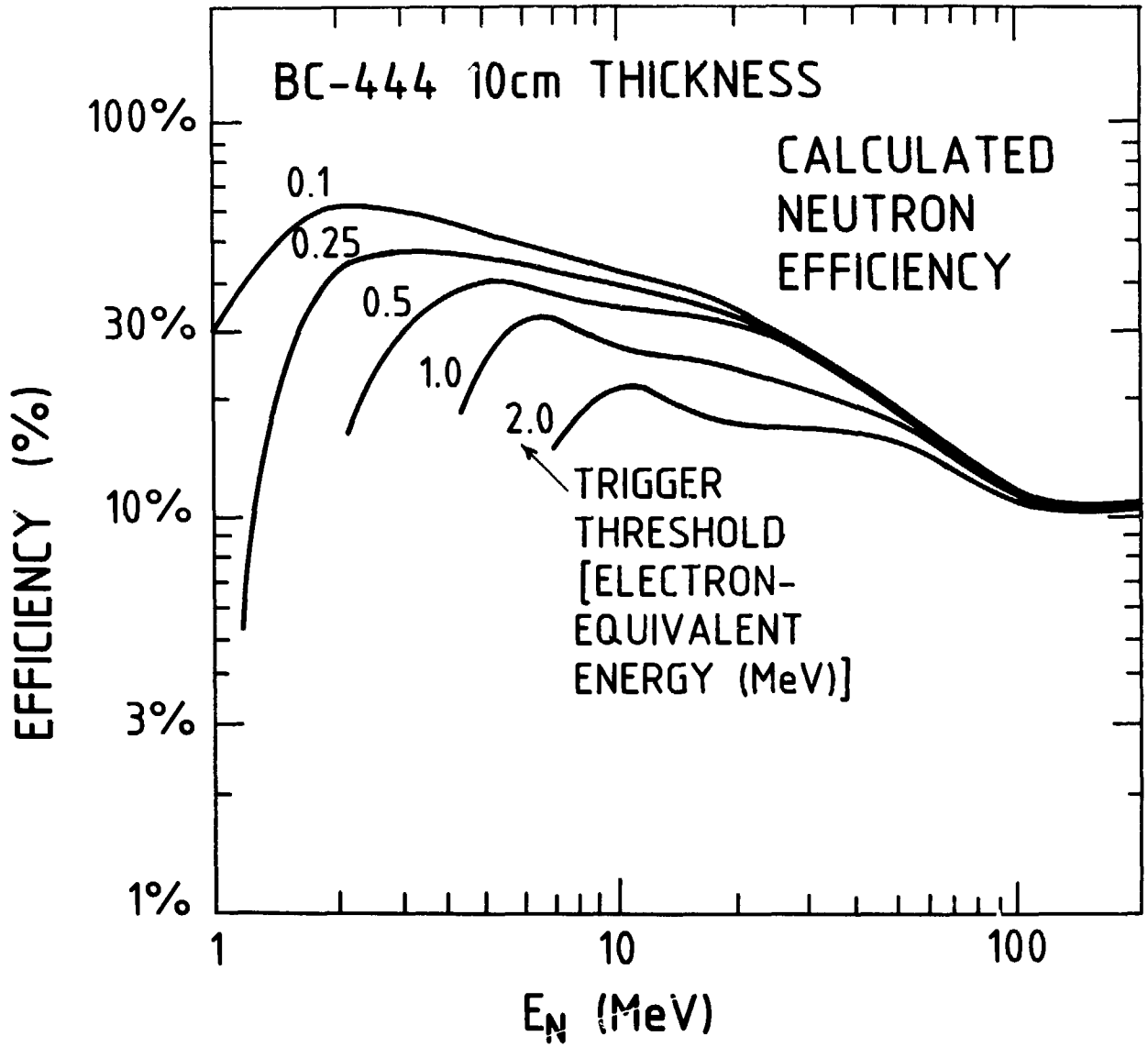

Figure 13. Efficiency of neutron identification as a function of neutron energy for 10 cm-thick scintillator. The present proposal calls for 7.6 cm thickness.

4.4 Stabilization and Calibration

Setup and reliable operation of the large array of phoswich detectors will require a mechanism for calibration and stabilization of the time and energy signals. The light output of organic scintillators is not linear in the energy loss when the ionization per unit path is large. In addition the energy calibration can change because of gain drifts in the photomultiplier due to temperature changes and large count rate fluctuations. Because of the large spatial dimensions of the array and low intrinsic efficiencies of the plastic scintillators for γ-rays, use of radioactive sources is impractical for the purpose of calibration or stabilization.

We plan to use an optical system shown in Figure 14 for calibration and gain stabilization of the array. The system is similar to that of Kapustinsky et al.[15] For long-term stability, the high voltage to each photomultiplier is controlled via CAMAC with reference to a light signal from a blue LED (e.g. Siemens LR-5410-H0). Because of the large dynamic range of light output required several LED's may be required. The outputs of these LED's and the typical fibre optic coupling are monitored via the stable PIN's for comparison and normalization. Each LED output can be calibrated in terms of the scintillation from a radioactive source. The LED's can be pulsed for setup and calibration of the timing signals and the delays between the array modules.

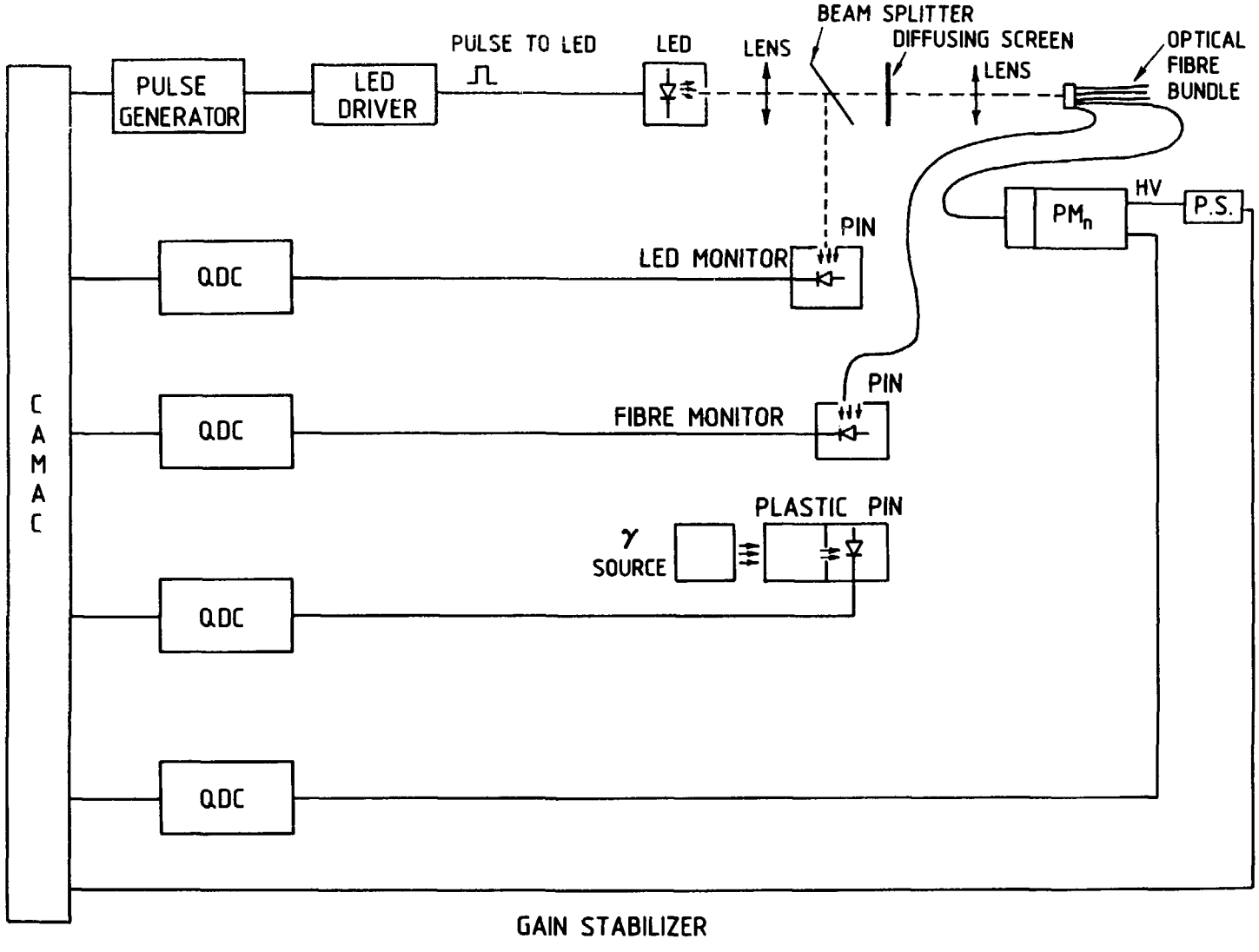

Figure 14. Scheme of the optical system to be used for calibration and gain stabilization of the phoswich detectors.

5. SCATTERING CHAMBER

5.1 Design

The scattering chamber for MARS is a horizontal-axis cylinder, 3 meters in diameter and 3.7 meters in length. The specification drawing is shown in Figure 15. Its basic dimensions were dictated by the size of the phoswich array, by the need for a 2-m flight path, and by the space requirements of gas-filled detectors for use in coincidence with the array. The chamber can also accept experiments unrelated to the array. For example, large area avalanche counters can be placed more than a meter from the target, even at $\theta > 90°$. The chamber, configured in much the same way as the Nautilus at GANIL, has the flexibility to accommodate future developments in detector technology and new experimental directions.

Entry into the chamber is through a manhole near the beam port. The entire front end of the chamber is flanged and may be removed to access the array and mount equipment. The chamber specifications are detailed in Appendix I. These contain a rather comprehensive set of requirements in terms of materials, construction methods, internal finish, cleanliness, documentation, quality assurance, and high vacuum performance. Of some technical interest is the field weld of two chamber sections to be performed on site by the manufacturer. This delivery in sections is necessary in order to bring the very large vacuum vessel through the permanent concrete passageways leading to the target area.

5.2 Vacuum System

The quality of the chamber vacuum system is of great importance. A slow pumpdown cycle can cause loss of valuable beam time when a modification is required during a run. A poor chamber

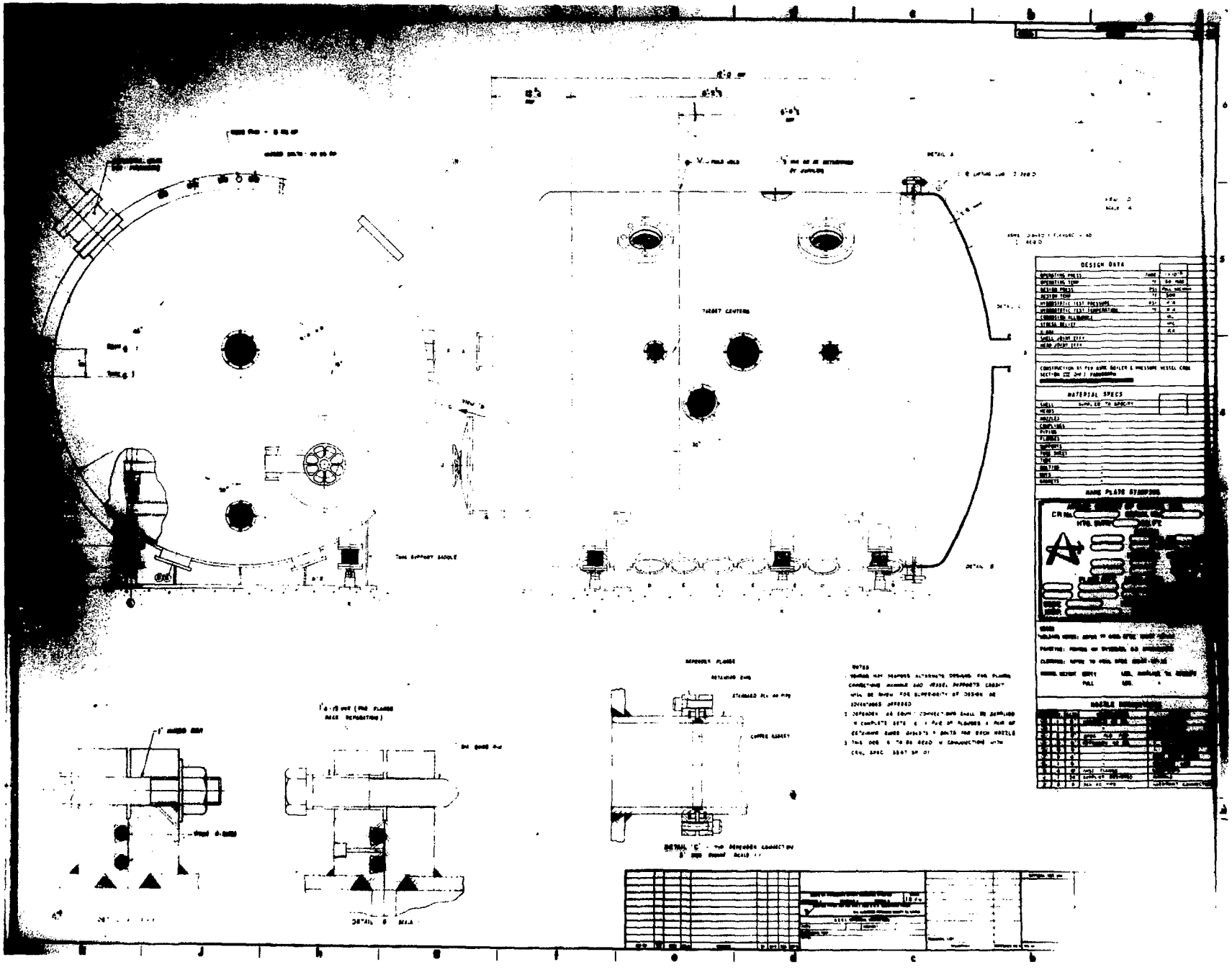

Figure 15. Specification drawing of the vacuum chamber.

vacuum can lead to high-voltage breakdowns in compact detector geometries and in cases when up to 50 kV must be applied to the target assembly for suppression of secondary electrons. It can also lead to pollution of the high quality vacuum of the TASCC beam transport system. A good vacuum is necessary if time-zero triggers that are based on electron multipliers are to be used. Cleanliness of the system is also a prime concern since contaminant buildup, chiefly of hydrocarbons, can be a significant problem in nuclear reaction studies. While high-energy, relatively light projectiles permit use of targets that are thick relative to the potential impurity buildup, the effect can never be completely neglected, and can be severe for thin target work. An oil-free system is therefore needed. A schematic illustration of the system proposed is shown in Figure 16. In order to evacuate the 26 000 L vessel from atmospheric pressure to 13 pascals (100 millitorr) in one hour or less, an average effective pumping speed of more than 65 L/s over that pressure range is needed. A number of roughing systems with average pumping speeds near 100 L/s for air have been considered, including a custom-built carbon vane/sorption system (see Figure 17) and various two-stage mechanical pumps coupled to roots blowers and equipped with traps to prevent backstreaming of oil vapor. Though a final decision has not yet been made, the major options are rather close in price.

Our criteria for the high-vacuum system are: i) no oil contamination, ii) attainment of specified 1.3×10^{-5} Pascal (1×10^{-7} Torr) base pressure in a clean, empty chamber, iii) pumpdown to 6.6×10^{-4} Pascal (5×10^{-6} Torr) in less than 4 hours for a

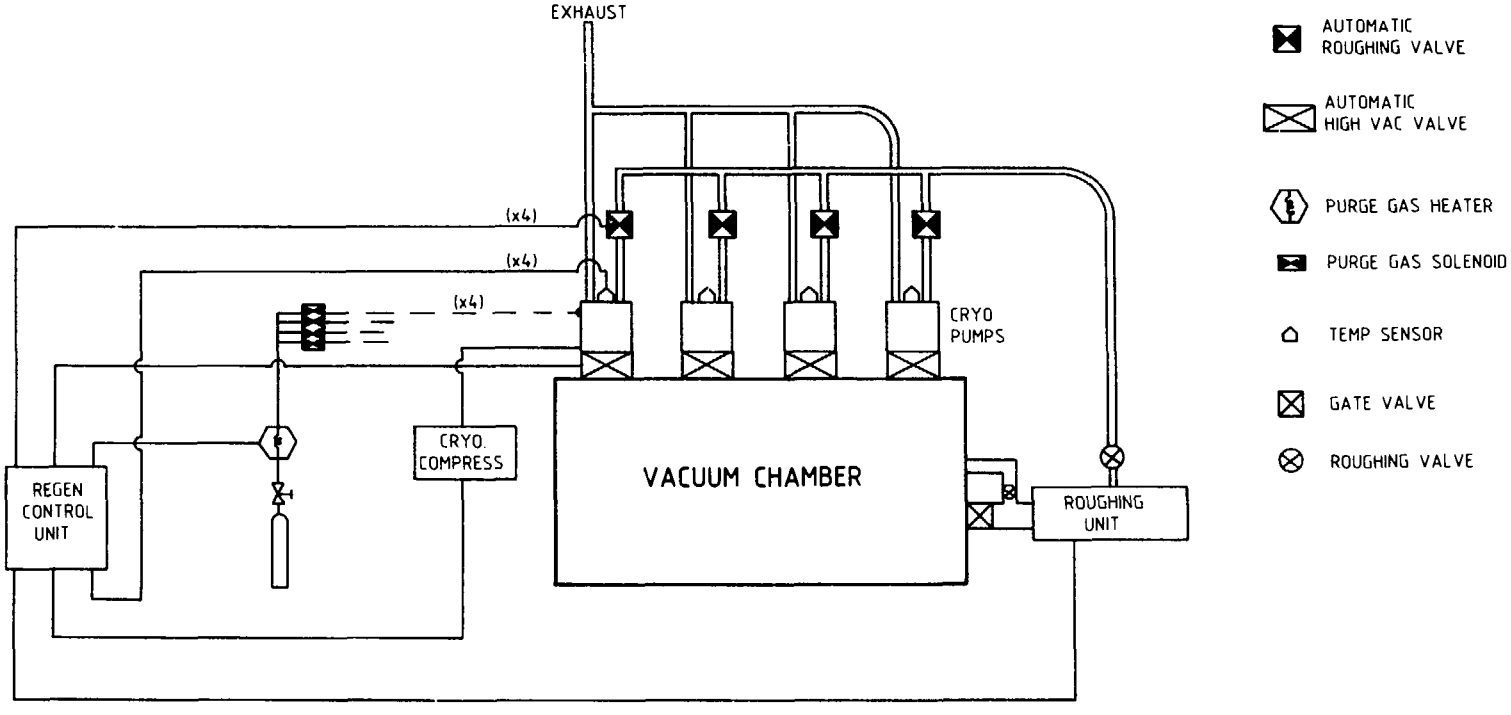

Figure 16. Flow diagrams for the vacuum pumping system.

fully "loaded" chamber, including one hour for roughing, and iv) routine attainment of 1.3×10^{-4} Pascal (1×10^{-6} Torr) after a day or more of pumping under normal experimental conditions. These criteria reflect the characteristics of the vacuum system for our existing 1.75 m chamber. It is therefore possible to estimate the pumping requirements for the MARS chamber by scaling up the gas load of the existing facility by an appropriate factor. For the large chamber, the increase in interior surface area is a factor of five, and in number of detectors, cables, phototubes, and bases it is a factor of four. Various other quantities were considered, and a required pumping speed of 12000 L/s for air deduced. This can be provided by cryogenic capture pumps, which require some safety precautions (see Appendix II) or by turbomolecular pumps, which require some precautions to avoid oil contamination. While Figure 16 shows these requirements being filled by four large cryopumps, a combination of the two types of pumps is also being considered.

5.3 Mechanical Supports

A crucial part of any design involving a large vacuum chamber concerns the structure on which the experiment itself is to be supported. Because order-of-magnitude variations in cross section can occur within a fraction of a degree in scattering angle, an accuracy of 0.05° is specified in the positioning of detection apparatus. Accordingly it is required i) that the initial position of any detector be known to a tolerance of 1 mm, ii) that subsequent deflection of the detector support and alignment structure be less than 1 mm, independent of loading, and iii) that neither the target nor the detectors must shift relative to the incident beam from

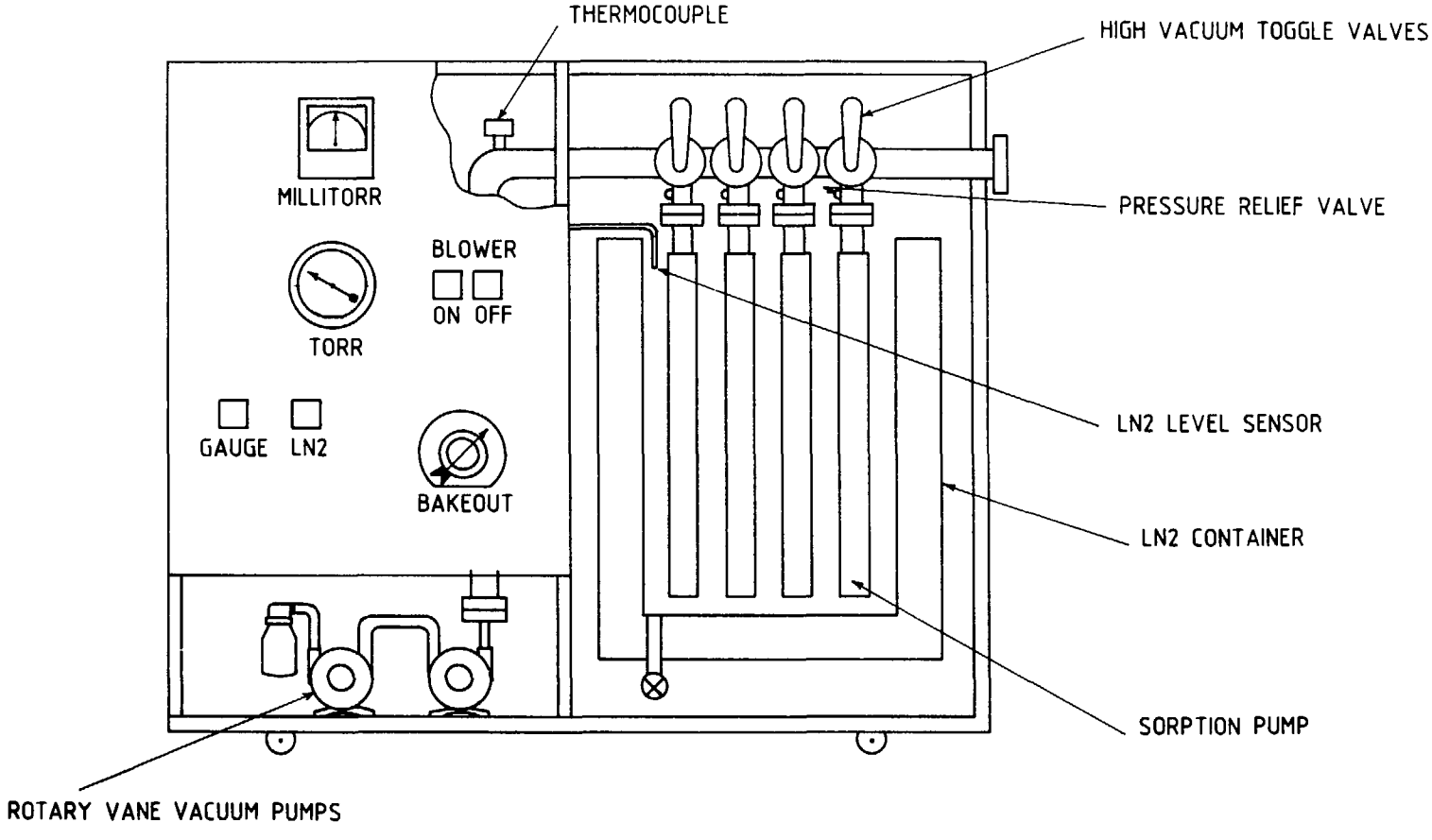

Figure 17. Contaminant-free rough pumping system consisting of two series-mounted carbon vane blowers and four large-capacity sorption panels.

deformation of the steel vacuum chamber upon evacuation. A set of "hard points" has therefore been designed for the chamber. These are six supports, fixed to the building floor and penetrating the steel vacuum shell, which form the legs of a massive steel table (see Figure 18). The vacuum at the penetration points is maintained with bellows, which leave the chamber free to deform under pressure, with no effect on target or detector alignment. The chamber itself rests independently on the floor of the building. The target assembly and any user-provided detector systems are attached to the table. Movement of the array occurs on two linear bearings, giving a choice of target-array distances as well as a means of removing the array.

6. ELECTRONICS

A modular diagram of the array electronics is shown in Figure 19. Our aim has been to decide very early in the electronic processing of an event whether that event is to be accepted or rejected. Processing of events that do not fulfill our criteria can then be terminated before any digital conversion has started. Changes of the conditions imposed on each event should also be easily implemented and verified.

The electronic circuit shown in Figure 19 can be broken down into five major areas: i) the initial treatment of each phototube signal; ii) the trigger logic, iii) the time determination, iv) the determination of ΔE and E, and v) inclusion of other detectors. Each of these major areas are discussed in more detail in the following five paragraphs.

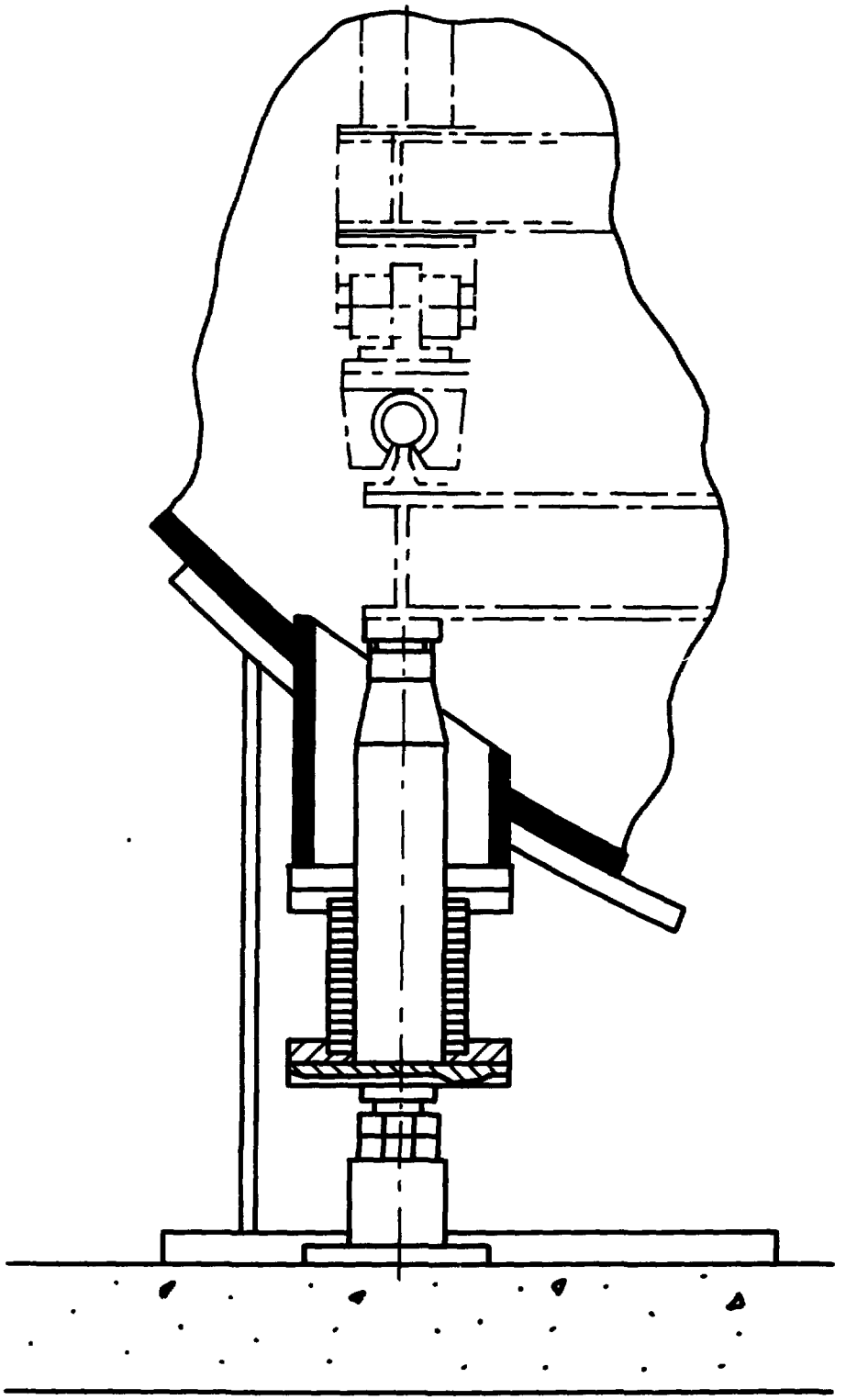

Figure 18. One of the six "hard points" which support the massive steel table and the detectors. These "hard points" allow the detectors and target to be aligned independently of the chamber walls, which will deform under atmospheric pressure.

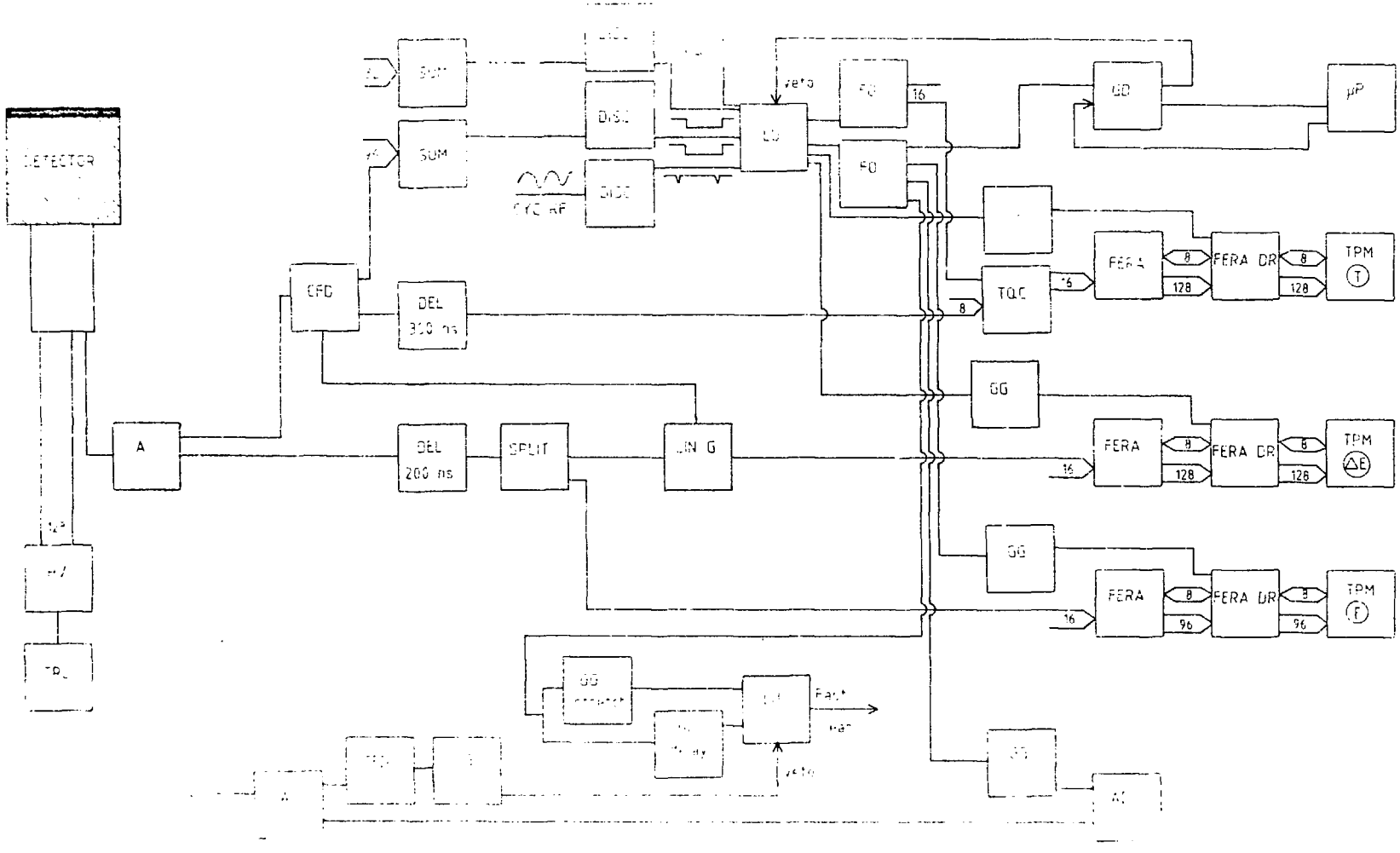

Figure 19. The front end electronics for MARS.

6.1 Initial Signal Treatment

The output from the phototube is amplified without any pulse-shaping by a fast amplifier with two outputs. One of these analog signals is analysed by a constant fraction discriminator (CFD) and the resulting logic outputs are used for trigger and time information. The other is fanned out and fed to the ΔE and E digitizers.

6.2 Trigger

The trigger logic is separated into two parts, that for the 32 thin plastic detectors of the two inner rings and that for the 96 fast-slow plastic sandwiches of the outer six rings. In both cases all CFD outputs are connected to an analog summing module. This module generates an analog output that is increased by 50 mV for each present NIM logic level input. The analog output is analysed by a discriminator. Multiplicity criteria can therefore be set independently for the two inner rings of detectors and the six outer rings. Alternatively, the CFD outputs from both types of rings may be connected to the same analog summing module and a single multiplicity criterion imposed. An event that passes the array multiplicity criteria will be presented to a logic unit (LU) where other selected criteria, such as the presence of other detector signals and the availability of the digitizers, are imposed. One input channel to the LU is derived from the cyclotron RF. The width of this input is set to be very narrow, whereas all others are stretched. The RF timing pick-off will be adjusted so that this narrow input arrives after the other stretched detector inputs. The

coincidence condition for this LU will thus be fulfilled with the arrival of the RF pulse. The output will then be timed with respect to cyclotron RF irrespective of any time jitter in the detector inputs. The output from the LU is fanned out and used to derive the gates for all digitizers as well as to provide a signal to the time determination circuit.

6.3 Time

A LeCroy FERA system will be used to digitize the signals from the detector. While the charge integration of those fast digitizers is ideal for phototube energy signals, no compatible time-to-digital converter can run at the same rate. Therefore, a time-to-charge-converter (TQC), started by the master trigger and stopped by the individual detector, delivers to the FERA an amount of charge proportional to the elapsed time. Note that the various electronic propagation delays allow the FERA gate to come on before the TQC pulse arrives. The common FERA gate width is set by a logic unit; positioning of this gate relative to the signal is with a single cable delay. A 128-channel delay of 300 ns in the "stop" of the TQC puts the time peak in the middle of a 500 ns window. If shorter time windows are required, the custom built 128-channel delay should be adjusted accordingly.

6.4 ΔE and E

The analog signal from the fast amplifier is delayed and fanned out two ways. Since the arrival times of particles within a single event can vary by as much as 50 ns, the ΔE part of the signal, which comes from the fast plastic part of the phoswich, is isolated with a linear gate positioned as a 30 ns window on the leading edge of the

analog signal. The resulting gated analog signal is then fed to the ΔE digitizer (FERA), while the ungated analog signal is fed to the E digitizer. The common ΔE and E FERA gate positions and widths are set by a GG 8000 gate and delay unit. The analog signals must be delayed in order that the FERA gates arrive before the signals. The width of the E gate will be set at about 700 ns to integrate the total ΔE + E analog signal. The ΔE gate width will be about 100 ns to accommodate the jitter in signal arrival times, though the fast analog ΔE signal has already been "pregated" and will only be about 30 ns wide.

6.5 Other Detectors

These detectors are labeled OD on the diagram. They do not form a part of the proposal, but the ability of the array to handle coincidences with additional instruments does. Fast detectors pose no particular problems; their logic can be merged with the array logic in the logic unit and the master trigger can be used to generate their ADC gates. Slow detectors, on the other hand, cannot be integrated with the forward array trigger logic. For these, a scheme like that illustrated at the bottom of the diagram must be implemented. A fast multiplicity requirement has to be met for the array and when it is fulfilled, that event goes ahead, though the status of the slow detectors is not yet known. If after a specified time, no slow detector signal has been received, then the array event in progress must be cleared by the ADC/QDC fast clear. This is accomplished by splitting the array master trigger in two. One signal is stretched to about 5 μs; the other is delayed by 4 μs and both are fed into a logic unit which is set to a twofold coincidence

requirement. If nothing else happens, then the requirement will be fulfilled after 4 μs and a fast clear issued. However, if a slow detector signal is detected during these 4 μs, the logic unit is vetoed and the event is allowed to continue.

7. DATA ACQUISITION

7.1 Design

Speed and versatility are the most important properties of an acquisition system for a large, multidetector array. It must be fast enough to handle the anticipated data rate and it must have the flexibility to operate in a variety of modes, ranging from serving as a simple pipeline to tape, to performing sophisticated preprocessing of the data. The data acquisition parameters and logic circuits should therefore be under computer control. Commercial availability, particularly of the more complex components, is highly desirable.

The front-end electronics have been discussed in the previous section. Here we consider the on-line computer system (a Perkin Elmer 3230), a microcomputer for monitoring and control, the data acquisition microprocessor, and the CAMAC logic and data stream.

7.2 The TASCC Data Acquisition Computer

The TASCC on/off line data acquisition system is based on a Perkin Elmer 3230, 32-bit minicomputer. The present hardware configuration is summarized in Table 5. The software is a modified version of the system developed at ORNL[16] for the Holifield Heavy Ion Research Facility. It is capable of high speed data rates, writing ≈500 KB/s to magnetic tape (6250 bpi). A second computer system for expanded on-line and off-line capabilities is planned for installation in 1988-89 if funding is approved. Both computer

TABLE 5: TASCC DATA ACQUISITION COMPUTER SYSTEM HARDWARE CONFIGURATION

Perkin Elmer 3230 CPU	16MB, WCS, FPP
4 disk drives	≈1 GB total
4 Mag tapes:	two -- 800/1600
	two -- 800/1600/6250

7 Vision 2000 Terminals (RS 232 interface)

1 Printronix Line Printer (parallel interface)

2 Chromatics Color Graphics terminals (CAMAC interface)

1 TRILOG hardcopy plotter/printer (CAMAC interface)

2 Modgraphs (Tektronix 4014 emulators) (RS 232 interface)

2 JORWAY 432 CAMAC Interfaces:

- 2 parallel branches (data rates 500KB/sec to tape)
- 1 serial highway

Several custom built CAMAC modules

General purpose Data Scanner 16 ADCs (singles/coin)

General purpose CAMAC acquisition system (CAB Microprocessor)

systems will have the necessary speed and data analysis capabilities to handle the type of data that would be generated by MARS. Links from the data acquisition hardware to the Perkin Elmer 3230 would be provided via a parallel CAMAC highway for high-speed transmission of data and via a serial highway for control, downloading of programs to the data acquisition microprocessor and other low-speed transmission requirements (see Figure 20).

7.3 Local Computer

Functions such as calibration, phototube voltage setting and stabilization, monitoring, and control of CAMAC would best be performed with a local computer. These functions could also be performed through the main acquisition computer; however, that would severely restrict facility software development and testing during times when the 3230 was in use for other experiments. With the availability of inexpensive, reliable microcomputers with standardized interfaces (RS-232, CAMAC, etc.), adaptation of a "PC" to these tasks becomes a viable and cost-effective option.

7.4 Data Acquisition Microprocessor (CAMAC Branch Driver)

The microprocessor coordinates the data taking-cycle for each event. It performs standard CAMAC functions as well as numerical and logical functions and finally outputs formatted data to the host computer. A variety of such devices exists, ranging from glorified CAMAC crate controllers to rather sophisticated bit-slice microprocessors.

The LeCroy 4805 CAB (CAMAC Booster) was chosen three years ago as the standard microprocessor for CAMAC-based data acquisition systems at TASCC. Its most complex application so far has been as

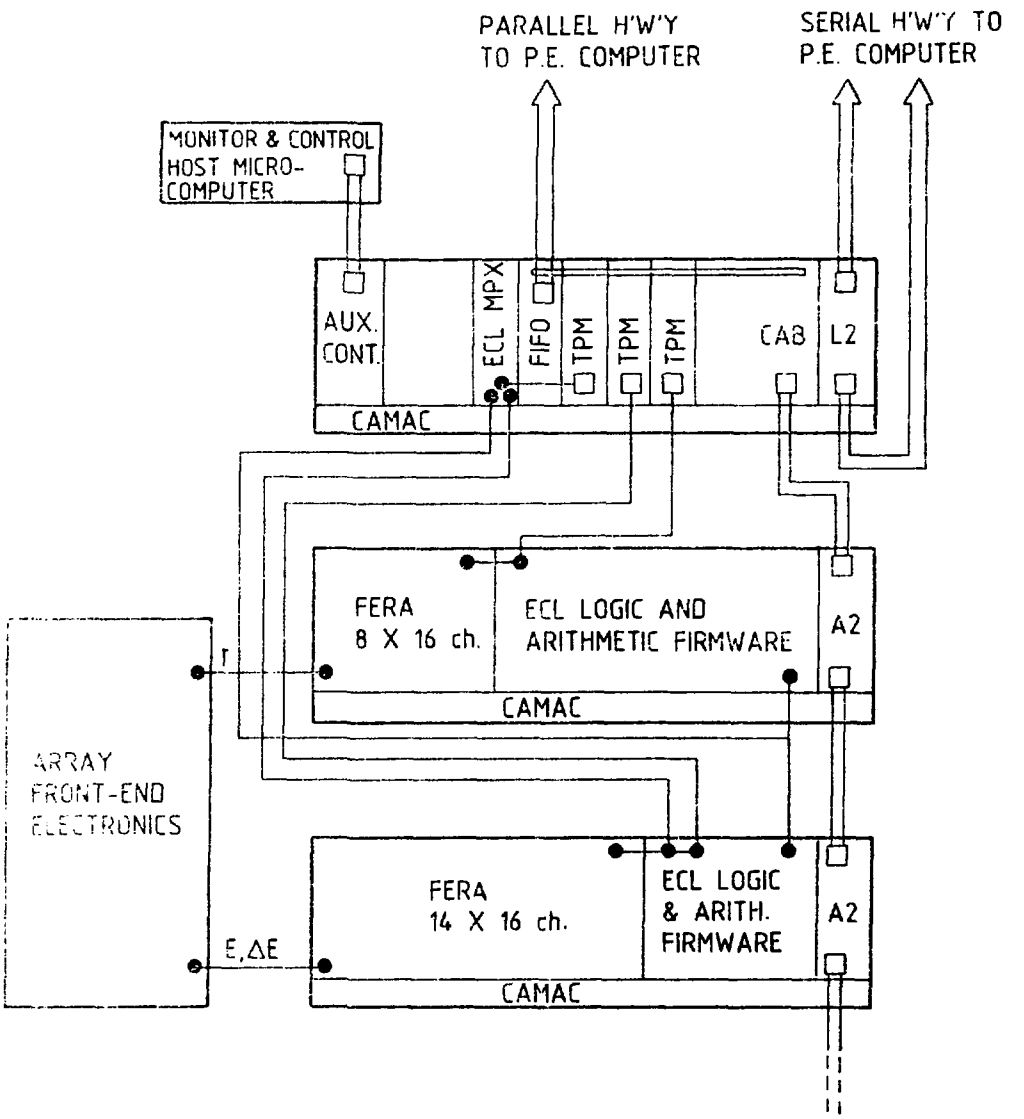

Figure 20. Layout of the complete data acquisition system for MARS.

the microprocessor for the 8π Spectrometer[17]. Other front-end microprocessors are available commercially; however, the CAB meets the requirements for the array, fits with the existing TASCC on-line computer architecture, and offers the benefits of proven hardware and software developed for the very successful 8π acquisition system. Nevertheless, alternatives, such as devices based on the very fast Motorola MC68020, will be carefully considered.

7.5 The CAMAC Data Stream

As indicated in section 6, the array signals are digitized in a LeCroy Fast Encoding and Readout ADC (FERA) system, selected because its charge integrating function is well suited for a fast-slow plastic combination and because of its performance in applications involving multiparameter data acquisition. It is already used in the 8π spectrometer and has been chosen for the MSU 4π Array[18] and DELF,[19] the new detector system for heavy fragments which is being developed at GANIL.

The FERA is a high speed charge integrating analog to digital converter with a gate width variable from 50 to 2000 ns. The important features are: 1) high density: 16 channels per CAMAC module, 2) fast conversion: 10 bits in 5 μs, 3) fast readout: 10 MHz via a front panel ECL port in zero suppressed mode, 4) fast external clear, and 5) fast preprocessing via commercially available logic and arithmetic firmware (e.g. LeCroy 4418 16-Channel Programmable Logic delay/fan-out, LeCroy 2372 memory Lookup unit 64K-bit, LeCroy 2375 Data Stack Module 256 by 16-bit memory, LeCroy 2365 Octal Logic Matrix 16 by 8).

Figure 2[illegible] shows schematically the flow of data from the FERAs to triple-port memories (TPM) connected directly to the micro-processor and to ECL logic and arithmetic firmware for a first stage of preprocessing. This permits fast clear decisions and storage on tape of higher-order, computed parameters, such as hit patterns, multiplicity, charge, mass, and energy, which could be generated by lookup tables in the MLUs.

The block diagram of a preliminary design of the preprocessing ECL firmware is shown in Figure 21. Pairs of ΔE and time data words flow simultaneously in parallel streams into two triple port memories (labelled 1 and 2) connected to the data-acquisition microprocessor through an internal private bus. A memory look up unit (LRS MLU 2372, labelled number 1) is used to compare 7-bit ADC identifier words, synchronizing the flow of ΔE energy-time pairs and rejecting those where the time or ΔE energy data words are missing. The dataflow timing synchronization and logic will be done with a programmable logic unit (LRS Octal Logic Matrix OLM 2365) to allow the dataflow logic to be adapted to various experimental situations without rewiring. The memory lookup unit labelled 2 in Figure 21 applies a digital window to all time data words which can be individually specified for each detector. The main purpose of these gates is to reject pile-up events from the computed hit pattern and multiplicity. If the time channel window is satisfied (T-OK in Figure 21) then the Bit Pattern and Multiplicity module uses the 7 bit ADC identifier to update a hit pattern and multiplicity register.

The readout method used for the ΔE and time data modifies the data words received from the FERAs so that the module number (7 bits)

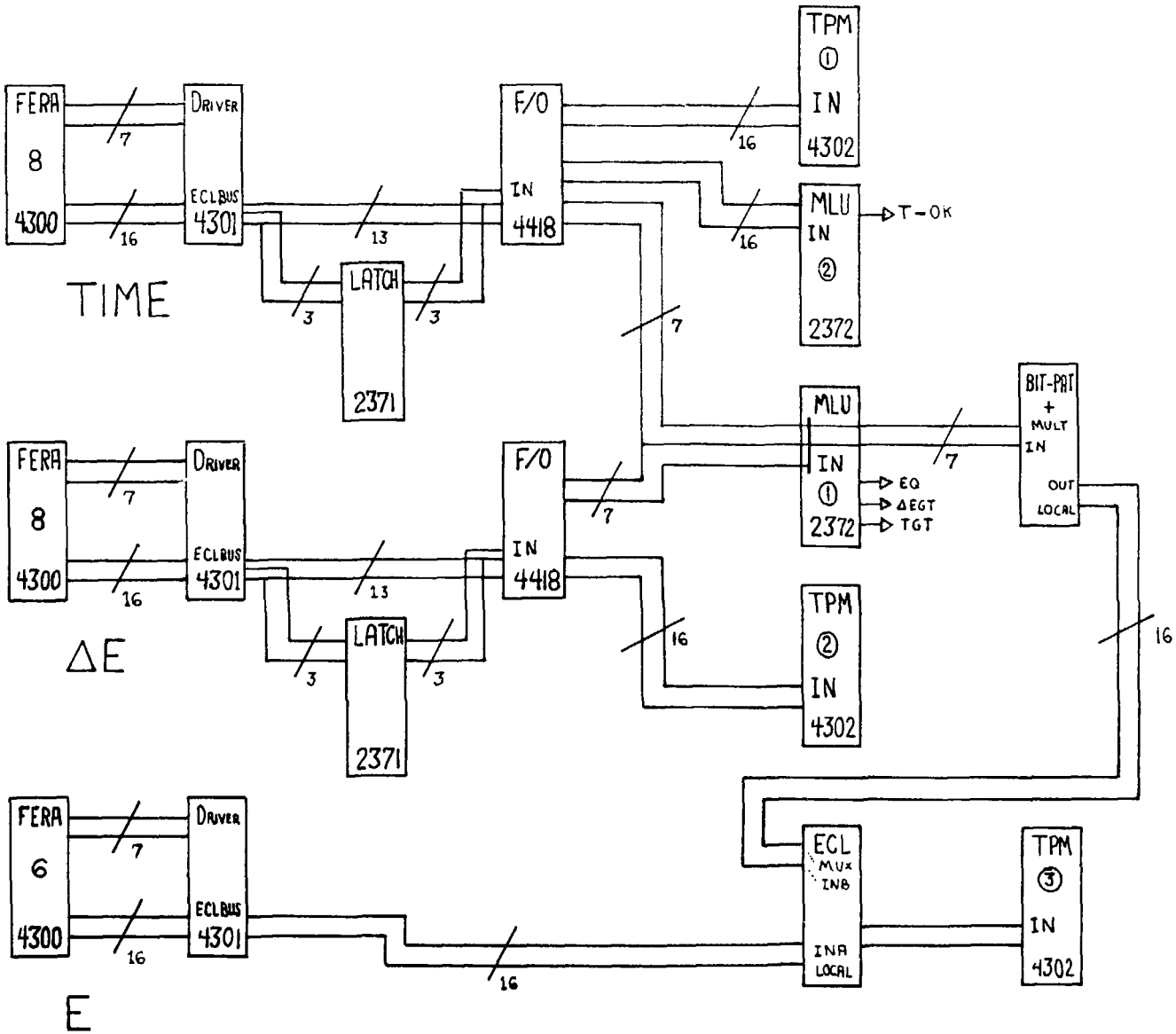

Figure 21. Data flow from the FERAs to the triple-port memories.

and data (9 bits) can be packed into one 16-bit word. Since 10 bits (1024 channels) are required for the energy signals, the unmodified FERA data words will be transferred directly to the TPM labelled 3 via a dual port ECL multiplexer module which is also used to transfer the hit pattern and multiplicity data words after all FERA data words have been sent.

7.6 Data Rates

The TASCC PE 3230 computer is capable of acquiring and writing data on magnetic tape at a rate of about 250K 16-bit words per second. For a typical central collision array event, involving a heavy fragment and 5-10 light charged particles, each with one ΔE, one energy, and one time parameter, about 30 16-bit words would be required. This corresponds to a maximum data rate of 8000 events per second at the limit of the computer. The FERA system deadtime would be less than 100 μs per event, i.e. comparable to the on-line computer dead time.

8. BUDGET AND SCHEDULE

The budget for MARS can be separated into three components: (i) chamber and supports, (ii) detectors, and (iii) electronics and acquisition. In making the cost estimates shown here, we have adjusted any earlier quotes or prices to correspond to dollars of the year 1987. The costs were summarized in Part I of this proposal (Table 2).

8.1 Chamber and Supports

The vacuum chamber, with associated mechanical support structure, vacuum pumps, etc. will be owned by AECL. Costs are indicated in Table 6. Three Canadian manufacturers have bid on the fabrication of the large vacuum vessel. Based on the information

contained in those quotations, the Plant Design Division of AECL, Chalk River recommends that we budget $233 330 plus 10% contingency, for the chamber purchase. Fabrication and materials costs for the support structure, including "hard points", table, linear bearings, and carriage have been quoted by the AECL Workshops, Estimating and Planning Branch at $64 000 with 20% contingency specified by them. The mounting bracket to hold and align the 128 detectors with an individual adjustable tile for each has been designed and costed at $116 000 with a 20% contingency. That amount includes $10 000 for surveyors and other specialists to do the labor-intensive procedure of mounting and aligning each detector. Preparation of the site for the chamber (plumbing and electrical work) movement of the chamber into the target room, surveying, installation of support hardware, and the cost of the beam exit line from the chamber total $37 000. Quotations for four high-capacity cryopumps with stainless steel valves were received from a prospective supplier in 1986. Including taxes and correction for dollars of the year, this gives $41 608 per pump plus 10% for contingency. A roughing system with the cleanliness and power demanded of this application costs $37 000. A variety of components yet to be designed, including vacuum plumbing, gauges, signal feedthrus, interlocks, target assembly, etc. add up to about $40 000. Plant Design Division of AECL has already completed work costing $21 200 which is not included in this proposal and has already been paid by Nuclear Physics Branch. Detailed drawings, mechanical design, and engineering required for fabrication is estimated by them at $57 750. The total cost of the chamber, supports, pumps, and associated components is $751 580 plus a contingency amount of $110 330 which represents 14.6%.

TABLE 6: COST ESTIMATES FOR CHAMBER AND SUPPORTS

COMPONENT	COST	SUBTOTAL	CONTINGENCY	
DESIGN CHARGES				
Engineering and drafting	57 750	57 750	11 550	(20%)
CHAMBER SHELL				
Delivered price	183 000			
P. & P. sales tax	34 770			
Coordination costs	15 560	233 330	23 330	(10%)
SUPPORTS (HARD POINTS, CARRIAGE, RAILS, TABLE)				
Machining and fabrication	43 000			
Materials	21 000	64 000	12 800	(20%)
DETECTOR MOUNTING & ALIGNMENT STRUCTURE				
Machining & fabrication	88 500			
Materials	17 500			
Detail detector mounting & alignment	10 000	116 000	23 200	(20%)
SITE PREPARATION & INSTALLATION				
Gas exhaust, electrical work	7 000			
Move & position chamber	10 000			
Install hard pts., rails, etc.	7 000			
Beam exit line, pedestal, dump	13 000	37 000	7 400	(20%)
HIGH VACUUM PUMPS w/GATE VALVES				
Delivered price	139 900			
P & P sales tax	26 600	166 500	16 650	(10%)
ROUGH PUMPING SYSTEM				
Welding & fabrication	11 000			
Materials & components	26 000	37 000	7 400	(20%)
VAC. PLUMBING, FEEDTHRU PANELS, MISC.				
Labor	20 000			
Materials	20 000	40 000	8 000	(20%)
TOTAL CHAMBER & SUPPORTS		751 580	110 330	

8.2 Detectors

The detectors will be owned by the Universities (NSERC). Their costs are detailed in Table 7. It is proposed to buy the phototubes and scintillator materials from commercial suppliers, but to cut and polish the detectors at the Universities. The workspace and labor to do this will be a contribution of the individual universities, rather than by NSERC. The technical manpower to assemble and test the detectors will be supported by an NSERC infrastructure grant (see accompanying request), and does not constitute a portion of this Major Installation Grant request. Scintillator costs are taken from budget estimates by a supplier and will be confirmed by quotations. Phototube prices are taken from quotation competitions and costs for other components from recent catalogues. (Note that only about 100 detectors need to be manufactured, since the phoswich detectors for rings 3 and 4 of the array will be constructed independently of this proposal in a shared U. Laval-AECL endeavor and will be used with existing electronics as a miniature forward array.) Total costs for detector materials is $243 100; a contingency factor of 15% has been applied to all items.

8.3 Electronics

Electronics costs are listed in Table 8. In general the electronics will be owned by the universities. An exception is a portion of the items under the category "custom-built". These will be built in the university and AECL laboratories; the AECL component is marked by asterisks in the table. Commercially available items carry a contingency of 10%; custom built items require 30%. The total electronics cost is $648 756, with a contingency of $106 396 (which constitutes an average of 16.4%).

TABLE 7: COST ESTIMATES FOR DETECTOR MATERIALS[a)]

(All items include 9% Quebec Sales Tax)

COMPONENT	QUANTITY	COST	CONTINGENCY (all 15%)
SCINTILLATOR			
Slow scintillator	6.0 m^2	71 800	10 770
Fast scintillator	5.5 m^2	34 600	5 190
PHOTOMULTIPLIER TUBES			
1 1/2" tubes	35	6 300	945
3" tubes	18	18 000b)	2 700
5" tubes	50	89 000	13 350
Shields, sockets, materials		7 000	1 050
OTHER DETECTOR COMPONENTS			
Lucite	0.8 m^3	12 400	1 860
Optical cement, jigs, etc.		4 000	600
TOTAL DETECTOR MATERIALS	243 100		36 465

a) 32 phoswich detectors compatible with the array are being built independently of this proposal. Their costs are not included in this table.

b) Estimate.

TABLE 8: ARRAY ELECTRONICS COSTS

Units costs include quantity discounts where applicable, and Quebec sales tax for all commercial items. Items marked by an asterisk will be owned by AECL. For both the PERA and the CFD components, which are required in large numbers, two modules more than required by the minimum setup will be purchased.

COMPONENT	MODEL	QUANTITY	UNIT COST	TOTAL COST
CAMAC				
PERA	LRS 4300	24	4263	102312
PERA DR	LRS 4301	3	2958	8874
TPM	LRS 4302	3	4891	14673
CAB	LRS 4805	1	19302	19302
Crate	BiRa 5000	5	3201	16005
V2 Controller	BiRa	3	1692	5076
L2 Controller	Jo 74	1	2038	2038
Latch	LRS 2371	2	2443	4886
SQ	LRS 4418	2	4940	9880
MQU	LRS 2372	2	3144	6288
QUM	LRS 2365	2	3204	6408
CCL MUX	Custom	1	2000	2000
Bit Pattern	Custom	1	2000	2000
CAS FIFO	Custom	1	2000	2000
LTM				
A	PS 776	9	1902	17118
CFD	PS 714	34	3459	117606
DISC	LRS 821	1	2267	2267
GH	LRS 365	1	2050	2050
FO	LRS 429	2	2875	5750
GG	ESN 8000	1	4060	4060
GD	LRS 222	1	2628	2628
Crate	OR 402D	6	2289	13734
LB	LRS 622	1	2010	2010

TABLE 8: ARRAY ELECTRONICS COSTS continued

CUSTOM BUILT (128 CHANNELS EACH OF:)				
TQC				27 000*
Mixer				5 000*
Linear gate				30 000
Splitter				13 700
Delay (200 ns)				16 400*
Delay (300 ns)				19 500*
Fiberoptics stabil. & calib. system				40 000
HV				
Mainframe	LRS HV 1449E	1	15432	15 432
Pods	LRS 1443/12	11	3199	35 189
CAMAC interface	LRS 2132	1	2350	2 350
MONITORING & CONTROL				
Microcomputer	Compaq 386	1	17000	17 000
CAMAC interface		1	3000	3 000
Crate controller		1	1500	1 500
RACKS & CABLING				
Cables with connectors	Custom	2000	25	50 000
Racks with fans		4	930	3 720
TOTAL ELECTRONICS				648 756
CONTINGENCY (10% for commercial, 30% for custom built)				106 396

REFERENCES FOR PART III

1. T.C. Awes, S. Saini, G. Poggi, C.K. Gelbke, D. Cha, R. Legrain, and G.D. Westfall, Phys. Rev. C25 (1982) 2361.

2. T.C. Awes, G. Poggi, C.K. Gelbke, B.B. Back, G. Glagola, H. Breuer, and V.E. Viola, Jr., Phys. Rev. C24 (1981) 89.

3. R. Bougault, D. Horn, G.G. Ball, M.G. Steer and L. Potvin, Nucl. Inst.and Meth. in Physics Research A245 (1986) 455.

4. D.F. Measday and C. Richard-Serre, Nucl. Inst. and Meth. 76 (1969) 45.

5. P.J. Karol, Phys. Rev. C11 (1975) 1203.

6. R. Bougault, *private communication.*

7. N. Brummond, C. Glasow, K.H. Kampert, R. Santo, K.D. Hildenbrand, U. Lynen, W.F.J. Muller, H.J. Rabe, R. Trockel, D. Pelte, and J. Pochodzalla, GSI Scientific Report 1984, GSI-85-1, (March 1985) 53.

8. C. Pruneau, Thesis, Université Laval (1987).

9. A. Baden, H.H. Gutbrod, H. Löhner, M.R. Maier, A.M. Poskanzer, T. Renner, H. Riedesel, H.G. Ritter, H. Spieler, A. Warwick, F. Weik, and H. Wieman, Nuclear Inst. and Meth. 203 (1982) 189.

10. C. Pastor, F. Benrachi, B. Chambon, D. Drain, A. Dauchy, A. Giorni, and C. Morand, Nucl. Inst. and Method. 212 (1983) 209; A. Giorni, Proc. Workshop on Heavy-Ion Reaction Dynamics Studied with Large Counter Arrays, U. Toronto (1987 March 26-27) 165; G.D. Westfall, op. cit. p51.

11. R. Mühlhans, W. Kühn, V. Metag, R. Novotny, D. Pelte, U. Winkler, A. Gobbi, and K.D. Hildenbrand, GSI Scientific Report 1986, GSI 87-1 (March 1987) 63.

12. F. Lidén, J. Nyberg, A. Johnson and A. Kerek, Nucl. Inst. and Meth. in Physics Research A253 (1987) 305.

13. R.A. Cecil, B.D. Anderson, and R. Madey, Nucl. Inst. and Meth. 161 (1979) 439.

14. M.A. Lone, A.J. Ferguson, and B.C. Robertson, Nucl. Inst. and Meth. 189 (1981) 515.

15. J.S.A. Kapustinsky, R.M. DeVries, N.J. Digiacomo, W.E. Sondheim, J.W. Sunier and H. Coombes, Nucl. Inst. and Meth. A241 (1985) 612.

16. W.H. Atkins, IEEE Trans. Nucl. Sci. NS30 (1983) 3797.

17. J.P. Martin, D.C. Radford, M. Beaulieu, P. Taras, D. Ward, H.R. Andrews, G. Ayotte, F.J. Sharp, J.C. Waddington, O. Häusser, and J. Gascon, Nucl. Inst. and Meth. in Physics Research, A257 (1987) 301.

18. G.D. Westfall, Proc. Workshop on Heavy-Ion Reaction Dynamics Studied with Large Counter Arrays, U. Toronto (1987 March 26-27) p. 51.

19. R. Bougault, J. Duchon, J.M. Gauthier, A. Genoux-Lubain, C. Le Brun, J.F. Lecolley, F. Lefebvres, M. Louvel, P. Mosrin, and R. Regimbart, submitted to Nucl. Inst and Meth. in Physics Research, and R.A. Dayras, Proc. Workshop on Heavy-Ion Reaction Dynamics Studied with Large Counter Arrays, U. Toronto (1987 March 26-27) p. 105.

APPENDICES

APPENDIX I CRNL SPECIFICATION 13547-SP-01

Equipment: High Vacuum Chamber

1. SCOPE

This specification covers the requirements for procurement of a high vacuum chamber for a multi-particle detector system to be installed at the Chalk River Nuclear Laboratories. The scope of supply includes the design, fabrication, inspection, testing and delivery of the chamber.

2. APPLICABLE DOCUMENTS

ASME Boiler and Pressure Vessel Code, Section VIII, Division 1.
CRNL Drawing E-13547-SK-2, Rev. 0.

3. REQUIREMENTS

3.1 Design Pressure: Full Vacuum

3.2 Design Temperature: 300°F

3.3 Operating Pressure: 1×10^{-6} torr

3.4 Bake-out Temperature: 300°F

3.5 Corrosion Allowance: None

3.6 Registration: Not Required

3.7 Materials of Construction:

Materials used in construction shall have outgassing rates suitable for high vacuum service. Carbon steel shall not be used inside the vessel. The shell, heads, flanges and nozzles shall be fabricated from stainless steel type 304. Elastomer O-rings, if used, shall have gas permeability rates equal to or lesser than Viton-A. Copper, if used, shall only be OFHC grade.

3.8 Welding:

Particular care shall be exercised in the design of weldments to avoid virtual leaks. Welding practices shall be suitable for high vacuum service. Wherever possible, components shall be welded on the vacuum side of a joint to eliminate the possibility of trapping gas in cracks or collecting dirt in crevices. Double butt joints shall be avoided.

If welds are required on both sides of a joint for strength, the strength weld shall be on the outside and made intermittently. The inner weld shall be continuous and, where feasible, be of single pass design.

3.9 Finish:

All interior surfaces of the vessel shall be polished to an equivalent of No. 4 (150-180 grit) finish. All inner welds shall be ground smooth and polished to match adjacent finish. As an option, the supplier shall quote for a No. 2B finish on all interior surfaces.

3.10 Cleaning:

All interior surfaces, internal components and flange faces shall be scrupulously cleaned employing a multi-stage procedure. The following steps shall be included as a minimum:

a) Remove visible contaminants mechanically

b) Clean with synthetic detergent

c) Rinse with hot distilled water

d) Rinse with acetone

e) Wipe with alcohol-soaked cloth

f) Dry in warm air.

Exterior surfaces shall be reasonably clean.

3.11 Leak Testing:

3.11.1 Helium Leak Test: The high vacuum chamber assembly or all of its sub-assemblies shall be helium leak tested using a purchaser-approved procedure. The acceptance criterion shall be a maximum leak rate of 1×10^{-9} std.cc/s.

3.11.2 Pressure Rise Test: The assembled chamber shall be pumped down to a pressure of 1×10^{-7} torr, using a purchaser-approved procedure. The pump shall be valved off and the rate of increase in pressure shall be recorded from a base of 1×10^{-6} torr. The time interval for the pressure to rise by an order of magnitude, i.e. to 1×10^{-5} torr, shall not be less than 75 minutes.

3.12 Documents:

General arrangement drawings of the vessel shall be submitted to the purchaser for acceptance and such acceptance obtained prior to scheduled start of construction. Four (4) copies of certified dimensional drawings shall be sent to the purchaser prior to shipment of the vessel.

Leak testing and cleaning procedures shall also be submitted to the purchaser for acceptance prior to use.

3.13 Special Requirements:

The CRNL drawing noted in paragraph 2 shows a field weld between shell sections in order to facilitate the installation of the vessel. The supplier shall take this requirement into account and propose the most practical and cost-effective method of accomplishing the leak testing requirements at either the supplier's plant or the purchaser's site.

As an option, the supplier shall quote on the following basis:

a) Design, fabricate, inspect and test the chamber using a temporary weld in place of the field weld shown.

b) Remove the temporary weld and refurbish the weld preps following successful completion of leak tests.

c) Deliver the vessel in two sections, to be rewelded on site by purchaser.

4. QUALITY ASSURANCE

The supplier shall apply a Quality Inspection Program as specified in CSA Standard Z299.4 that will assure the purchaser that materials, inspection and documentation fully meet the requirements. The purchaser shall have the right of access to the supplier's premises for verification of technical and quality assurance requirements.

5. PREPARATION FOR DELIVERY

The supplier shall preserve and package the product according to the best commercial practice. The vessel shall be shipped in a sealded condition to prevent recontamination of interior surfaces.

APPENDIX II SAFETY CONSIDERATIONS FOR CRYOGENIC CAPTURE PUMPS

A. HAZARDS:

Cryopumps are capture pumps. Therefore, if toxic or explosive gases are pumped these could accumulate in significant quantities in the pump and, without proper precautions, a dangerous situation could result. In the MARS vacuum system, the only substantial sources of gases other than air are the detectors and their associated gas lines. Toxic gases are not used; however, hydrocarbons (e.g. methane, isobutane) are common components of counter gases. When these gases enter the vacuum system, there is no immediate danger of explosion since air is not present. The gases are then captured by the cold head. Thus, a hazard could arise upon warming up of the cold head as hydrocarbon gases are released in a mixture with air. (Since N_2 is released before O_2 during the warming of a pump and since O_2 is never a counter gas, oxygen-enriched mixtures will not occur.) The limits of inflammability, in percent by volume at atmospheric pressure, are 5-15% for methane in air and 1.8-8.4% for isobutane in air. If these mixtures were present and were ignited, an explosion could occur. Events that might release such mixtures include:

- normal pump warmup and purge
- power failure
- pump failure

B. MANUFACTURER'S RECOMMENDATIONS

It is recommended that in order to pump explosive gases safely, one should:

- eliminate any source of ignition (e.g. ion gauges, high voltage) between the pump head and the high vacuum valve.
- vent relief valve through a sealed "path into a controlled environment."
- clearly mark pumps to indicate potential hazard.

C. PRECAUTIONS FOR MARS VACUUM SYSTEM

Two members of the CRNL Radiation and Industry Safety Branch were consulted upon installation of the existing 1.75 m scattering chamber, which also is used with potentially explosive counter gases and cryopumps. They inspected the explosive gas-vent line going to the roof of the TASCC complex and recommended its use. The MARS vacuum system will also couple into this line. The following precautions will be incorporated:

- no spark sources between pump head and gate valve.
- cryopump vent valves couple directly to explosive gas vent line.
- explosive gas-vent line is metal conduit going directly to roof; no blowers or other possible spark sources in line.
- high-vacuum gate valves close upon power failure; when power is restored, they do not automatically reopen, since released gases could then enter chamber and be ignited by ion gauge or high voltage breakdown.
- to protect against pump failure and against human error on warmup, high-vacuum valves automatically seal off cryopumps when chamber pressure goes over 150 μm.
- warning notices posted on pump controls and gas handling system.